TECH LIBRARY KAFB, NM

NASA CONTRACTOR
REPORT

NASA CR-2841

NASA CR 2

STATIC AND WIND TUNNEL
NEAR-FIELD/FAR-FIELD
JET NOISE MEASUREMENTS
FROM MODEL SCALE SINGLE-FLOW
BASELINE AND SUPPRESSOR NOZZLES -
SUMMARY REPORT

Carl L. Jaeck

NATIONAL AERONAUTICS AND SPACE ADMINISTRATION • WASHINGTON, D. C. • JUNE 1977

1. Report No **NASA CR-2841**	2. Government Accession No.	3. Recipient's Catalog No.
4. Title and Subtitle Static and Wind Tunnel Near-Field/Far-Field Jet Noise Measurements from Model Scale Single-Flow Base Line and Suppressor Nozzles—Summary Report		5. Report Date **June 1977**
		6. Performing Organization Code
7. Author(s) Carl L. Jaeck		8. Performing Organization Report No. D6-44121-3
		10. Work Unit No.
9. Performing Organization Name and Address Boeing Commercial Airplane Company P.O. Box 3707 Seattle, Washington 98124		
		11. Contract or Grant No. NAS 2-8213
		13. Type of Report and Period Covered Contract Report
12. Sponsoring Agency Name and Address National Aeronautics and Space Administration Ames Research Center Moffett Field, California 98035		
		14. Sponsoring Agency Code

15. Supplementary Notes

NASA project manager, Adolph Atencio, Jr.

16. Abstract

A test program was conducted in the Boeing Large Anechoic Test Chamber and the NASA-Ames 40- by 80-Foot Wind Tunnel to study the near- and far-field jet noise characteristics of six baseline and suppressor nozzles. The objectives of the study were to (1) determine static and wind-on noise source locations, (2) establish a technique for extrapolating near field jet noise measurements into the far field, (3) determine if flight effects measured in the near field are the same as those in the far field, and (4) determine the flight effects on the jet noise levels of the baseline and suppressor nozzles. Test models included a 15.24-cm round convergent nozzle, an annular nozzle with and without ejector, a 20-lobe nozzle with and without ejector, and a 57-tube nozzle with lined ejector. The static free-field test in the anechoic chamber covered nozzle pressure ratios from 1.44 to 2.25 and jet velocities from 412 to 594 m/s at a total temperature of 844^0 K. The wind tunnel flight effects test repeated these nozzle test conditions with ambient velocities of 0 to 92 m/s.

The noise source locations were derived from acoustic measurements along multiple sideline locations. The static and wind tunnel noise source locations were determined to be distributed along the jet and varied as a function of Strouhal number and a noise source radiation or propagation angle. Analysis techniques were developed to interpret near-field noise data and extrapolate noise measurements from relatively close to the sources to the far field. Analysis of data from the wind tunnel test indicates that flight effects on jet noise measured in the near field are the same as those measured in the far field. Data from all six nozzles at most conditions indicates that forward speed results in jet noise reduction in the aft quadrant, and little or no reduction in the forward quadrant. At supersonic conditions some of the configurations displayed an increase in noise in the forward quadrant due to forward speed. All subsonic data indicate that there is no noise increase in the forward quadrant with forward velocity. Shock cell noise was shown to increase in the forward quadrant with forward speed and causes an eventual crossover of wind-on overall sound pressure level (OASPL) and perceived noise level (PNL) directivities relative to the wind-off values. Flight effects for the round convergent (RC) nozzle measured in the 40- by 80-foot wind tunnel were shown to be in good agreement with flight test results from a turbojet-powered F-86 airplane. The F-86 flight test results were obtained from a taxiby test.

17. Key Words (Suggested by Author(s)) Jet noise Flight effects Source locations Suppressor nozzles Model scale Wind tunnel	18. Distribution Statement Unclassified, unlimited STAR Category – 07

19. Security Classif. (of this report) Unclassified	20. Security Classif. (of this page) Unclassified	21. No. of Pages 100	22. Price* $5.00

*For sale by the National Technical Information Service, Springfield, Virginia 22161.

CONTENTS

FIGURES

FIGURES (Continued)

STATIC AND WIND TUNNEL NEAR FIELD/FAR FIELD JET NOISE MEASUREMENTS FROM MODEL SCALE SINGLE-FLOW BASELINE AND SUPPRESSOR NOZZLES

SUMMARY REPORT

C. L. Jaeck
Boeing Commercial Airplane Company

SUMMARY

A test program was conducted in the Boeing Large Anechoic Test Chamber and the NASA-Ames 40- by 80-Foot Wind Tunnel to study the near- and far-field jet noise characteristics of six baseline and suppressor nozzles. The objectives of the study were to (1) determine static and wind-on noise source locations, (2) establish a technique for extrapolating near field jet noise measurements into the far field, (3) determine if flight effects measured in the near field are the same as those in the far field, and (4) determine the flight effects on the jet noise levels of the baseline and suppressor nozzles. Test models included a 15.24-cm round convergent nozzle, an annular nozzle with and without ejector, a 20-lobe nozzle with and without ejector, and a 57-tube nozzle with lined ejector.

The static free-field test in the anechoic chamber covered nozzle pressure ratios from 1.44 to 2.25 and jet velocities from 412 to 594 m/s at a total temperature of 844°K. The wind tunnel flight effects test repeated these nozzle test conditions with ambient velocities of 0 to 92 m/s.

The noise source locations were derived from acoustic measurements along multiple sideline locations. The static noise source locations were determined to be distributed along the jet and varied as a function of Strouhal number and a noise source radiation or propagation angle. In addition, the noise source locations for the 20-lobe and 57-tube nozzles were a function of jet Mach number or pressure ratio. The wind-on peak noise source locations exhibited the expected shift downstream due to a stretching of the potential core, while the peak noise propagation angles indicated the effect of sound convection. The distributed sound source locations for the wind-on data were found to agree with the static correlations when Strouhal number was based on relative velocity and the noise propagation angle includes sound convection.

Analysis techniques were developed to interpret near-field noise data and extrapolate noise measurements from relatively close to the sources to the far field. An empirical correlation was defined that accounts for the deviation from spherical spreading loss in the near field caused by distributed noise sources, non-point sources, and pseudosound effects. The extrapolated static and wind-on data from the 0.6-m and 1.5-m sidelines were observed to agree with the measured 3.0-m data when the proper corrections were applied. Analysis of data from this test indicates that flight effects on jet noise measured in the near field are the same as those measured in the far field. Data from all six nozzles at most conditions indicates

that forward speed results in jet noise reduction in the aft quadrant, and little or no reduction in the forward quadrant. At supersonic conditions some of the configurations displayed an increase in noise in the forward quadrant due to forward speed. All subsonic data indicate that there is no noise increase in the forward quadrant with forward velocity. Shock cell noise was shown to increase in the forward quadrant with forward speed and causes an eventual crossover of wind-on OASPL and PNL directivities relative to the wind-off values.

In general the flight peak PNL suppression for all of the suppressor nozzles was less than that measured statically. Forward speed reduces the peak PNL of the suppressor and the baseline nozzles. The amount of the reduction for the baseline is larger, and therefore results in a reduction of peak noise suppression in flight. Only the annular nozzle with lined ejector tended to maintain peak PNL suppression with forward speed.

Flight effects for the RC nozzle measured in the 40- by 80-Foot Wind Tunnel were shown to be in good agreement with flight test results from a turbojet-powered F-86 airplane. The F-86 flight test results were obtained from a taxiby test.

The near-field jet noise analysis techniques which were developed and verified during this study proved that engine flight jet noise levels can be determined from near-field measurements in the 40- by 80-Foot Wind Tunnel. The wind tunnel dimensions and the reverberant field forces one to make the engine noise measurements relatively close to the sources. The agreement between the near- and far-field model scale jet noise levels and increments indicates that wind tunnels provide an accurate means for simulation and measurement of the effect of ambient velocity on aircraft engine jet noise.

Two previous reports have been published that describe the two test series and related analysis. These reports are NASA-CR 137913 and 137914.

INTRODUCTION

One method of simulating flight effects on engine noise is to test the engine in a facility such as the NASA-Ames 40- by 80-Foot Wind Tunnel. Noise measurements are made in the near field and thus must be extrapolated into the far field, namely, flight certification altitudes and sideline distances. The far-field flight noise levels and directivity must be determined by direct extrapolation of the wind tunnel measurement or by determination of a flight effects noise increment which is corrected for near-to-far-field directivity changes and added to a static far-field noise measurement. In both cases a near-field to far-field extrapolation technique plus knowledge of apparent noise source locations and propagation angles are required to derive the flight noise levels. The basic problem is to relate flight effects measured near and far from the noise sources.

The approach used during this program was to study near- and far-field jet noise only, by using model scale single-flow nozzles. The model test program consisted of:

1. A reverberation test in the 40 by 80 to define optimum nozzle and free-field measurement locations.

2. A static jet noise test in the Boeing Large Anechoic Test Chamber under free-field conditions to obtain near- and far-field data.

3. A jet noise flight effects test in the 40 by 80 which used the same nozzle hardware and measurement locations as were used in the anechoic chamber.

In the first phase of the study, noise source locations were determined using the multiple sideline technique, and procedures were established for the extrapolation of static near-field jet noise measurements into the far field. The established techniques were then verified for wind tunnel conditions with ambient air velocity. The presence of ambient velocity results in a convection of sound and in a shifting of the noise sources downstream due to a stretching of the jet potential core. These effects of forward speed on jet noise were studied by means of a test in the 40 by 80 wind tunnel. This test provides the important link between near- and far-field flight effects.

ABBREVIATIONS AND SYMBOLS

A   area, m^2

a   speed of sound, m/s

ARC   Ames Research Center

D   diameter, m

f   one-third octave band center frequency, Hz

L   length, m

LTC   Boeing Large Anechoic Test Chamber

M   Mach number

m   meters; static velocity exponent, see equation 5

n   flight velocity exponent

NASA   National Aeronautics and Space Administration

NPR   nozzle pressure ratio (upstream total to ambient static)

OASPL   overall sound pressure level, dB

1/3 OBSPL   one-third octave band sound pressure level, dB

P   pressure, N/m^2

PNL   perceived noise level, PNdB

R   radial distance from sound source to observer, m

RC   round convergent

RH   relative humidity, percent

S   Strouhal number, $fD/(V - V_A)$

SL   sideline distance, m

SPL   sound pressure level, dB

T   temperature, $^{\circ}C$, $^{\circ}K$

V_j	fully expanded jet velocity, m/s
$\overline{V}^2$	RMS velocity fluctuation, m/s
X	axial distance from nozzle or ejector exit plane, m
Y	radial distance, m
θ_I	angle relative to nozzle or ejector exit plane center and inlet axis
θ_S	angle relative to source location and inlet axis without ambient velocity (noise radiation angle), deg
λ	wavelength, m
ρ	density, kg/m^3
ρ_j	fully expanded jet density, kg/m^3
ψ	angle relative to source location and inlet axis (noise propagation angle, includes convection), deg
ω	density exponent

SUBSCRIPTS

A	ambient
cl	centerline
E	extrapolated; ejector
eq	flow equivalent
I	inlet
j	jet
M	measured; microphone
S	source

SUBSCRIPTS (Continued)

T   total

1   static noise resource location

2   wind-on noise source location

SUPERSCRIPTS

$--$ time averaged

TEST DESCRIPTION

TEST HARDWARE

The following six nozzle configurations were tested in the Boeing Large Anechoic Test Chamber (LTC) and NASA-Ames 40- by 80-Foot Wind Tunnel (40 by 80):

- 15.24-cm round convergent (RC) reference nozzle

- Annular (plug) nozzle

- 20-lobe nozzle

- Annular nozzle with lined ejector

- 20-lobe nozzle with lined ejector

- 57-tube nozzle with lined ejector

The test nozzles have nearly equal flow areas, which are equivalent to a diameter of 15.24 cm. Photographs of the nozzle hardware are provided in figures 1 to 4. Important dimensions and geometric descriptions are given in references 1 and 2.

TEST FACILITIES

The Boeing LTC consists of an acoustically treated room, 22.9 m wide, 19.8 m long, and 9.1 m high (75 by 65 by 30 ft). The acoustic treatment on the interior surfaces consists of 30.5-cm-square, 32-kg/m^3 polyether/polyurethane foam wedges with a depth of 40.6 cm. The foam wedges have been treated with a chemical fire retardant. The chamber provides acoustic data within ±1 dB of free field down to 200 Hz.

The NASA-Ames 40 by 80 is a closed-circuit tunnel driven by six 12.2-m-diameter fans. The tunnel test section is 12.2 m high, 24.4 m wide, and 24.4 m long. The tunnel cross section has semicircular sides with a flat horizontal ceiling and floor. The test section walls are constructed of steel plate and therefore the tunnel is quite reverberant. Four hundred square meters of 7.62-cm-thick polyurethane foam was installed on the internal wind tunnel walls and floor in the general vicinity of the test model and microphone installations to improve the acoustic characteristics. This material provides sufficient absorption to permit free-field noise measurements on a 3.0-m sideline for frequencies of 500 Hz to 40 kHz.

The hot gas source for the test nozzles in the LTC and the 40 by 80 were a propane and kerosene burner, respectively, designed to match a nozzle with a 180-square-cm exit area. The burner in the 40 by 80 was mounted on the floor to minimize flow disturbances by immersion in the tunnel boundary layer. The nozzle nacelle length and boundary layer growth were minimized by the floor mounting of the burner and use of two 135° elbows. The internal pipe and flow system diameters were made as large as possible to maintain low

internal flow velocities. Airflow for the burner in the 40 by 80 test was supplied by a Viper/J-85 turbocompressor installed beneath the wind tunnel. Air was ducted through a bypass system, up through an airflow-measuring nozzle, and into the kerosene fuel burner where the temperature was raised to 844° K, and exhausted through the nozzle. Photographs of the LTC and 40 by 80 installations are displayed in figures 5, 6, and 7.

ACOUSTIC INSTRUMENTATION

The acoustic instrumentation for the LTC test consisted of 35 microphones mounted along 0.6-, 1.5-, and 3.0-m sidelines. For the RC nozzle, measurements were also made along a 5.33-m sideline. Noise measurements in the 40 by 80 were made with three pairs of microphones mounted on mechanisms which traversed along 0.6-, 1.5-, and 3.0-m sidelines. Acoustic measurements in the 40 by 80 tunnel were made with a continuously moving traverse (sweep mode).

TEST CONDITIONS

The static free-field test in the anechoic chamber covered nozzle pressure ratios from 1.44 to 2.25 and jet velocities from 412 to 594 m/s at a total temperature of 844° K. The wind tunnel flight effects test repeated these nozzle test conditions with ambient velocities of 0 to 92 m/s. The 40 by 80 test also included a series of runs at a nozzle pressure ratio of 2.6 for the RC and 57-tube nozzle configurations.

DATA ANALYSIS

PHYSICAL MODEL

The jet noise generation and propagation problem can be broken into three regions: the flow field, the near field, and the far field. Siddon (ref. 3) defines the near field as the region from the line of maximum shear to the location where spherical divergence or 6 dB per doubling of distance begins. The near-field pressure fluctuations are composed of two parts: (1) the pseudosound or nonpropagating part, and (2) the acoustic or propagating fraction.

The near-field jet noise cannot be represented by a single-point source or by a series of point sources whose location is only a function of frequency. Assuming the jet can be represented by a cylindrical source, the noise at a given frequency is generated throughout the finite length cylindrical noise source and radiates sound in a highly directional manner. In a jet there are the additional effects of sound source convection and refraction, which influence sound directivity.

The presence of ambient velocity or forward speed produces changes in the jet flow field, noise generation, and sound propagation. Ambient velocity produces a stretching of the potential core that results in a shift of the jet noise source locations downstream.

To estimate the effect of ambient velocity on potential core length and peak noise source locations, an analytical study was conducted using the Lu/Berman flow/noise analysis (refs. 4 and 5). The results are useful for understanding the jet fluid mechanics and noise generation problem, and to point out possible noise source location correlating parameters. The effect of ambient velocity on the jet centerline velocity and turbulence intensity is shown in figure 8. The tip of the potential core, indicated by the arrows in figure 8, is observed to shift downstream by two diameters for an increase in ambient velocity of 91.5 m/s. The radial velocity profile (fig. 9) in the region of peak shear is only slightly affected by ambient velocity. The turbulence intensity profile is substantially changed, with the peak intensity decreasing from 14.5% to 12%.

The flow/noise analysis was also used to obtain the analytical peak power source locations as displayed in figures 10 and 11. The static results are presented in figure 10 for nozzle pressure ratios of 1.44 and 2.25. The analytical results collapse into a single line, and show a concentration of peak noise sources at or slightly downstream from the tip of the potential core. Ambient velocity produces a stretching of the potential core and shifting of the noise source locations downstream. This effect has been observed to be largest for the low frequencies or Strouhal numbers. The collapse of the analytical results onto a single straight line at a constant Strouhal number indicates a means of correlating the measured peak noise source locations, which will be discussed later.

The presence of ambient velocity also changes the noise propagation by convecting the sound as shown in figure 12. The noise source propagation angle (ψ) is related to the static noise source radiation angle (θ_S) by the following relationship:

$$\tan(\psi - 90^\circ) = \frac{\sin(\theta_S - 90^\circ) + M_A}{\cos(\theta_S - 90^\circ)} \tag{1}$$

Comparison of equation 1 and wind tunnel test results will be presented later in this report.

NOISE SOURCE LOCATIONS

A proposed model and method of analysis of the near-to-far-field jet noise data has been suggested by Strout (refs. 6 and 7). The jet noise generated at a given frequency is represented by a series of directional point sources. The sound radiates at a fixed angle relative to the jet axis and propagates from the source location in the jet through the near field and into the far field. The level is reduced by spherical divergence (with near field corrections) and atmospheric absorption. The sound level/distance (on a sideline basis) relationship is assumed to be the same for all radiation or emission angles, excluding atmospheric absorption effects. This assumption of a constant SPL increment is based on the following considerations:

1. $20 \log(SL,2/SL,1) = $ constant

2. The near-field effects on SPL at a given frequency and sideline distance are constant

3. The differences in atmospheric attenuation over any two propagation paths is small (between the same two sidelines)

The latter requirement is not true for high frequencies, where atmospheric attenuation corrections are required.

The noise source locations and radiation angles are defined by acoustic measurements on multiple sidelines. The anlaysis is accomplished by plotting the one-third-octave-band SPL directivities for the multiple sidelines at a given jet condition as shown in figure 13. The four points indicated by the angles for the peak or maximum one-third-octave-band SPL specify the noise propagation path. Assuming the SPL increment between the peak for the far field and a near-field sideline remains constant for all locations or propagation paths, the nonpeak emission angles are defined in figure 13 by the dashed lines. To illustrate the procedure, assume an angle of 90° on the 5.33-m sideline and then add the ΔSPL between the peak 5.33-m and 3-m sidelines to the SPL at 90° on the 5.33-m sideline. One then determines where this corrected SPL intersects the 3-m sideline, which is 93° for this case. This procedure is repeated for the remaining two sidelines to complete the tracing of the noise propagation path. This procedure is then repeated for other propagation paths to determine the variation of source location as a function of noise radiation angle for a given frequency or Strouhal number.

The procedure illustrated in figure 13 is repeated for each frequency to define a series of emission angles and apparent axial source locations for each jetflow condition. The noise sources were assumed to be located radially along a line of maximum shear, or at a radial position (Y) equal to the nozzle radius as shown in figure 14. The peak source locations and emission angles are shown in figures 15 and 16.

The peak noise source locations from the multiple sideline technique are compared with the wall isolation results (from ref. 8) in figure 15. Although the two sets of results are nearly equal in magnitude, the detail trends are quite different. The noise source locations from the multiple sideline technique do not stratify with Mach number and exhibit a flat region that indicates most of the peak noise is generated at the tip of the potential core at $X/D = 5.0$, similar to the analytical results. The similarity of the analytical and experimental peak source locations for the RC nozzle adds credence to the multiple sideline technique. All noise source locations for the six nozzle configurations at both static and wind-on conditions were derived from experimental results using the multiple sideline technique.

Peak noise source locations are only one piece of information required in the near-field/far-field analysis of jet noise data. Knowledge of the noise source radiation angles is also required to perform a near-to-far-field extrapolation of jet noise results. The peak noise radiation angles, like the noise source locations, were found to correlate with Strouhal number as presented in figure 16.

The peak noise source locations and radiation angles only partially define the noise generation in the jet. The noise at one frequency or Strouhal number is generated along the jet, and different parts of the jet radiate at different angles, as was shown earlier in figure 14. The previous correlations for peak noise source locations and radiation angles as functions of Strouhal number suggest a means of correlating the distributed noise source effects. The nondimensional noise source locations (X_S/D) can be correlated as a function of radiation angle (θ_S), but at constant Strouhal number (fD/V), as shown in figure 17, using the procedures and results of figures 13 and 14.

The distributed source location correlations indicate that for a given nozzle diameter, if the jet velocity and frequency are both doubled, the source locations (X_S/D) and radiation angles for the two cases are equal. This occurs because as frequency is increased, the noise sources tend to shift toward the nozzle exit, but as velocity is increased the jet core length is increased and the noise sources tend to move downstream.

These distributed noise source correlations indicate that the noise generation region at a given Strouhal number is limited in size, and extends from a point just downstream of the nozzle exit to a point near the end of the jet plume. These results are consistent with jet noise and flow phenomena.

As discussed earlier, the static distributed noise source locations can be correlated as a function of the noise radiation angle (θ_S) and Strouhal number (fD_j/V_j). For the wind tunnel

data the correlation parameters must be modified to account for ambient velocity, core stretch, and convection. The previous static noise source correlation parameters are modified as follows:

$$fD_j/V_j \longrightarrow fD_j/(V_j - V_A)$$

$$\theta_S \longrightarrow \psi \qquad\qquad (2)$$

These distributed noise source correlations were used to extrapolate static and wind-on near-field data into the far field, and to correct the wind-on angular location for convection and core stretch.

Peak wind-on noise source locations (X_S/D) and noise propagation angles (ψ) were determined for the RC nozzle as shown in figure 18. The experimental peak noise radiation angles show the effect of sound convection by the ambient velocity. The measured results agree with the trend calculated by equation 1. The static or initial value of the sound radiation angle was obtained from the correlation presented in figure 17.

The peak noise source locations shift downstream as the ambient velocity is increased due to the stretching of the potential core. The experimental peak noise source locations display the same linear trend observed in the analytical results. The faired line drawn through the data was established by using the noise propagation angle to enter figure 17 to determine the noise source locations. Stated another way, the peak noise source locations agree with the previous static correlations when θ_S is changed to ψ, and Strouhal number is based on the relative velocity ($V_j - V_A$).

Distributed noise source locations and propagation angles were determined for subsonic and supersonic jet conditions, with static and wind-on tunnel conditions as presented in figure 19. The 40 by 80 data are shown to agree and correlate with the LTC measurements (faired curves).

EXTRAPOLATION PROCEDURE

Application of the apparent jet noise source locations to the extrapolation of near-field data on an absolute level basis requires the assumption of a noise/distance scaling relationship, namely spherical divergence. Near a jet the assumption of spherical divergence or pressure doubling breaks down due to:

1. Pseudosound (nonpropagating), which increases the noise above spherical divergence close to the jet source region.

2. The fact that noise generation and sources are distributed over a volume in the jet. This is related to the differences between a point and line source as discussed by Rathe (ref. 9). The sound emitted by a line source falls off by a 10-log relation and then by a 20-log relation. The sound attenuation with distance is a function of the sideline distance and the position of the observer (i.e., the viewing angle, which spans the length of the source). The results of Rathe, though not directly applicable, are informative.

14

To account for the two effects, peak static near-field noise levels at varying frequencies or wavelengths were correlated as presented in figure 20. The correlation indicates the deviation of the peak near-field one-third-octave-band SPL from the peak far-field SPL extrapolated to the near-field location using spherical divergence. This near-field noise increment was found to be a function of the following correlation parameters:

1.   SL/D, sideline distance to jet diameter

2. (R/λ) (V_j/a_A), ratio of path length from noise source location to observer (R) to the wavelength (λ) multiplied by the acoustic Mach number (V_j/a_A)

The section of the curves to the right of the peak is attributed to the distributed source effects, while the left part of the curve is due to near-field effects. The near-field and distributed source effects on the acoustic spreading loss diminish for sideline distances (SL/D_j) greater than 20 diameters. For the wind-on or flight case, V_j must be replaced by the relative velocity, $V_j - V_A$.

The near-field jet noise data is extrapolated into the far field by correcting both the SPL and angular location. The correction in level is given by:

1/3 OBSPL (far field) = 1/3 OBSPL (near field)

$$- 20 \log_{10} \frac{R_{S,E}}{R_{S,M}} - \frac{\Delta dB}{305} \frac{R_{S,E} - R_{S,M}}{305} + \Delta SPL_1 - \Delta SPL_2 \qquad (3)$$

where:

$R_{S,M}$ = acoustic path length from source location to near-field microphone location which has been corrected for core stretch and convection, m

$R_{S,E}$ = acoustic path length from source (through near-field location) to far-field sideline, m

$\dfrac{\Delta dB}{305}$ = atmospheric attenuation (ARP 866, ref. 10), dB/305 m

ΔSPL_1 = from figure 20, where R = $R_{S,M}$ and SL = SL,M

ΔSPL_2 = from figure 20, where R = $R_{S,E}$ and SL = SL,E

The equivalent static microphone angle for the extrapolated wind-on data is given by the following equation:

$$\theta_I - 90^\circ = \arctan \frac{X_{S2} + (SL_E - Y_S) \, TAN \, (\psi - 90^\circ) - M_A R_{S,E} - (X_{S2} - X_{S1})}{SL_E} \quad (4)$$

which accounts for the effect of source locations, core stretch, and convection on directivity.

The measured data from the 40 by 80 flight effects test was extrapolated, analyzed, and presented in the following manner:

a. Measured spectral data extrapolated to a 3.0-m sideline at measurement day temperature and relative humidity covering frequencies of 200 Hz to 40 kHz.

b. PNL (ref. 11) and OASPL calculated from measured spectral data extrapolated to a 305-m sideline and 0 altitude including corrections for a scale factor of 5, Doppler frequency shift (but not level), and ambient conditions of 25°C and 70% relative humidity. The extrapolation to 305 m was performed in two steps: (1) to a 15.24-m sideline using the distributed source locations and model frequencies, and (2) from 76.2 m (5 x 15.24) to 305 m using point source located at the nozzle exit plane and scaled frequencies of 50 Hz to 8 kHz.

The data from the static free-field test in the LTC was extrapolated and analyzed as described in item (a). Extrapolated static and wind-on data for each of the six nozzles are presented in references 1 and 2. The extrapolated data from the 0.6- and 1.5-m sidelines were observed to be in excellent agreement with the 3-m far-field data.

BASELINE NOZZLE FLIGHT EFFECTS

The baseline nozzle used in the 40 by 80 flight effects test was a 15.24-cm convergent (RC) nozzle. The RC nozzle was tested at subsonic and supersonic jet Mach numbers, and at tunnel velocities up to 92 m/s. Flight effects on jet noise were studied on both an incremental and absolute level basis.

The near-to-far-field extrapolation technique, described earlier, was used to extrapolate measured data from 0.6- and 1.5-m sidelines to the 3.0-m location. Subsonic data from the RC nozzle at a pressure ratio of 1.75 and tunnel velocities of 3, 46, and 69 m/s are compared in figure 21 on the basis of overall and one-third-octave-band SPL directivity. The resulting extrapolated data from the three locations indicate the same effect of ambient velocity on jet noise. Ambient velocity results in a large reduction in subsonic jet noise at angles in the aft quadrant and small reductions in the forward quadrant. In addition, the comparisons do not indicate any noise increase in the forward quadrant.

16

Previous investigations (refs. 12 through 14) have developed flight effects prediction procedures based on a velocity exponent in a power law applied to the OASPL. In general, these studies have also shown that the flight noise spectrum changes shape relative to the static spectrum.

An attempt was made during this study to correlate the effect of ambient velocity on the subsonic jet noise spectra. Since the normalized (1/3 OBSPL - OASPL) jet noise spectra for an RC nozzle at a given jet total temperature is a function of Strouhal number and velocity ratio (V_j/a_A), the wind-on spectra should be compared with the measured static case where the jet velocity is equal to the wind-on relative velocity ($V_j - V_A$). These 1/3 OBSPL increments are presented in figure 22 as a function of angle and Strouhal number, $fD/(V_j - V_A)$. The subsonic results presented in figure 22 also represent the deviation of the measured flight effect from the full relative velocity effect, and are a measure of the distortion of the jet flow field and noise generation mechanisms by the ambient velocity. The results presented in figure 22 can be used to predict the effect of ambient velocity on subsonic and supersonic shockfree jet noise. The prediction procedure would consist of the spectral correction and an increment in OASPL due to the relative velocity ($V_j - V_A$). The effect on the OASPL can be calculated using the velocity and density exponents given in figure 23, and the following equation:

$$m = - \frac{\left[OASPL - 10 \log_{10} (\frac{\rho_j}{\rho_A})^\omega\right]_{V_j} - \left[OASPL - 10 \log_{10} (\frac{\rho_j}{\rho_A})^\omega\right]_{V_j - V_A}}{10 \log (\frac{V_j}{V_j - V_A})} \qquad (5)$$

The static velocity and density exponents for the RC nozzle were based on the collected and normalized clean jet noise data of reference 15, since the data was much larger in quantity than that measured in these test series and covers a wider range of jet conditions.

The model scale acoustic data from the 0.6-, 1.5-, and 3-m sidelines were also extrapolated to a flight condition at a 305-m sideline with corrections applied for:

- Scale factor of 5

- Source location and near-field effects

- Core stretch

- Convection

- Ambient conditions, 25°C and 70% RH

- Doppler frequency shift (but not level)

The OASPL and PNL directivities based on the scaled spectral data for NPR = 1.58 and 2.25 at a flight (wind-on) Mach number of 0.2 are displayed in figures 24 and 25. The absolute noise levels are shown in the upper part of each figure and change or increment in noise due to forward speed is shown in the lower part. The static and wind-on measurements from the three sidelines agree reasonably well. The increment in noise level due to flight measured in the near field (0.6 m and 1.5 m) and the far field (3.0 m) are in good agreement. The subsonic cases do not show an increase in noise with forward speed in the forward arc, while the supersonic cases do show an increase. The increase in noise for the supersonic case is due to shock cell noise.

FLIGHT EFFECTS ON SUPERSONIC JET NOISE

A set of extrapolated static and wind-on data for a supersonic test condition (NPR = 2.25) is displayed in figures 26 and 27. The extrapolated static data are compared with empirical predictions for clean, shockfree jet mixing noise (ref. 15) and shock cell noise (ref. 16). The shock cell noise component is shown to dominate the peak and high-frequency region of the forward arc spectra. The shock cell noise can be seen to act as a noise floor, which minimizes the effect of ambient velocity on jet mixing noise. In addition, when the shock noise is the dominant noise source, ambient velocity produces a noise increase in the forward quadrant.

The shock cell structure in a supersonic jet from an underexpanded nozzle generates noise in the middle to high frequencies and at angles in the forward arc. The shock-cell-related noise is generated by shock-shock, shock-edge, and by shock-turbulence interactions. Little is presently known about these noise generation processes or the effect of ambient velocity on these shock-associated noise sources.

To isolate the flight effect on shock cell noise, the measured supersonic jet noise must be broken up into a jet mixing component and a shock cell component. The two effects have been separated in the far field by using PNL based on scaled extrapolated data from the 40 by 80 and static predictions (refs. 15 and 16) as shown in figure 28. The variation of jet mixing noise with ambient velocity has been suggested by references 12 and 13 to be of the form

$$PNL_{flight} = PNL_{static} - 10 \, n \log_{10} \frac{V_j}{V_j - V_A} - 10 \log (1 - M_A \cos \theta_I) \qquad (6)$$

The value of n at 40° and 140° was obtained from a "best" fit of the subsonic data.

The effect of forward speed on shock cell noise has been shown in reference 14 to follow:

$$PNL_{flight} = PNL_{static} - 40 \log_{10} (1 - M_A \cos \theta_I) \qquad (7)$$

18

At $\theta_I \doteq 40^o$, the data at NPR = 2.25 lay slightly below the shock cell prediction, but well above the jet mixing noise. At NPR = 2.6 the data follow the prediction given by equation 7. From these results, it can be concluded that shock cell noise increases in flight in the forward quadrant as predicted by equation 7. Shock cell noise represents one cause of the increase in forward arc noise in flight.

FLIGHT VELOCITY EXPONENTS

As indicated in the previous section, one of the methods of normalizing the flight effects data is through the use of a velocity exponent. The flight velocity exponent (OASPL) can be given by

$$10\,n \log \frac{V_j}{V_j\text{-}V_A} = \text{OASPL}_{static} - \left[\text{OASPL}_{flight} + 10 \log_{10}(1 - M_A \cos\theta_I)\right] \quad (8)$$

The variation of OASPL and PNL velocity exponents with angular position and NPR is summarized in figure 29. The data are observed to vary with nozzle pressure ratio. The results presented in the figure are similar to those presented by other investigators in references 7, 12, and 17.

WIND TUNNEL–FLIGHT COMPARISON

A comparison of the 40 by 80 RC nozzle data and taxi-by flight data (ref. 18) from the F-86 Sabre Jet aircraft are displayed in figure 30. The Orenda 14 turbojet engine which is installed in the F-86 Sabre Jet aircraft was ground static tested at Paine Field, Washington with the airplane parked near the middle of a 61-m-wide runway. Ground microphones were positioned on a 29-m sideline at angles from 20° to 160°. The Orenda 14 engine exhaust system consists of a tailpipe 57.4 cm in diameter and 2.4 m long, with a 48.0-cm-diameter conical nozzle. Prior to acoustic testing the engine exhaust conditions were determined as a function of engine power.

The F-86 static data used in figure 30 are an average of three runs, while the flight data are an ensemble average of 10 microphones. The flight effects increment in OASPL from the wind tunnel and flight test are in good agreement. This comparison further verifies the extrapolation procedures and use of a wind tunnel to simulate flight effects on jet noise.

FLIGHT EFFECTS ON JET NOISE OF SUPPRESSOR NOZZLES

The flight effects program in the 40 by 80 included testing five suppressor nozzle configurations both at static and wind-on conditions. These configurations consisted of a 20-lobe nozzle with and without lined ejector, an annular nozzle with and without lined ejector, and a 57-tube nozzle with lined ejector. The effect of forward speed on PNL directivity (305-m sideline) for each of the suppressor nozzles is presented in figures 31 to 35. Measured static and wind-on data from each of the three sidelines are compared on both an absolute and incremental basis.

In all cases the noise levels in the aft quadrant are reduced with forward speed. At the forward arc locations most of the suppressor nozzles indicated a noise increase with the increasing forward speed for the supersonic test conditions due to shock cell phenomena. The extrapolated results from the three sidelines are in good agreement on both an absolute and incremental basis.

One of the purposes of the test series in the 40 by 80 was to determine if static jet noise suppression levels are altered by forward speed. Jet noise suppression is not achieved only by a reduction of peak sound pressure level. Since aircraft are certified on the basis of a duration-weighted or effective perceived noise level (EPNL), jet noise reduction must be accomplished by a reduction of both the peak PNL and PNL on either side of the peak to be effective.

The PNL directivity for the RC nozzle was compared with that from the two bare nozzles and three ejector/suppressor configurations as shown in figures 36 to 39. The two bare nozzles maintain their levels relative to the RC nozzle in flight at NPR = 1.75, but the levels are reduced at NPR = 2.25.

In the case of the two bare suppressor and three ejector/suppressor nozzles, their peak PNL suppression (relative to the RC nozzle at the ambient velocity) is reduced as jet velocity is reduced and ambient velocity is increased. For example, the peak to peak static PNL suppression for the 57-tube nozzle with lined ejector at NPR = 2.25 is reduced from 10 ΔPNdB to 4.0 ΔPNdB at 92 m/s as displayed in figure 40. The 20-lobe ejector/suppressor static peak suppression is reduced from 10 ΔPNdB to 5 ΔPNdB. Only the annular nozzle with and without a lined ejector tends to maintain its peak PNL suppression as ambient velocity is increased.

Also presented in figure 40 are the measured suppression values for the JT8D engine with a 20-lobe ejector/suppressor configuration. These JT8D data were obtained during a static ground test, a 40 by 80 test (ref. 7), and a 727 flight test (ref. 19). The model results are shown to correlate with the engine wind tunnel measurements and 727 aircraft flight test results.

The PNL suppression characteristics for the five configurations are shown in figures 41 and 42 at NPR = 2.25, but on an angle-by-angle basis.

The annular nozzle both with and without ejector displays a uniform noise reduction statically and in flight. The 20-lobe and 57-tube nozzle configurations attain maximum suppression both statically and in flight at angles near the jet axis (150°). At the NPR = 2.25 test condition a maximum suppression of 20 PNdB was attained by the 57-tube nozzle configuration as displayed in figure 42. The 20-lobe and 57-tube nozzle configurations tend to lose suppression near the peak noise angles (120° to 140°) as presented in figure 41. The 20-lobe nozzle with lined ejector gains 2 to 3 PNdB at angles of 140° to 160°. These results indicate that the effect of forward speed on noise generation and suppression is highly dependent on nozzle geometry, nozzle flow conditions, and location of the noise sources.

20

CONCLUSIONS

Noise measurements were made in the Boeing Large Anechoic Test Chamber and the NASA-Ames 40- by 80-Foot Wind Tunnel along three sideline locations for each of six model scale nozzles extending from the near to the far field. The objectives of the tests were to:

- Determine jet noise source locations

- Verify a technique for the extrapolation of data measured in the near field into the far field

- Establish the wind tunnel as a simulation technique for flight effects on the engine jet noise component

- Determine the flight effects in the near and far field for the six baseline and suppressor nozzle configurations

Near-field jet noise analysis techniques were developed and verified during this study and proved that engine flight jet noise levels can be determined from near-field measurements in the 40- by 80-Foot Wind Tunnel. The engine noise measurements in the wind tunnel must be made close to the sources due to tunnel size limitations. However, the agreement between near- and far-field model scale jet noise measurements observed during this study indicates that wind tunnels can be used to simulate and measure engine jet noise flight effects.

Conclusions regarding the data analysis techniques and jet noise flight effects are summarized as follows:

1. Jet noise source locations and emission angles can be derived from acoustic measurements along multiple sideline locations. Experimental peak noise source locations based on the multiple sideline technique follow the same trends based on analytical calculations for the baseline nozzle.

2. Noise levels and flight noise increments measured in the near field agree with those in the far field at the same acoustic angle when the following corrections are applied:

   - Source location

   - Near-field effects

   - Spherical divergence

   - Atmospheric attenuation

   - Core stretch (wind-on only)

   - Convection (wind-on only)

3. The effect of forward speed on jet noise was measured for six model scale baseline and suppressor nozzles. In general the effect of forward speed resulted in a reduction in subsonic jet noise at all angles with the greatest reduction occurring in the aft quadrant. For an RC nozzle at supersonic conditions, the noise in the forward quadrant increased with increasing forward speed. This effect was caused by supersonic shock cell noise that was observed to follow a $10 \log (1 - M_A \cos \theta_I)^{-4}$ relationship.

4. Flight effects for the RC nozzle as measured in a wind tunnel were shown to be in good agreement with flight test data from the turbojet-powered F-86 aircraft. This comparison adds further confirmation that wind tunnels provide an accurate means for simulation and measurement of the effect of forward speed on aircraft engine jet noise.

5. The jet noise suppression characteristics are altered by the effects of forward speed. The peak to peak PNL suppression (relative to RC nozzle) was reduced as ambient velocity was increased for the two bare suppressor and three ejector/suppressor nozzles. The multi-element nozzles such as the 20-lobe and 57-tube nozzles suffered a large reduction in the peak suppression values.

REFERENCES

1. Jaeck, C. L.: *Static and Wind Tunnel Near Field/Far Field Jet Noise Measurements from Model Scale Single Flow Baseline and Suppressor Nozzles. Volume 1—Noise Source Locations and Extrapolation of Static Free Field Jet Noise Data.* NASA CR-137913, September 1976.

2. Jaeck, C. L.: *Static and Wind Tunnel Near Field/Far Field Jet Noise Measurements from Model Scale Single Flow Baseline and Suppressor Nozzles. Volume 2—Forward Speed Effects.* NASA CR-137914, November 1976.

3. Siddon, T. E.: *Comments—Noise Mechanisms.* AGARD Conference No. 131, AGARD CP-131, pp. A2 to A4.

4. Berman, C.; Jaeck, C.; and Lu, H.: *Analytical Prediction of Jet Noise Generation.* Boeing document D6-40614TN, July 1974.

5. Lu, H.: *Multiannular Axisymmetric Jet Flow Prediction Using a Two Equation Model of Turbulence.* Boeing document D6-42606, September 1975.

6. Strout, F. G.: *Procedure for Evaluating Near Field Wind Tunnel Noise Data for Flight Effects.* Boeing document D6-42745TN, November 1975.

7. Strout, F. G.: *Flight Effects on Noise Generated by the JT8D-17 Engine in a Quiet Nacelle and a Conventional Nacelle as Measured in the NASA-Ames 40- by 80-Foot Wind Tunnel.* NASA CR-137797 (Boeing document D6-42813), January 1976.

8. McGregor, G. R.; and Simcox, C. D.: *Location of Acoustic Sources in Jet Flows by Means of "Wall Isolation Technique".* AIAA paper 73-1041, presented at AIAA Aero-Acoustics Conference, Seattle, Washington, October 1973.

9. Rathe, E. J.: "Note on Two Common Problems of Sound Propagation". *J. Sound Vibration,* 10 (3), pp. 472-479, 1969.

10. *Aerospace Recommended Practice 866 by the Society of Automotive Engineers, Inc.,* issued August 31, 1964.

11. "Definitions and Procedures for Computing the Perceived Noise Level of Aircraft Noise", Society of Automative Engineers, Inc., *Aerospace Recommended Practice 865A,* revised August 15, 1969.

12. Cocking, B. J.; and Bryce, W. D.: *Subsonic Jet Noise in Flight Based on Some Recent Wind Tunnel Results,* AIAA paper 75-462, March 1975.

REFERENCES (Continued)

13. Bushell, K.: *Measurement and Prediction of Jet Noise In Flight,* AIAA paper 75-461, March 1975.

14. Drevet, P.; Duponchel, J. P.; and Jacques, J. R.: *Effect of Flight on the Noise from a Convergent Nozzle as Observed on the Bertain Aerotrain,* AIAA paper No. 76-557, July 1976.

15. Jaeck, C. L.: *Empirical Jet Noise Predictions for Single and Dual Flow Jets with and without Suppressor Nozzles. Volume I–Single Flow Subsonic and Supersonic Jets.* Boeing document D6-42929, April 1976.

16. Evans, T.: *Predictions of Single Stream Shock-Cell Noise,* SAE A-21 Jet Noise Subcommittee, April 2, 1975.

17. Belleval, J.; Chen, C.; and Perulli, M.: *Investigation of In-Flight Jet Noise Based on Measurements in an Anechoic Wind Tunnel.* Sixth International Congress on Instrumentation, Ottawa, September 1975.

18. Oas, S.: *Relative Velocity Jet Noise Test Using an F-86 Airplane in Taxi and Flyover.* Boeing document T6-6104, 1977.

19. Munoz, L.: *727/JT8D Jet and Fan Noise Flight Effects Study.* FAA-RD-76-110, August 1976.
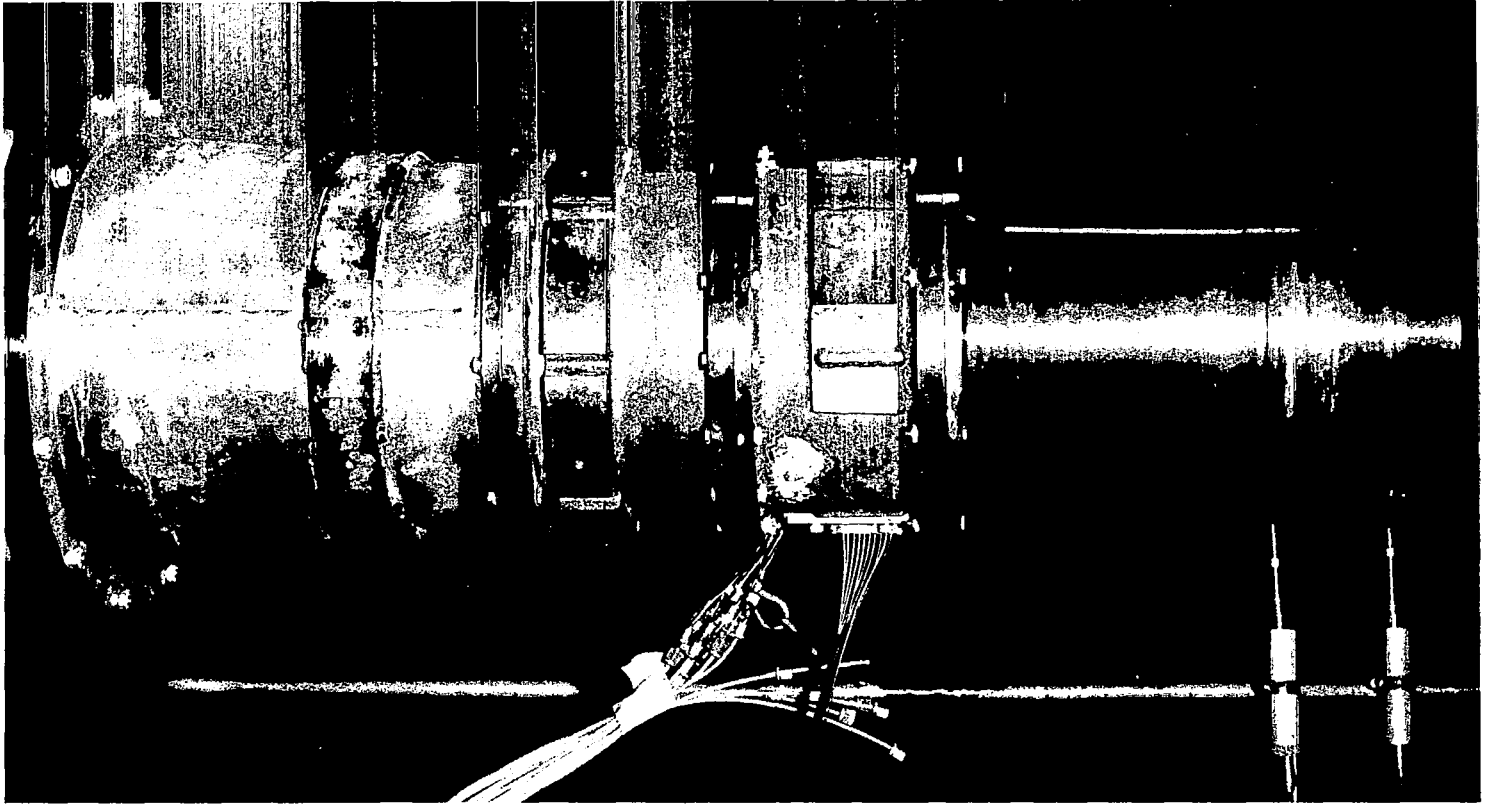
Figure 1.—15.24-cm RC Nozzle
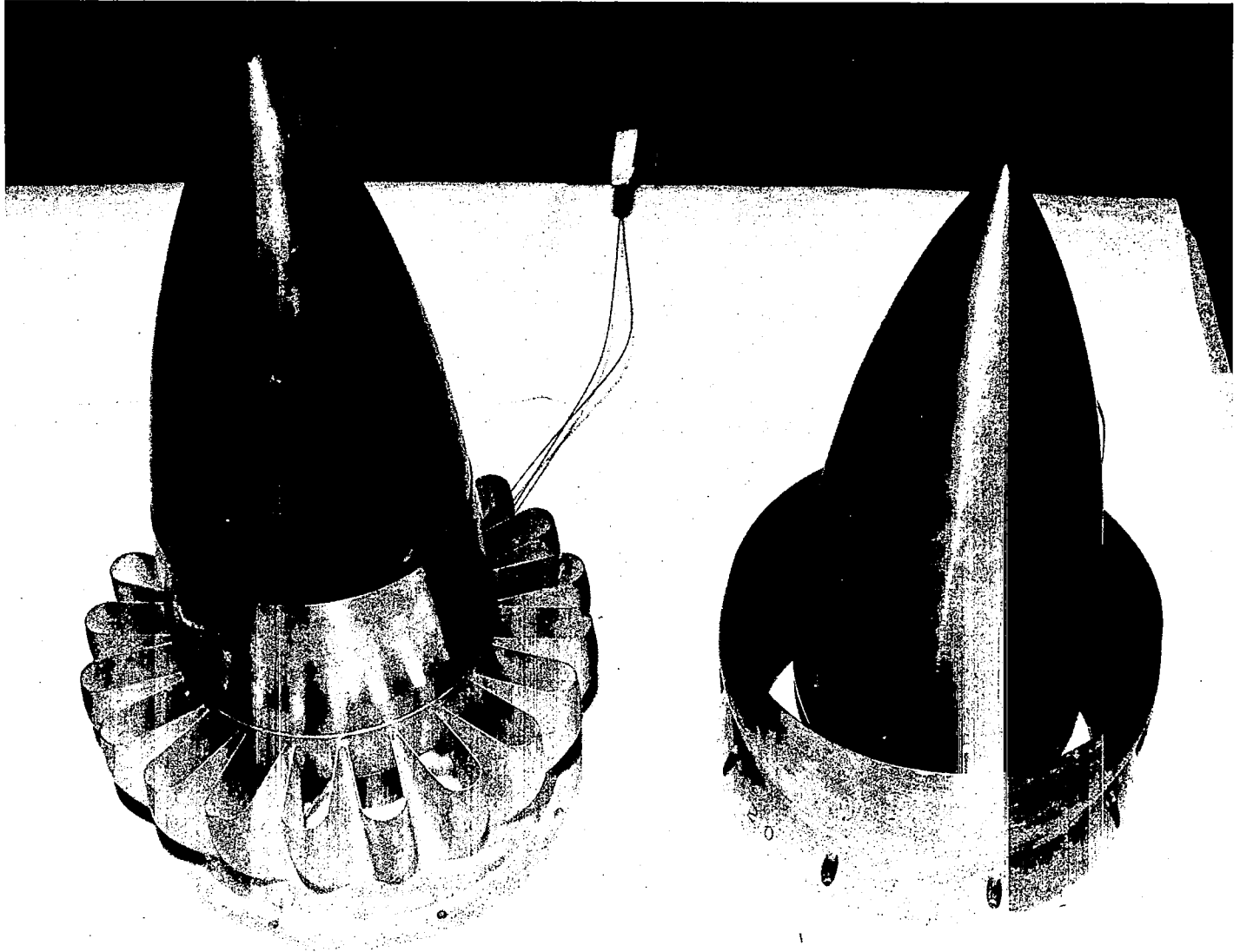
Figure 2.—20-Lobe and Annular Nozzles

Lined ejector

Upstream nozzle
aerodynamic fairing
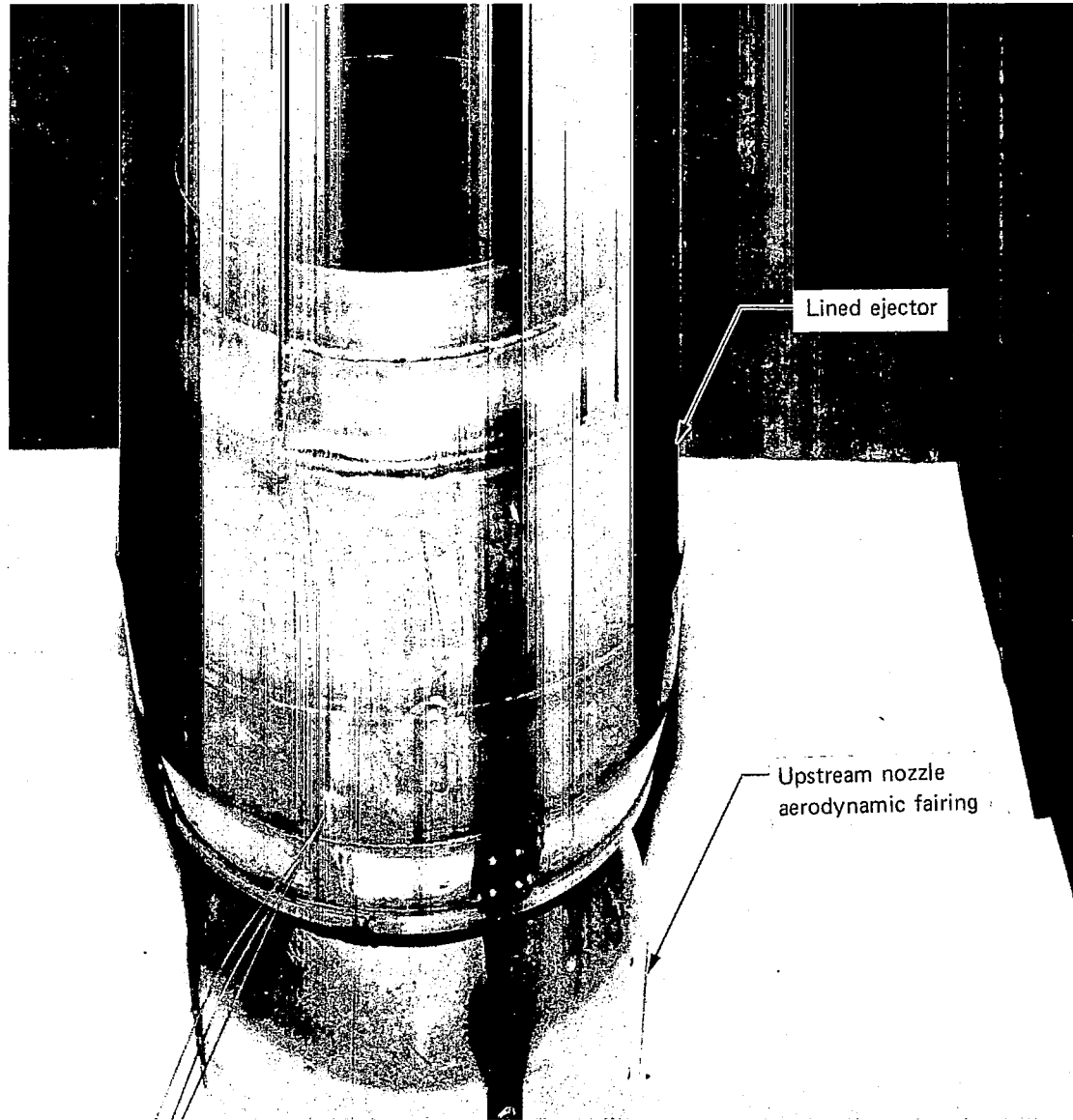
Figure 3.—Lined Ejector for 20-Lobe and Annular Nozzles
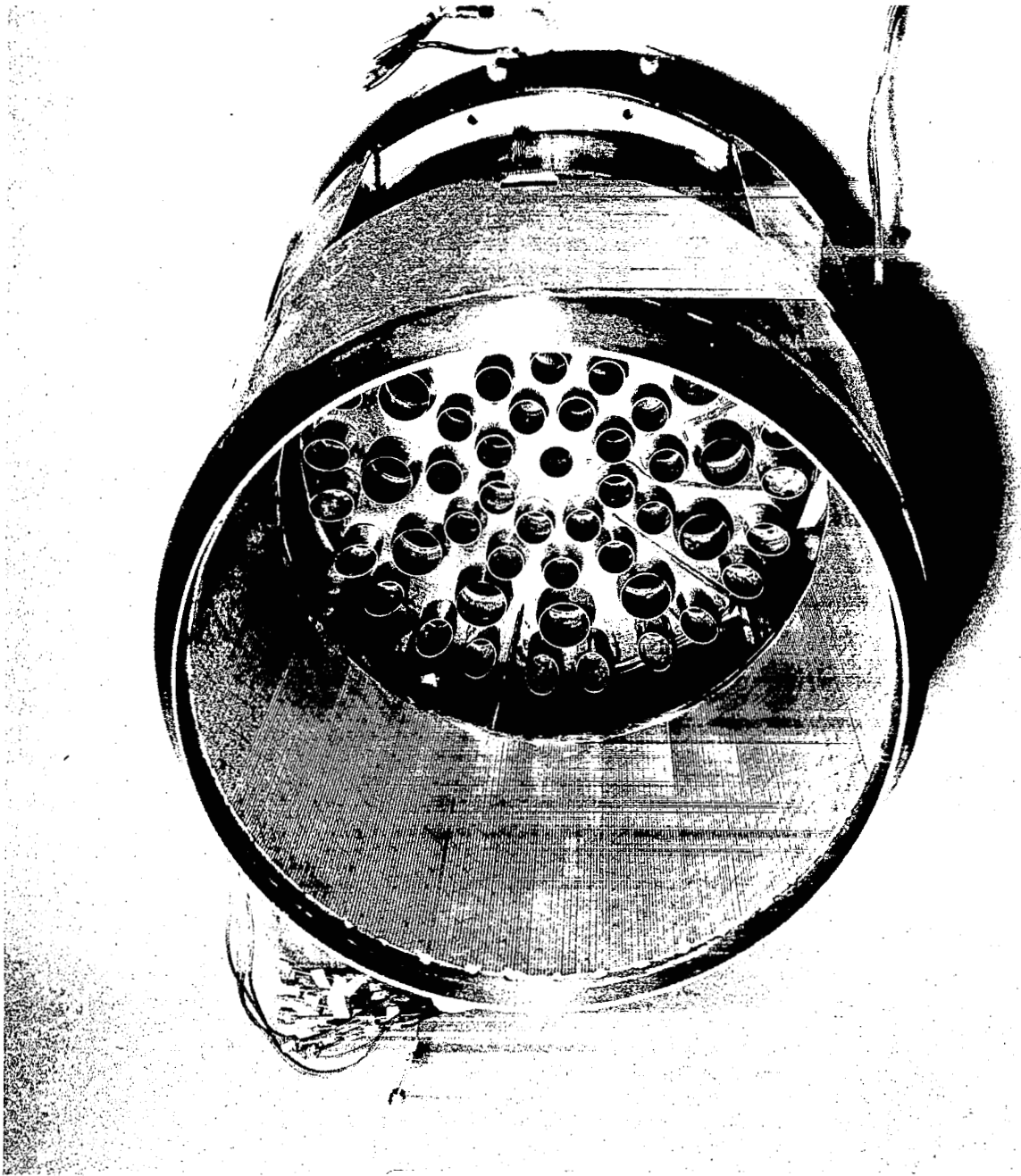
Figure 4.—Lined Ejector for 57-Tube Nozzle
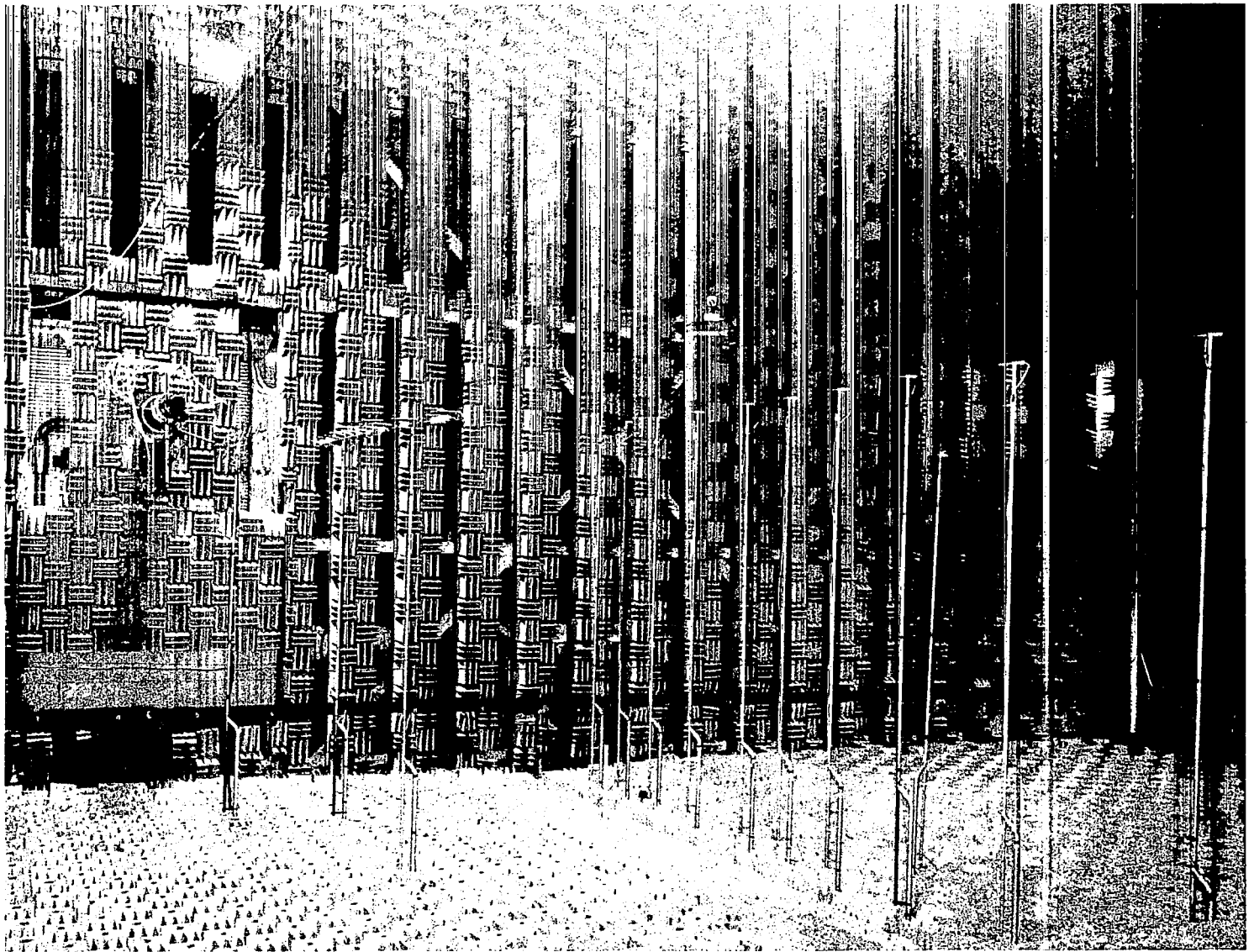
Figure 5.—Anechoic Chamber With 0.6, 1.5-, and 5.33-m Sideline Arrays
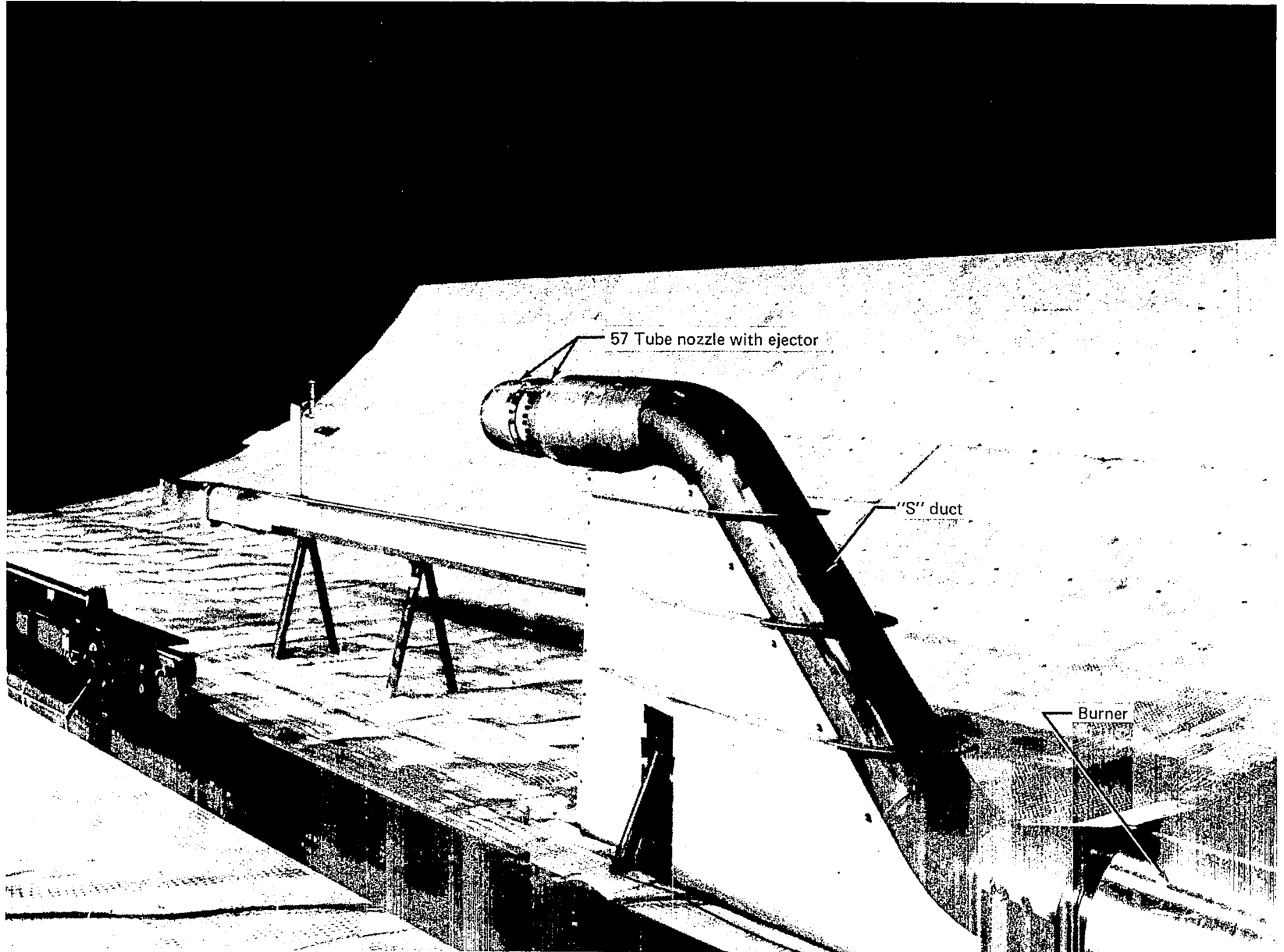
Figure 6.—Nozzle Nacelle, Hot Flow "S" Duct and Burner Installation
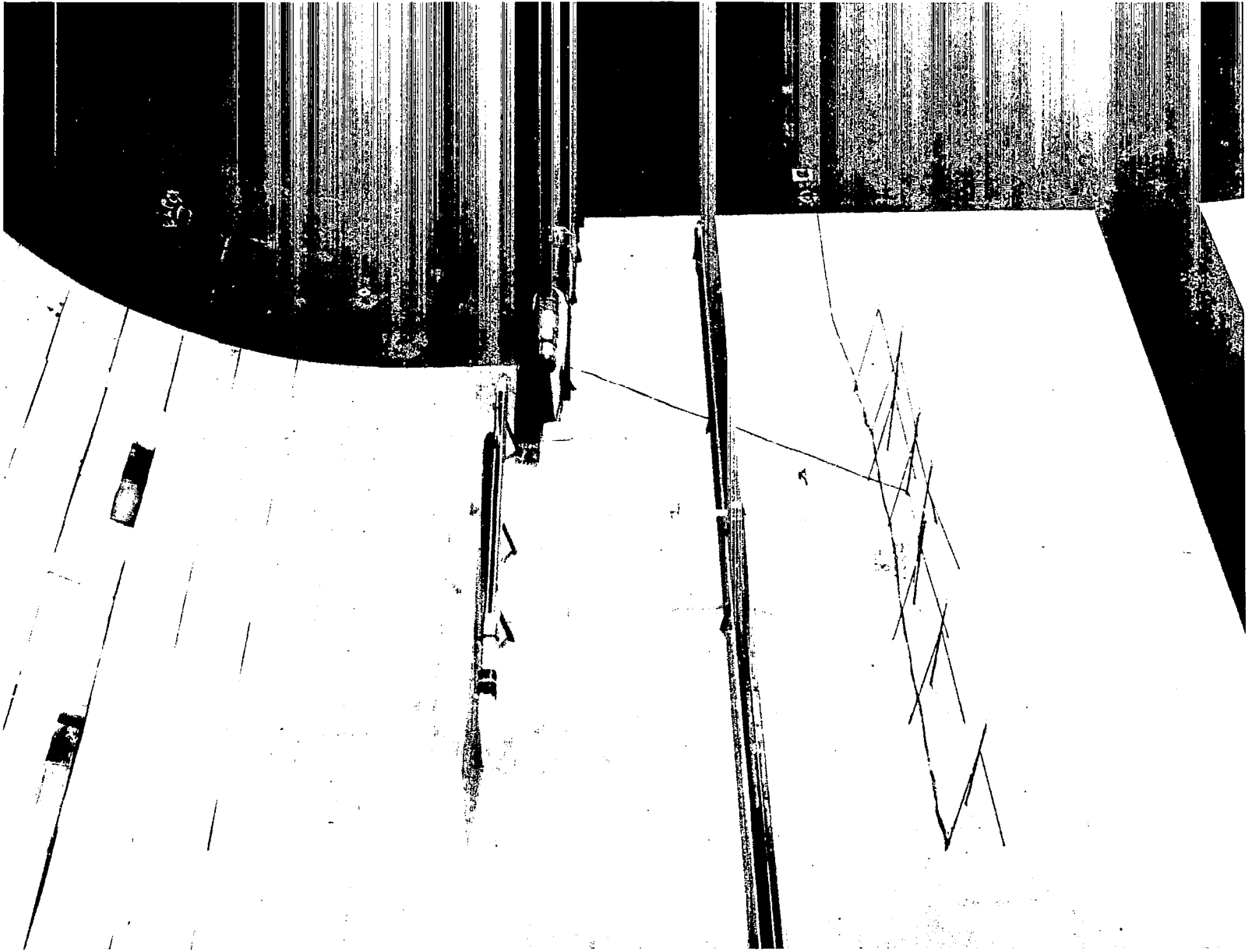
Figure 7.—Lining, Flow and Microphone Installations
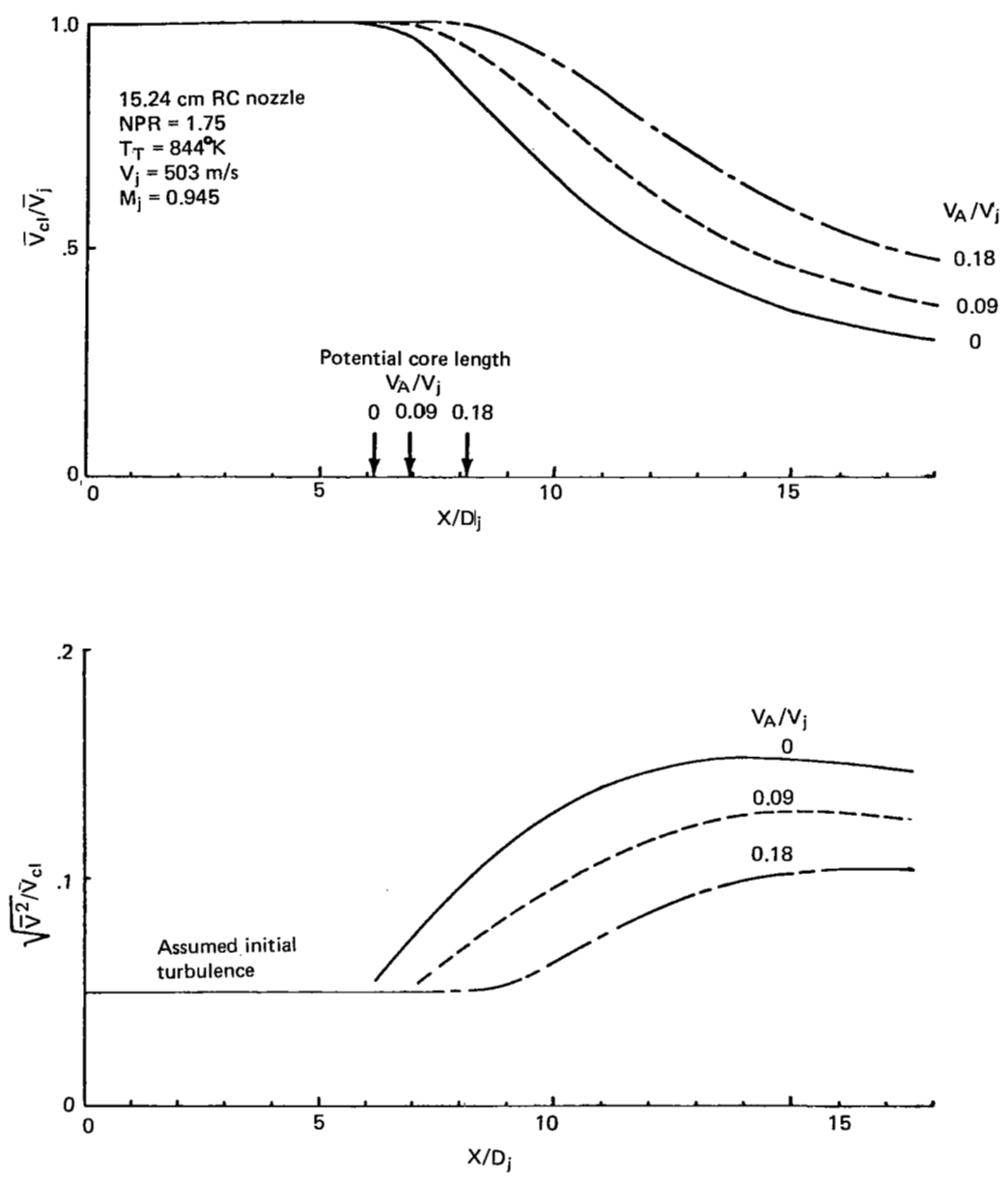
Figure 8.—Centerline Velocity and Turbulence Intensity Distribution
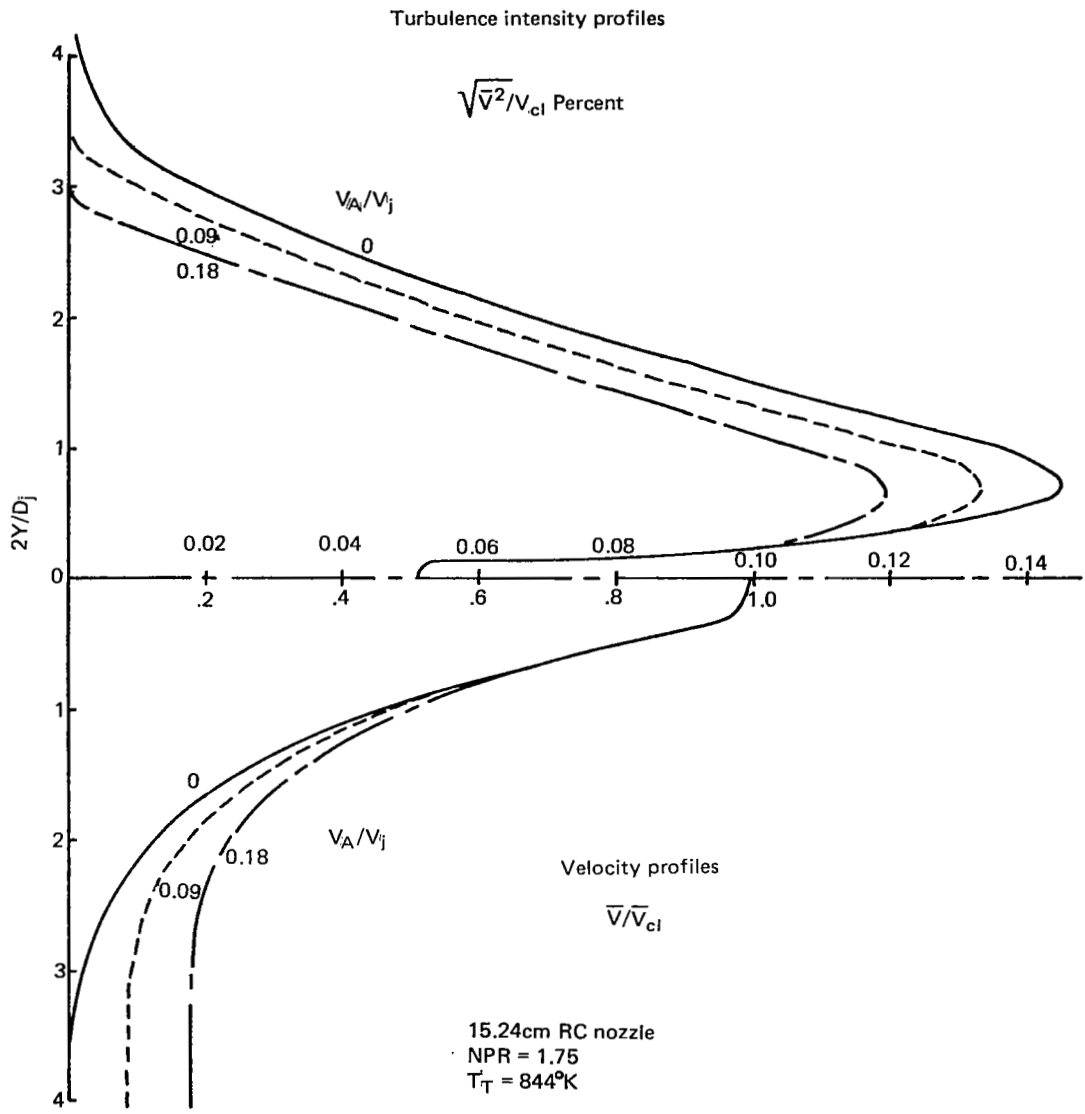
Figure 9.—Velocity and Turbulence Profiles at the Tip of the Potential Core

33
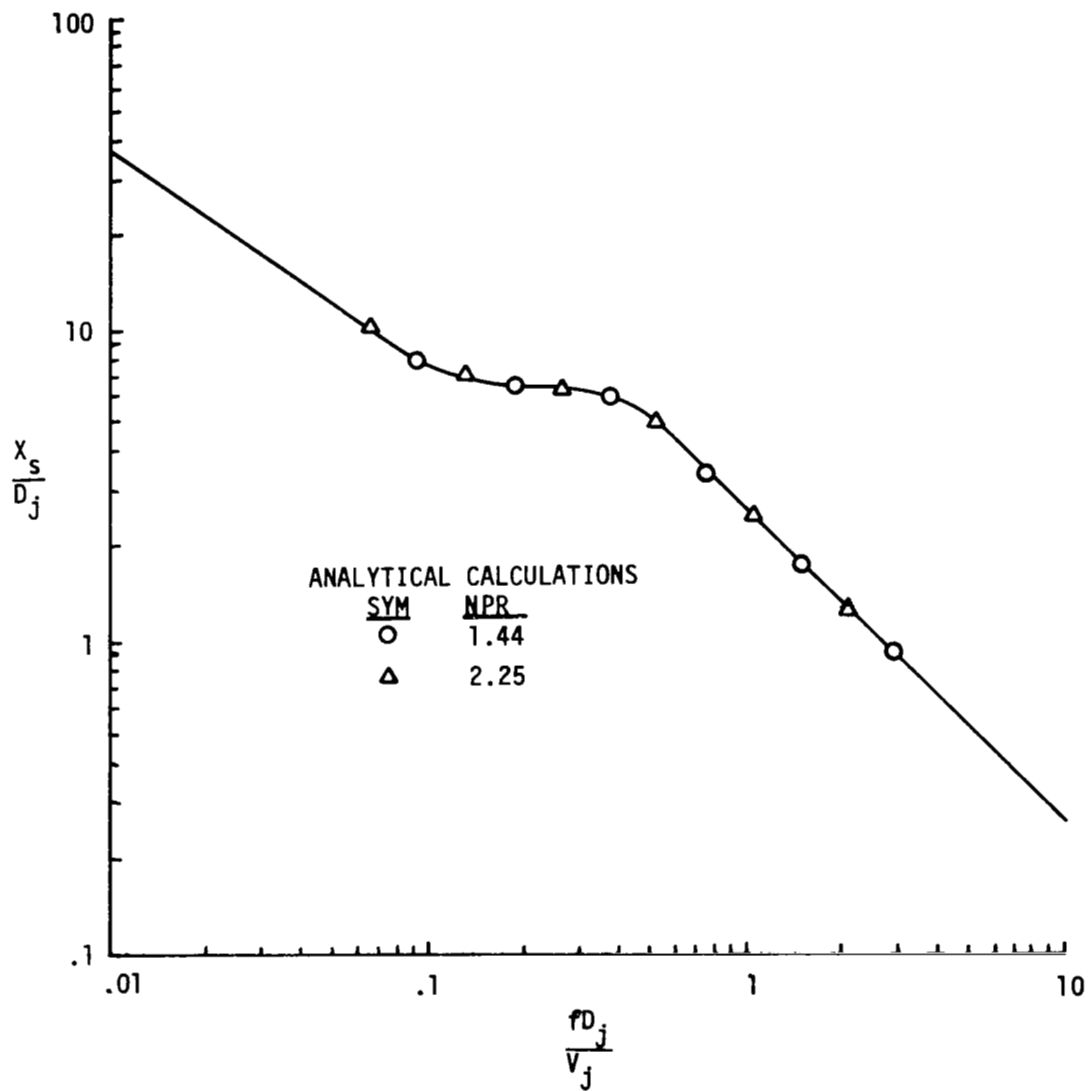
Figure 10.—Analytical Prediction of Noise Source Locations for a
15.24-cm Nozzle Using the Lu/Berman Flow/Noise Analysis
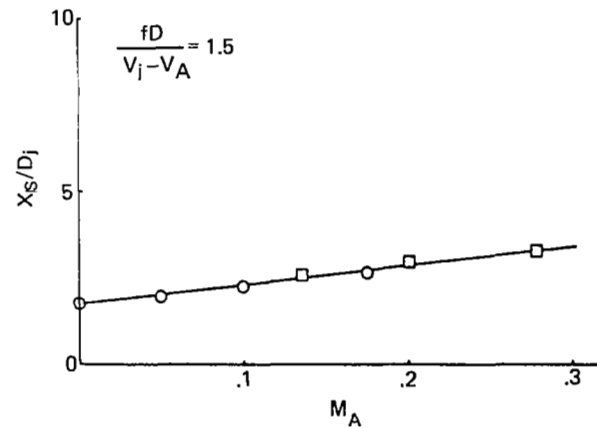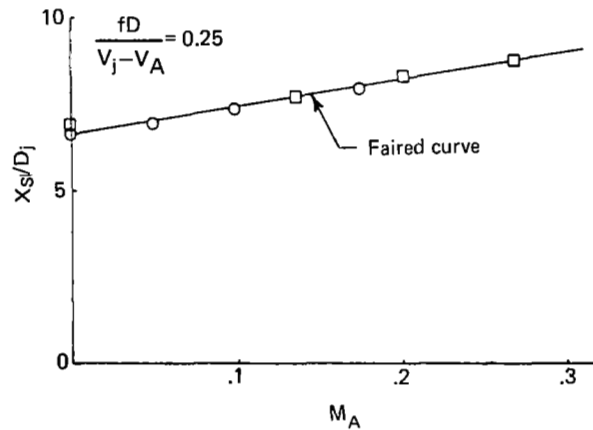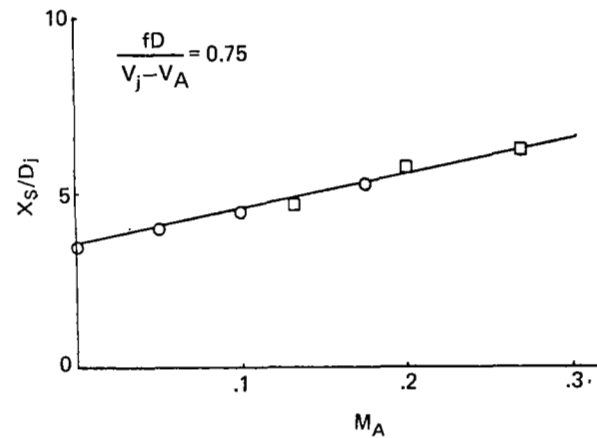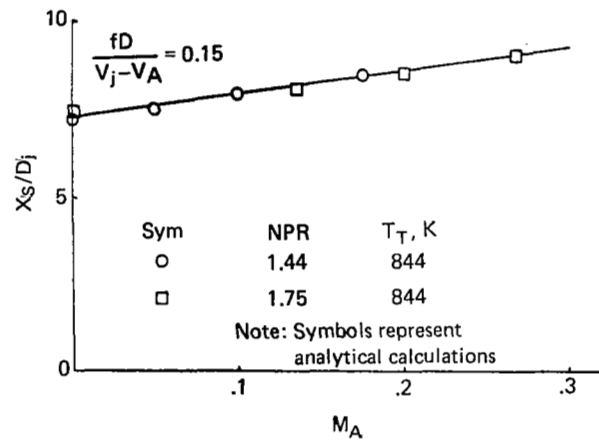
Figure 11.—Calculated Peak Noise Source Locations Using the Lu/Berman Flow/Noise
Analysis, 15.24cm RC Nozzle

$$TAN\ (\psi - 90°) = \frac{Sin\ (\theta_S - 90°) + M_A}{Cos\ (\theta_S - 90°)}$$

θ_S

Ψ

$R_{S,E}$

$M_A\ R_{S,E}$

Extrapolated
sideline location
SL_E

$M_A\ R_{S,M}$

$R_{S,M}$

Microphone

Measured sideline
location SL_M

Y_S

θ_I

Y

X

Max. shear line
centerline

Nozzle or
ejector exit

Wind-on noise source location $X_{S,2}$

Static noise source location $X_{S,1}$
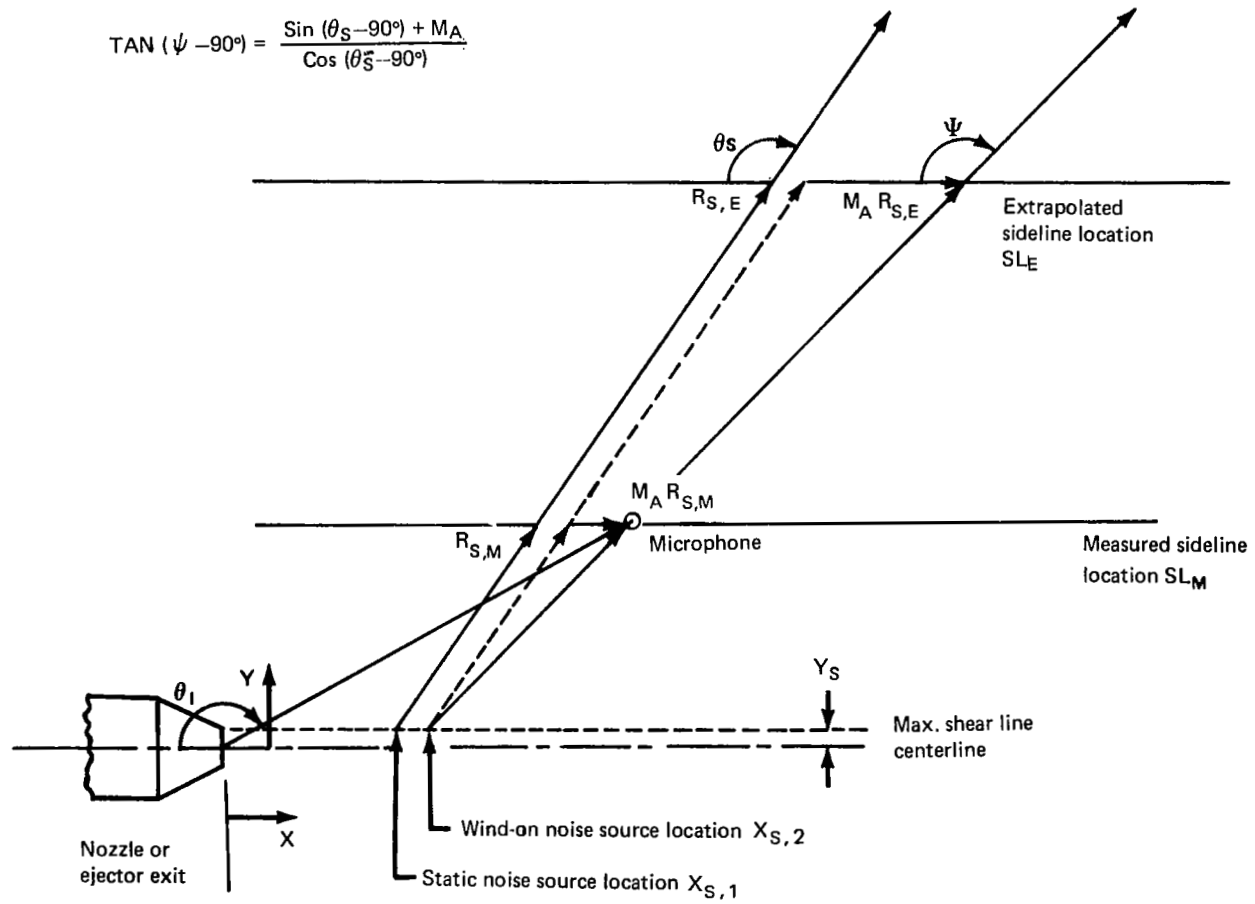
Figure 12.—Coordinate System and Nomenclature

- 15.24-cm RC nozzle
- NPR = 1.75
- T_T = 844 K
- Frequency = 250 Hz
- S = 0.075

Symbol Sideline distance, m

Symbol	distance
O	0.6
□	1.5
△	3.0
◇	5.3

Dotted lines indicate noise propagation paths. Arrows indicate propagation path locations on the 0.6m sideline.

One-third-octave-band SPL, dB re 2×10^{-5} N/m^2

Angle, re inlet axis and nozzle exit
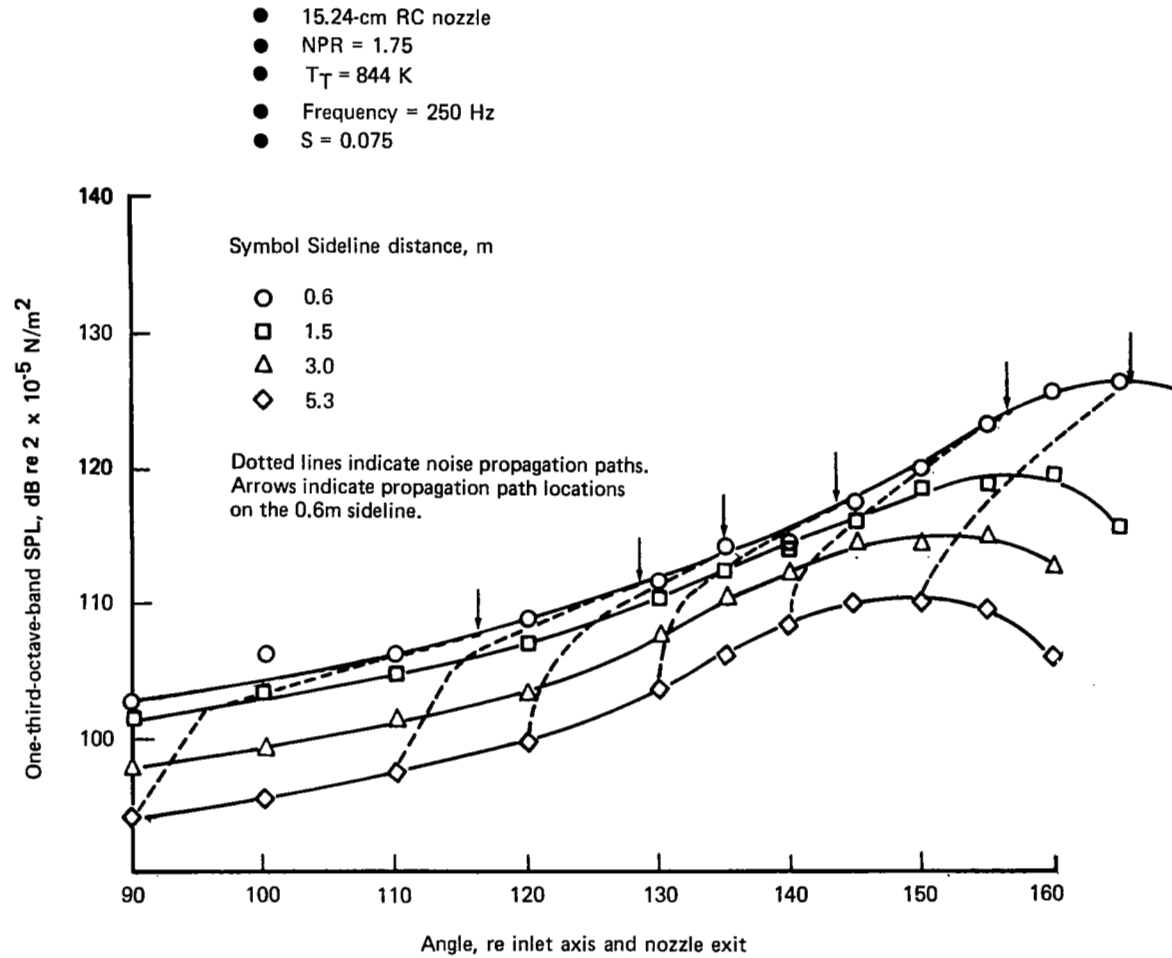
Figure 13.—Multiple Sideline Source Location Technique

- 15.24-cm RC nozzle
- NPR = 1.75
- T_T = 844 K
- Frequency = 250 Hz
- S = 0.075

Symbols refer to figure 13 where dashed lines cross each of the solid lines.

Noise radiation angles

Sideline location

86° 107° 117° 126° 135° 146°

Peak noise

5.33 m

3.0 m

1.5 m

0.6 m

Max shear line

0   5   10   15   20

X_S/D_j

Axial noise source locations
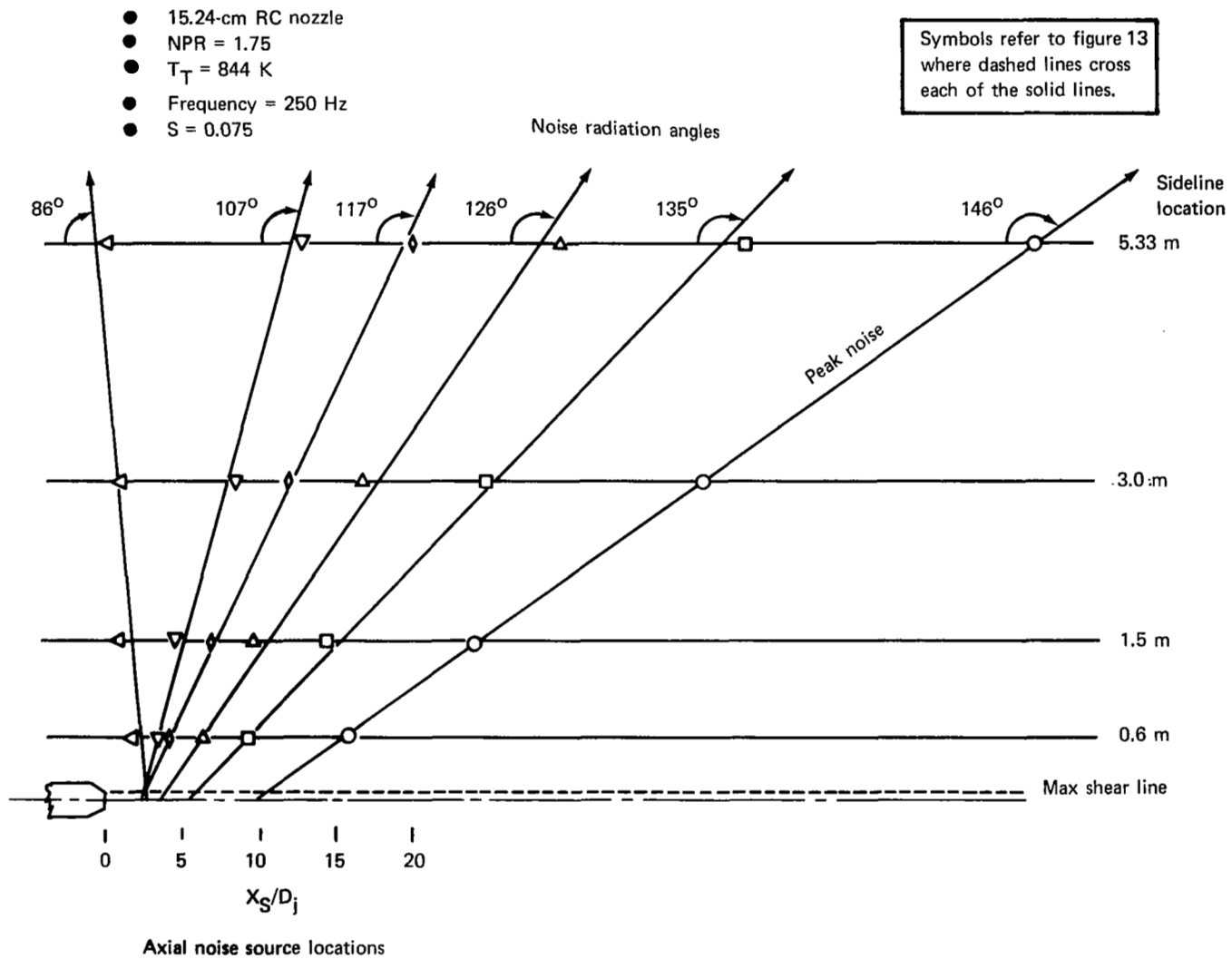
Figure 14.—Determination of Apparent Noise Source Locations and
Noise Radiation Angles
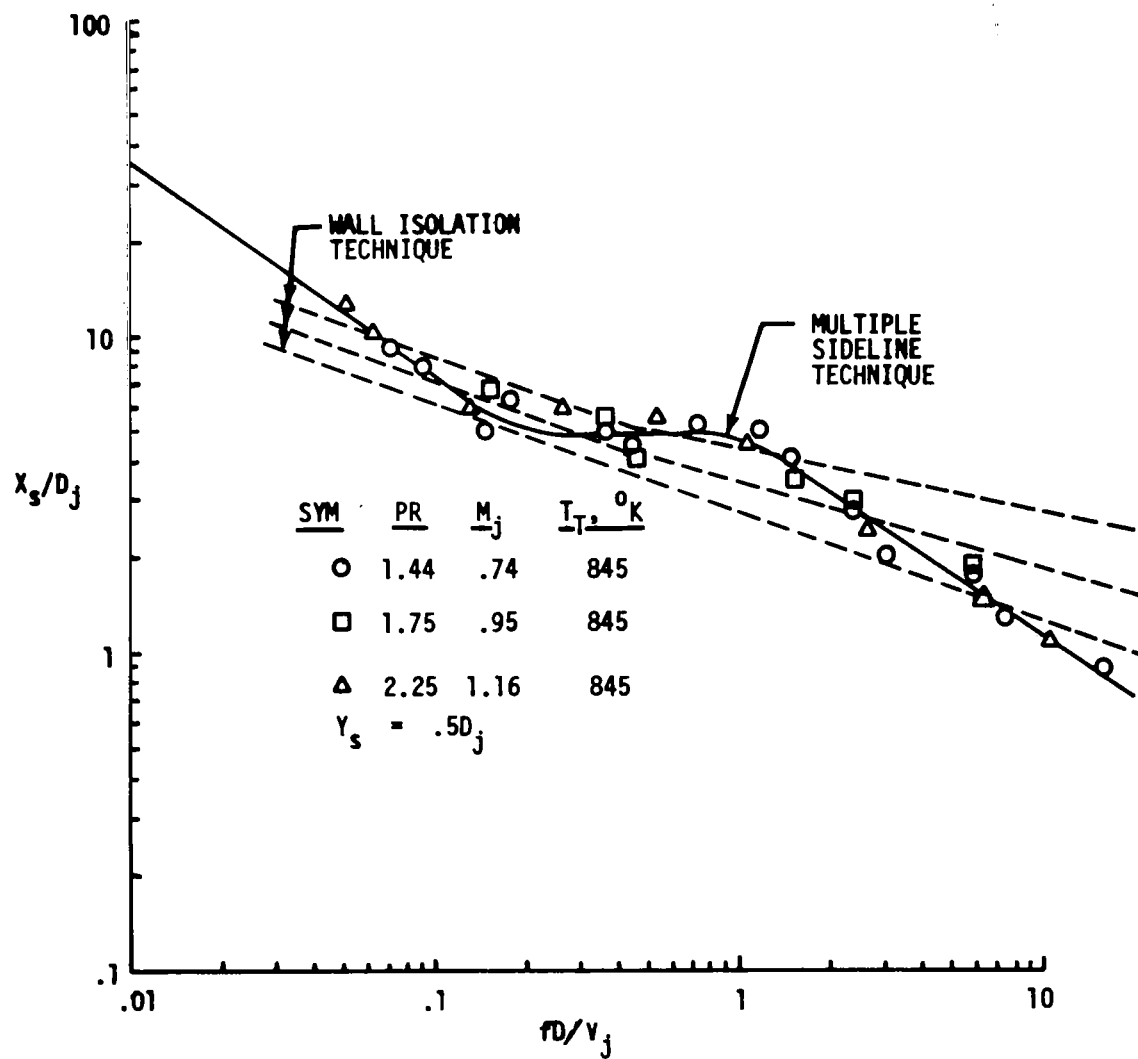
Figure 15.—Comparison of Peak Axial Noise Source Location for a 15.24-cm RC Nozzle
Using the Wall Isolation and Multiple Sideline Techniques
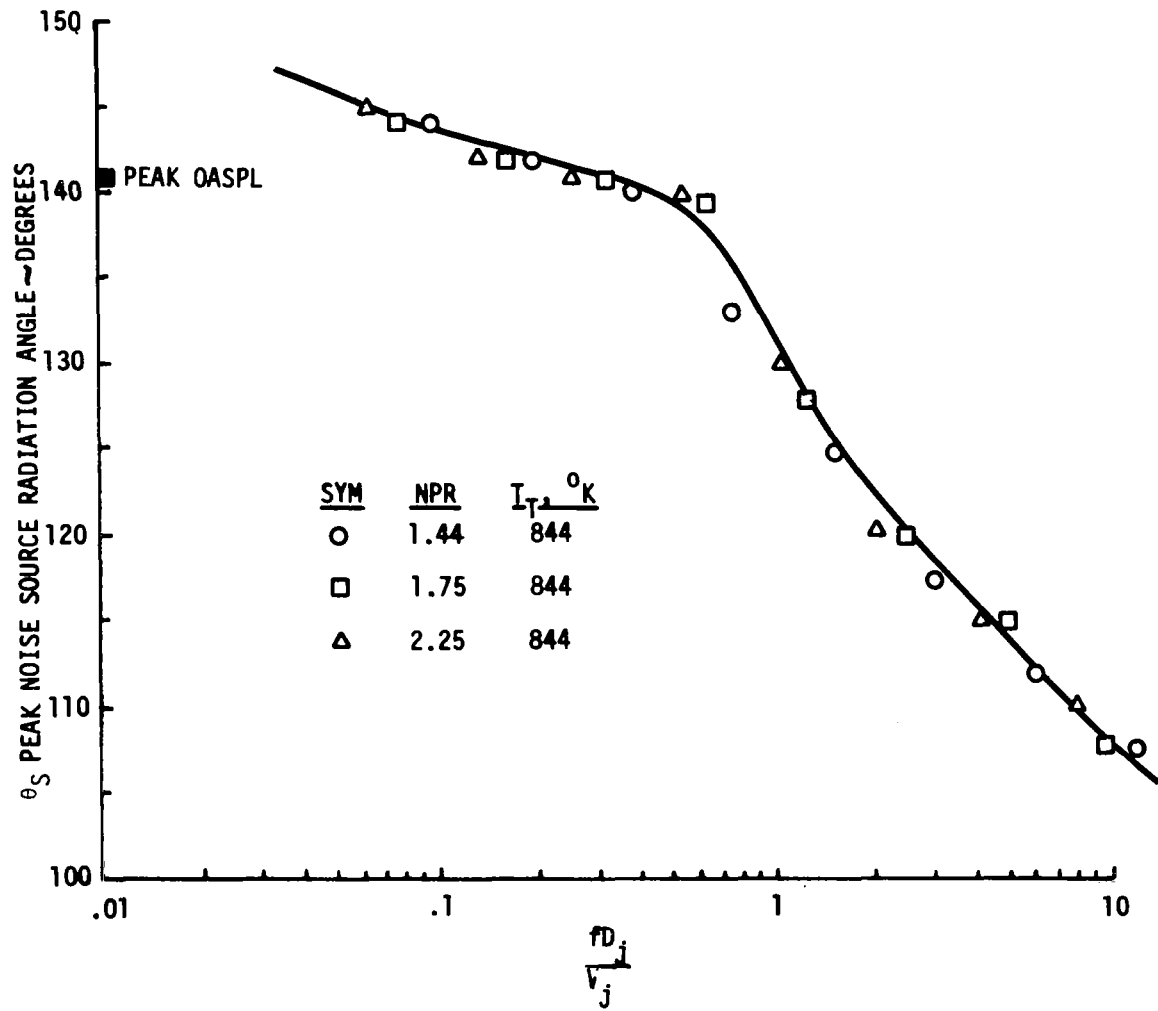
Figure 16.—Correlation of Peak Noise Source Radiation Angle for a 15.24-cm Nozzle
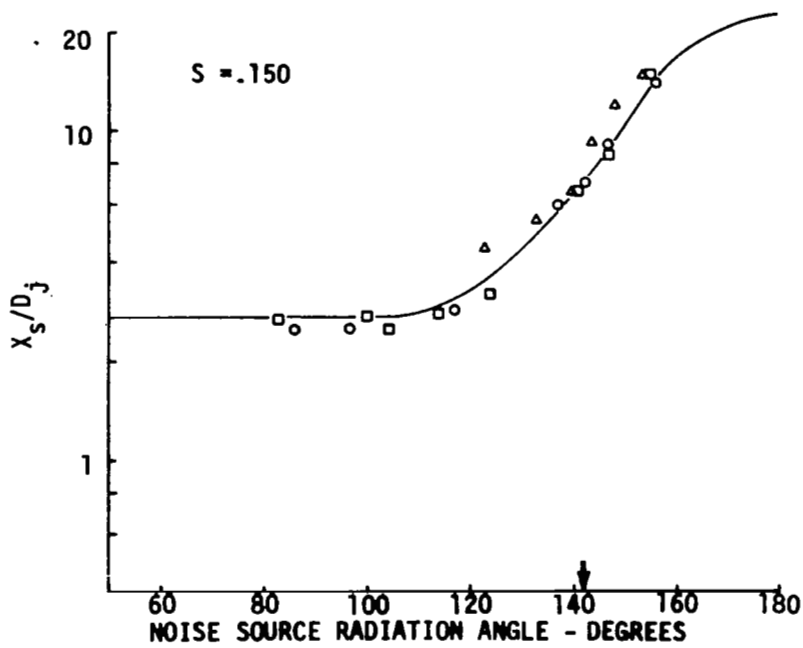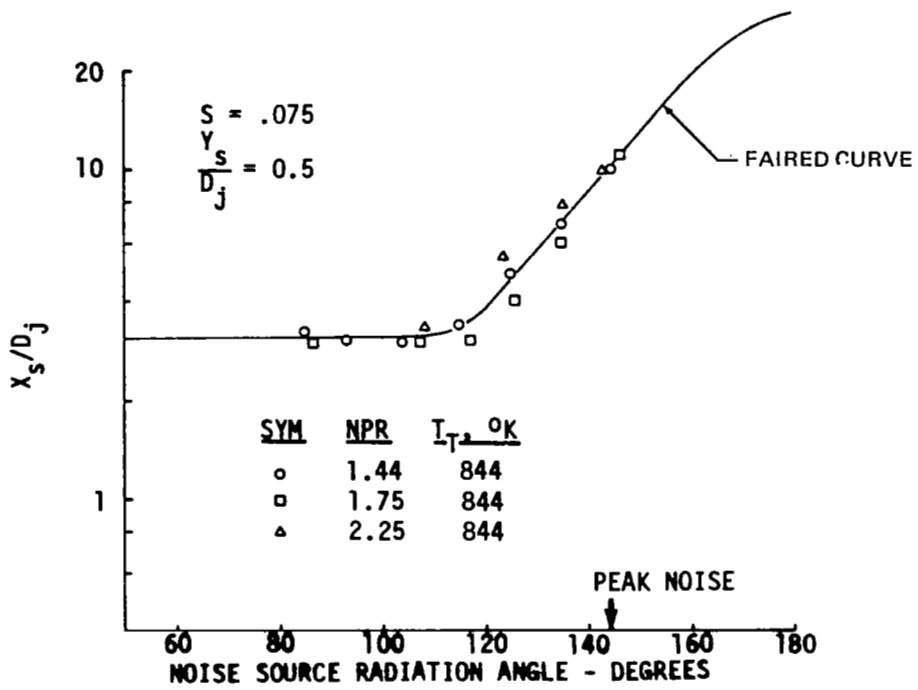
Figure 17.—Distributed Noise Source Locations for a Jet From a 15.24-cm RC Nozzle
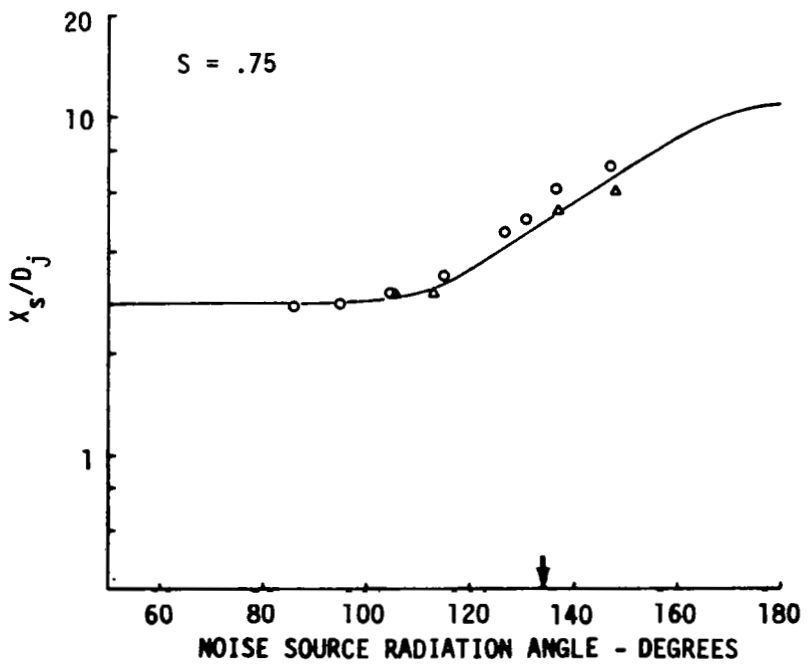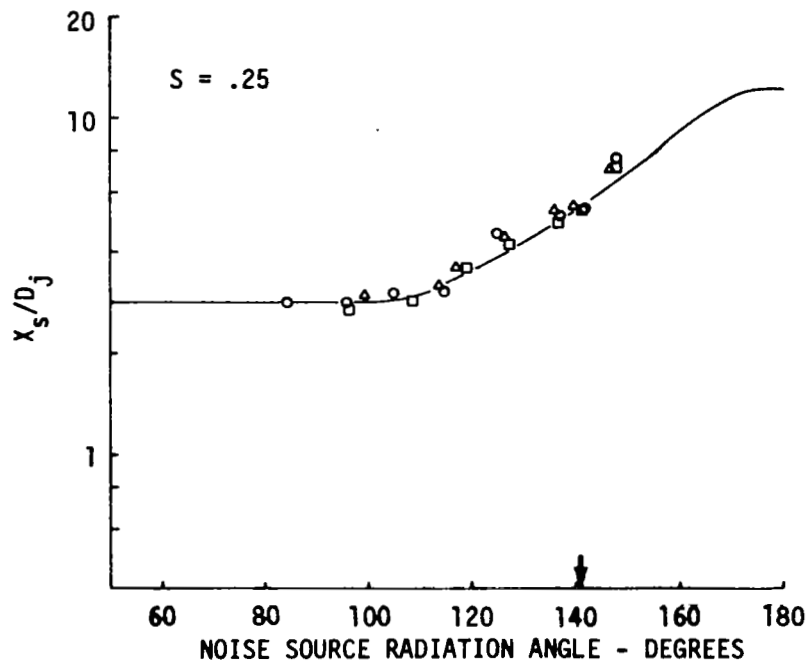
Figure 17.—(Continued)
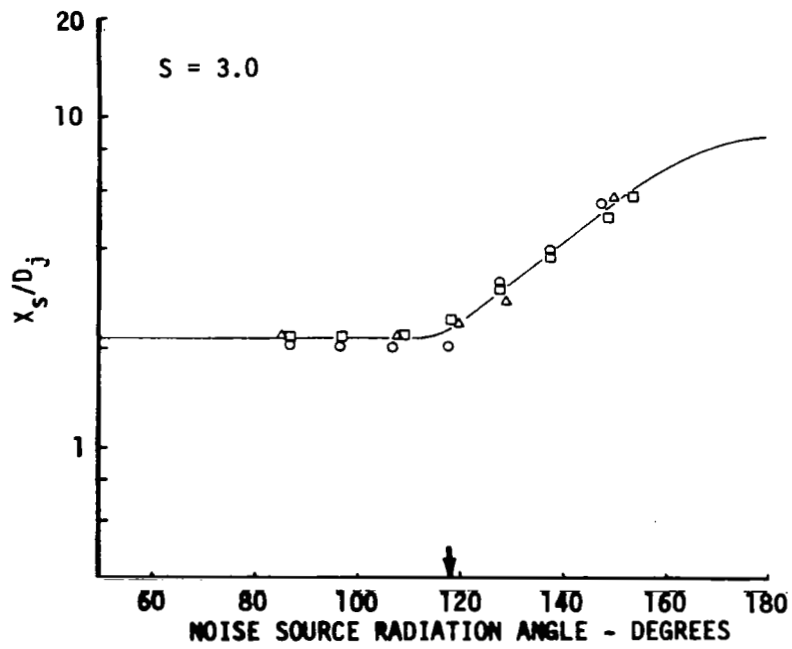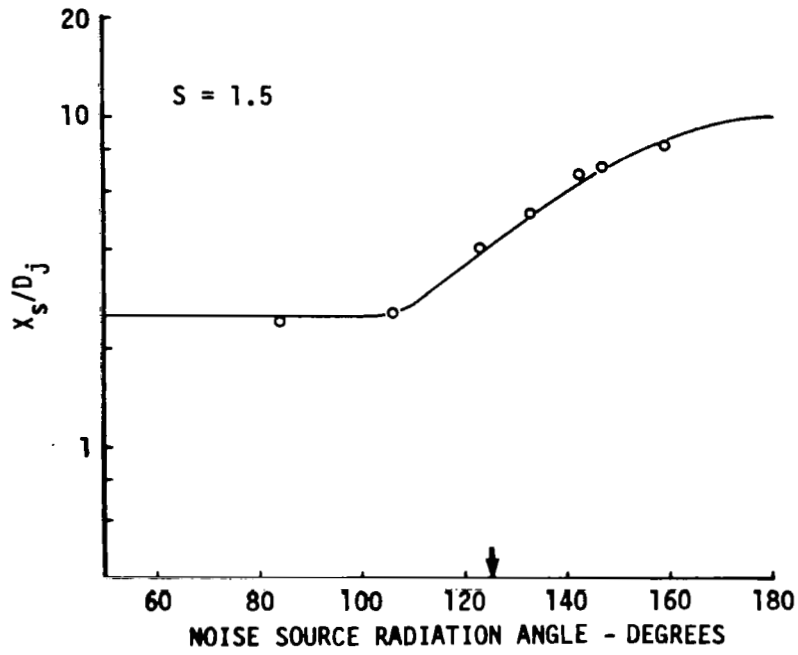
Figure 17.—(Continued)
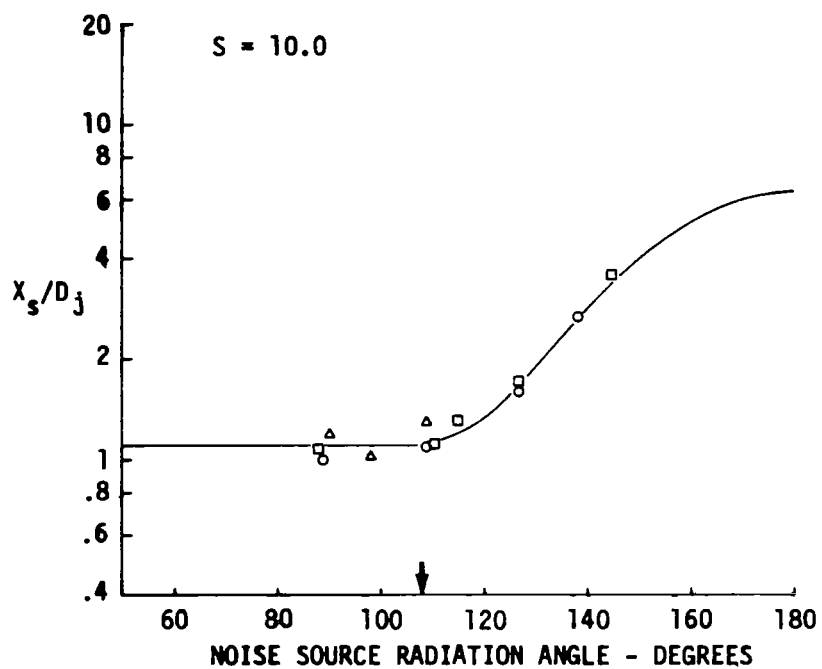
Figure 17.—(Continued)
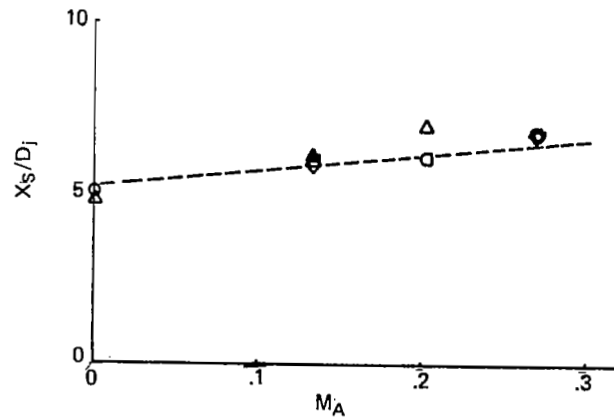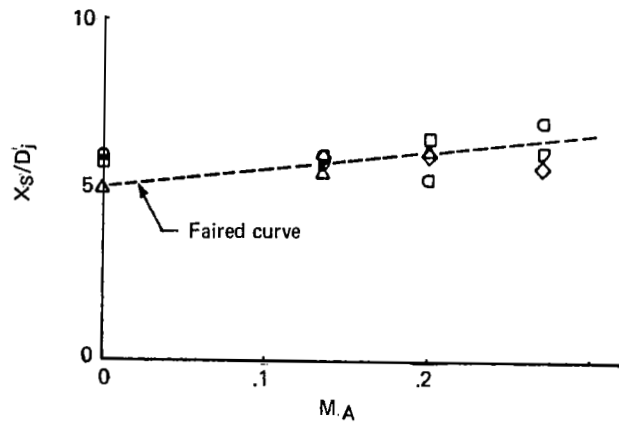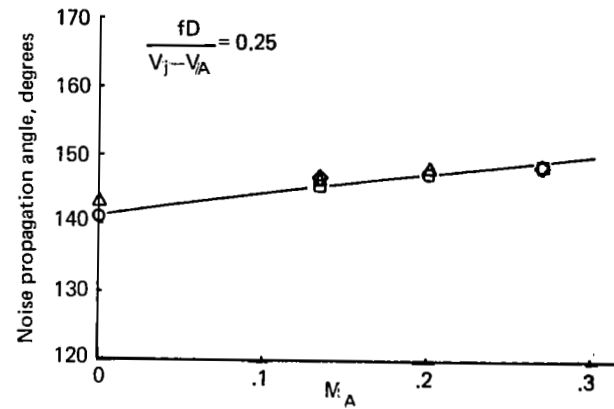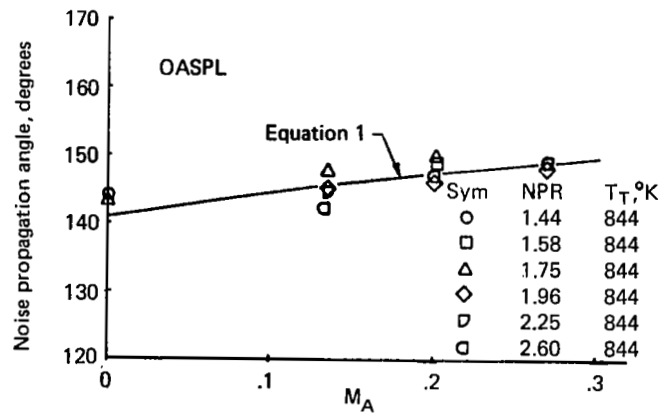
Figure 18.—Effect of Ambient Velocity on Peak Noise Source Locations and Noise Propagation Angles for the 15.24-cm RC Nozzle
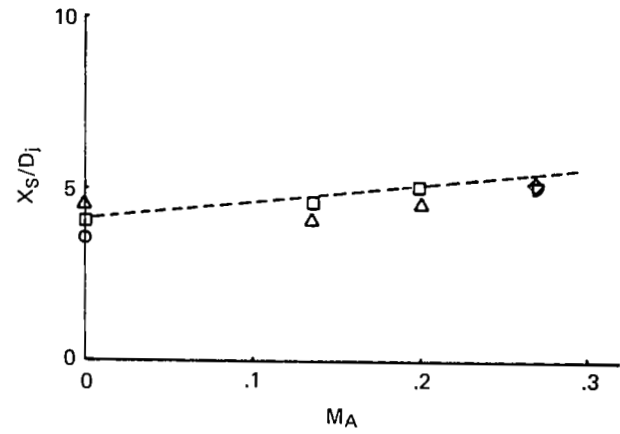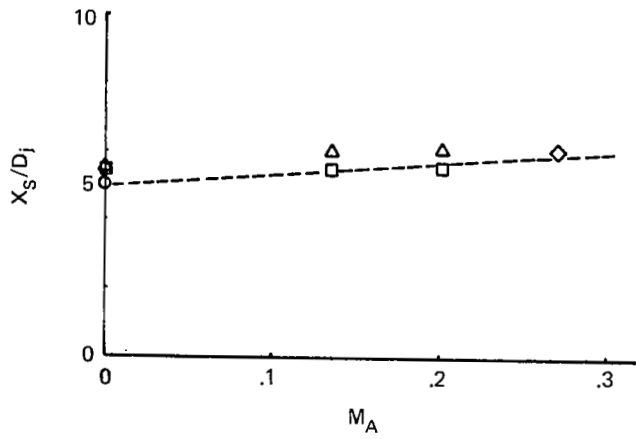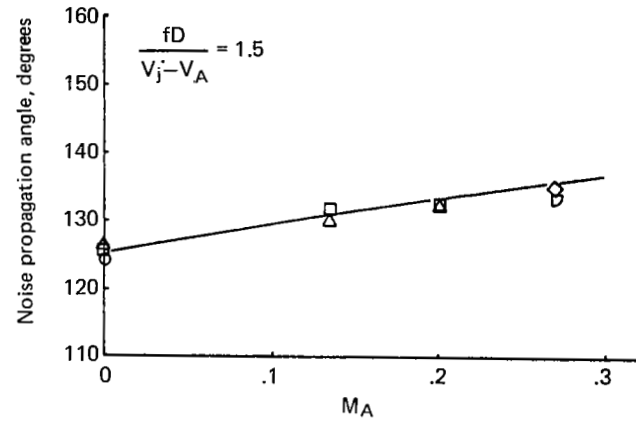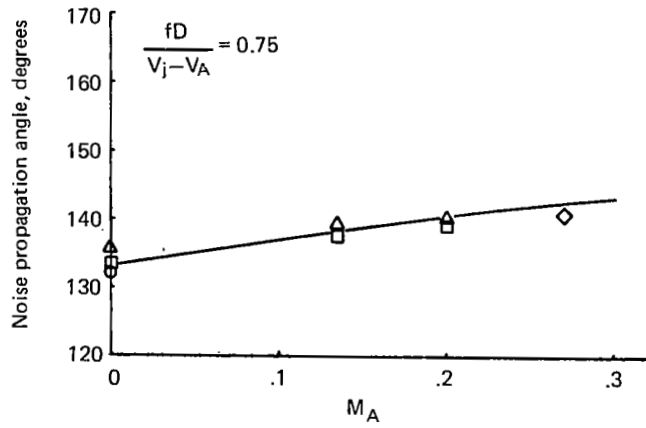
Figure 18.—(Continued)
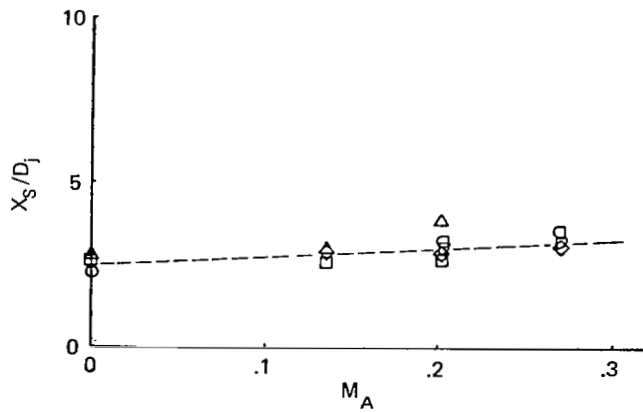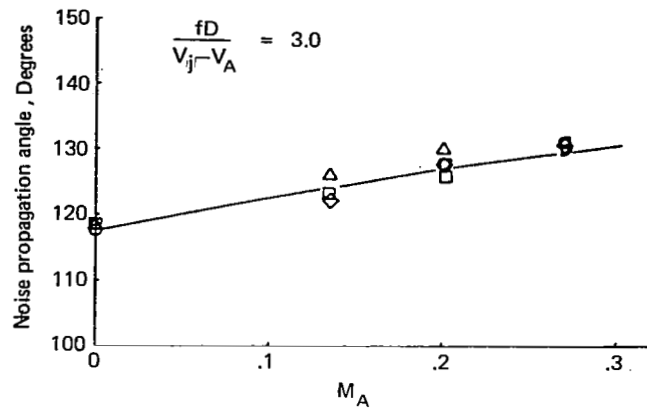
Figure 18.—(Continued)
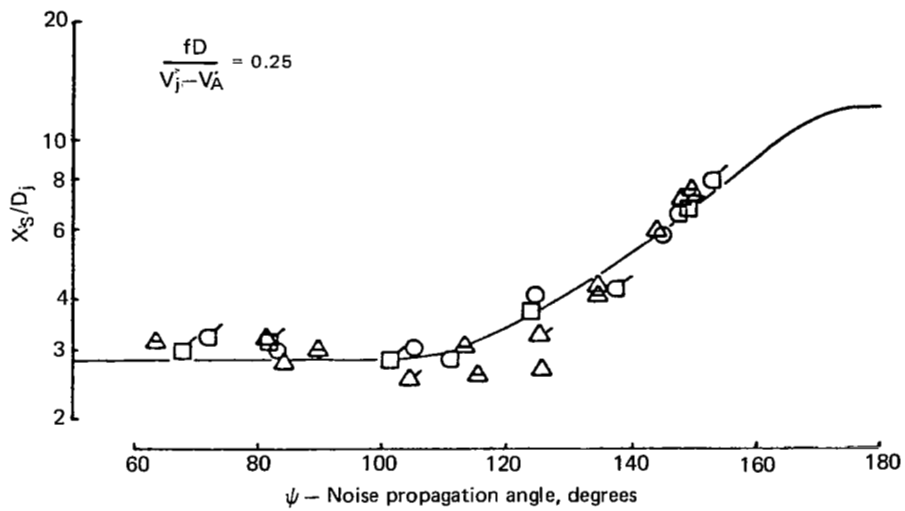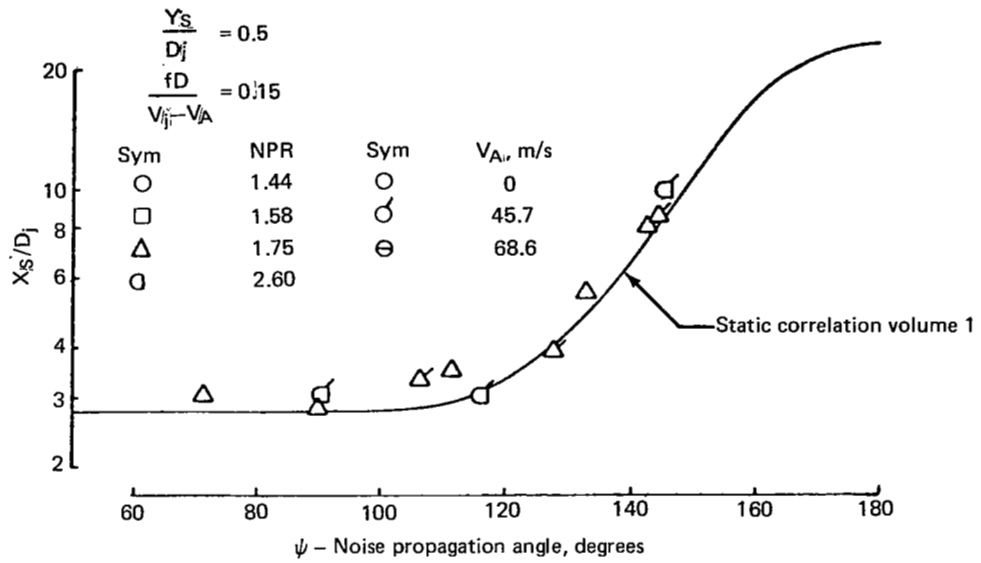
Figure 19.—Effect of Ambient Velocity on the Distributed Noise Source Locations for a 15.24-cm RC Nozzle

48
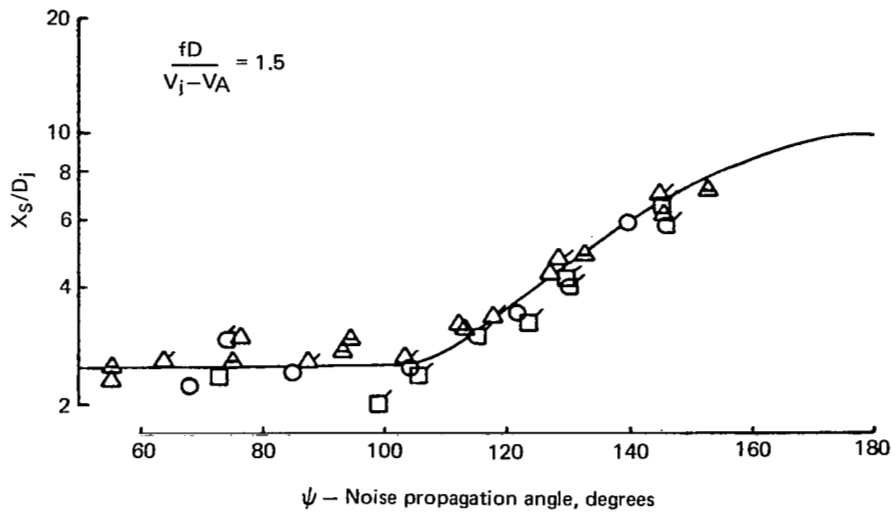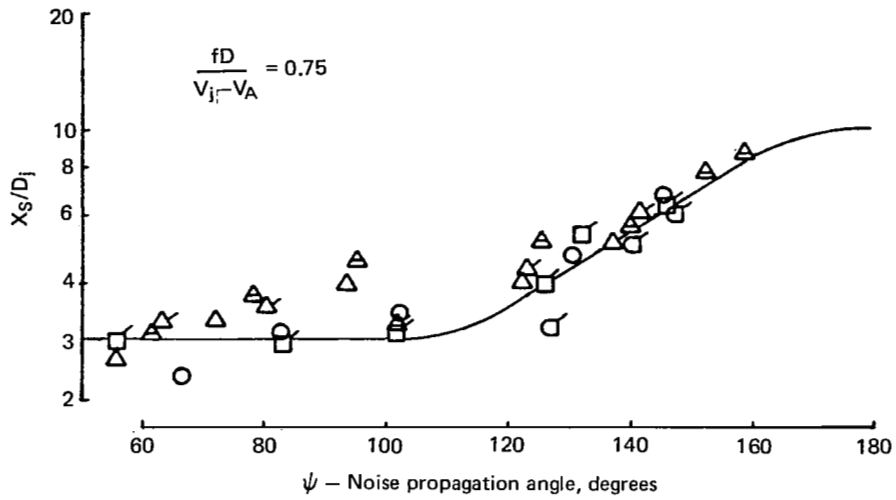
Figure 19.—(Continued)
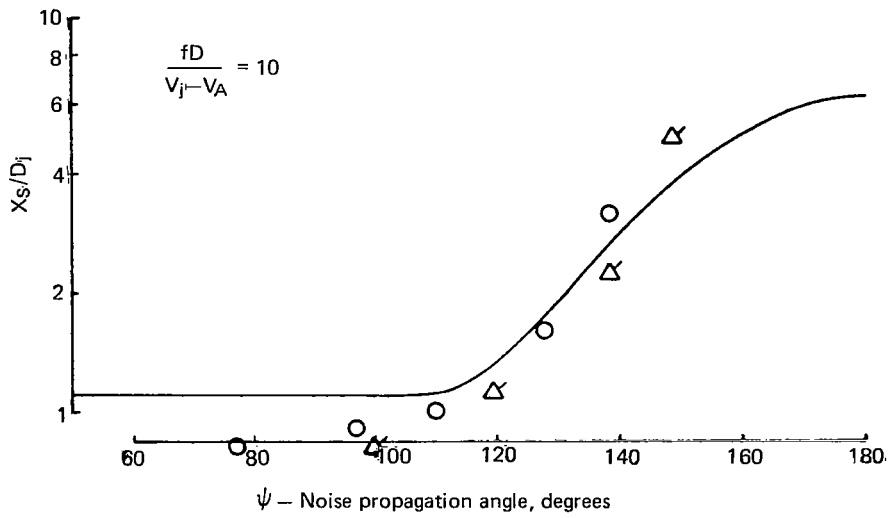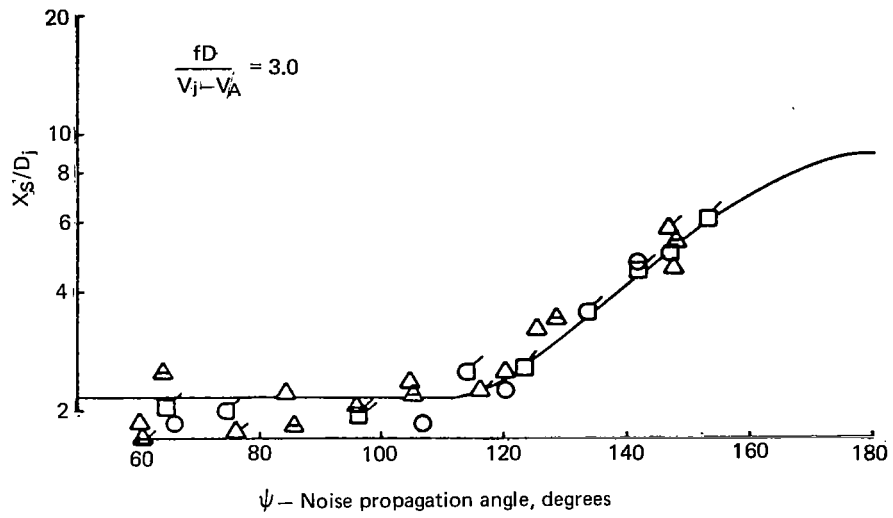
Figure 19.—(Continued)
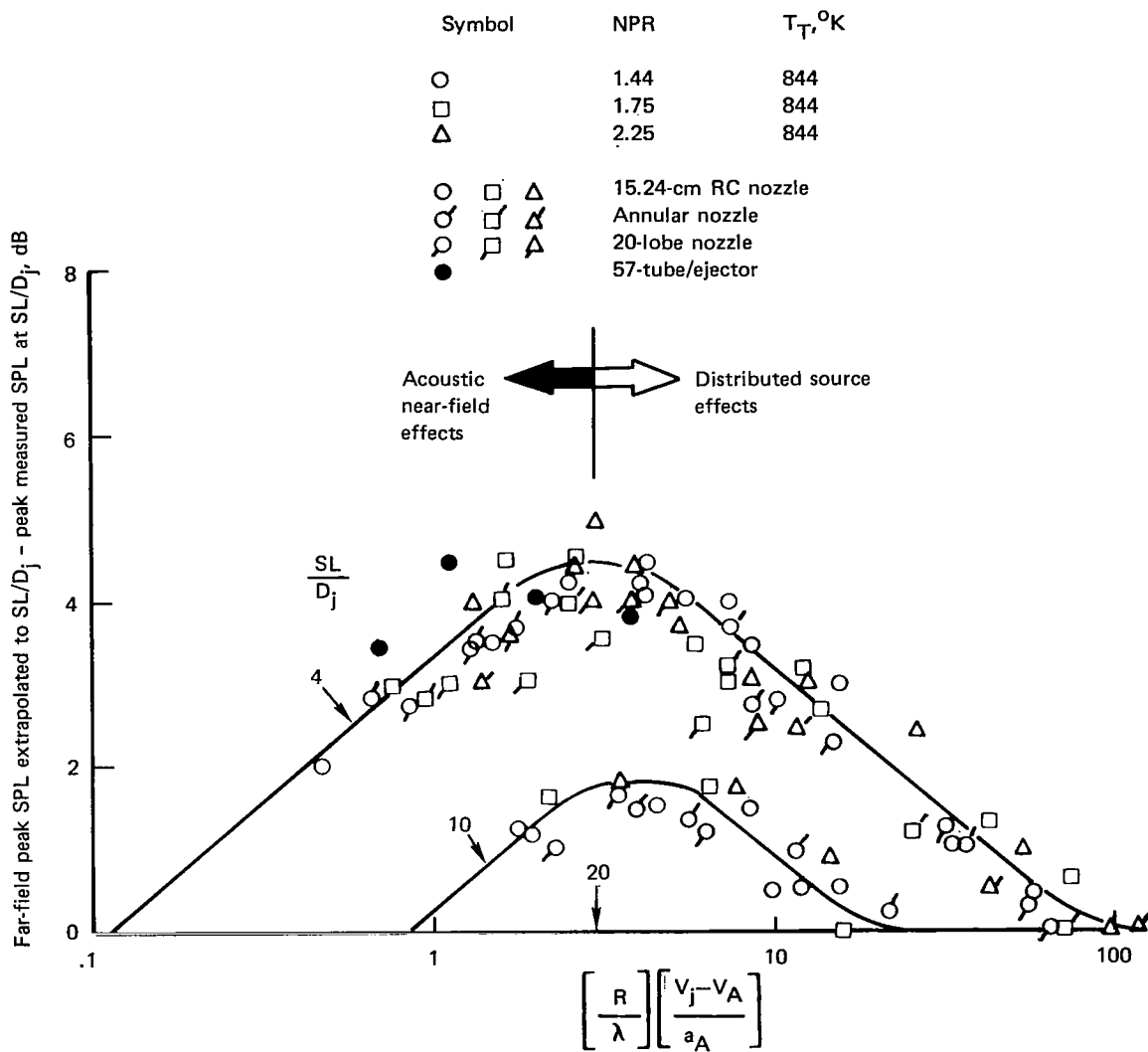
Figure 20.—Deviation of Jet Noise Measurements From the Spherical Divergence/Point Source Assumption
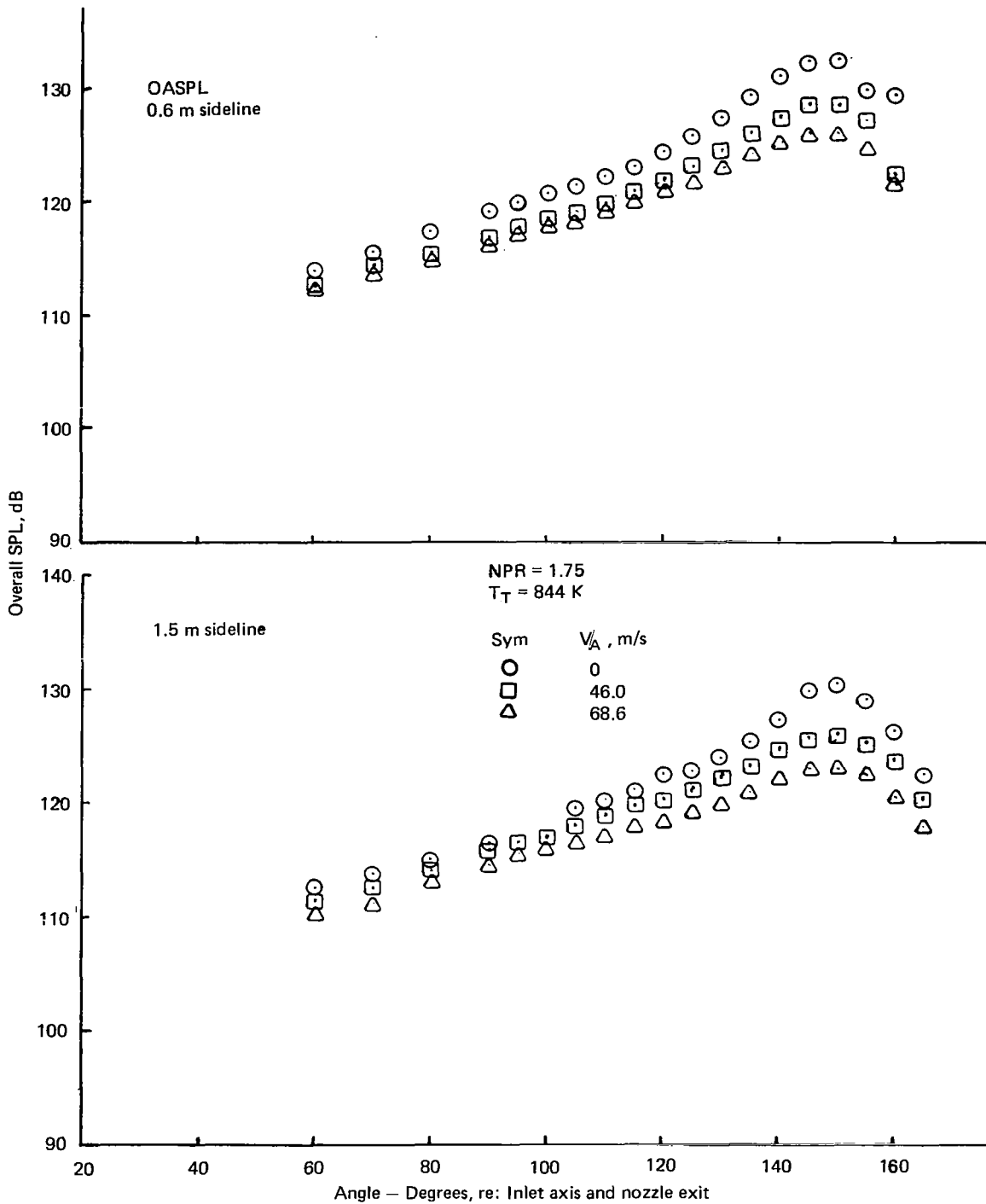
Figure 21.—Comparison of Flight Effects Measured for a 15.24 cm RC Nozzle on a 0.6, 1.5 and 3 m Sidelines Extrapolated to a 3.0 m Sideline.
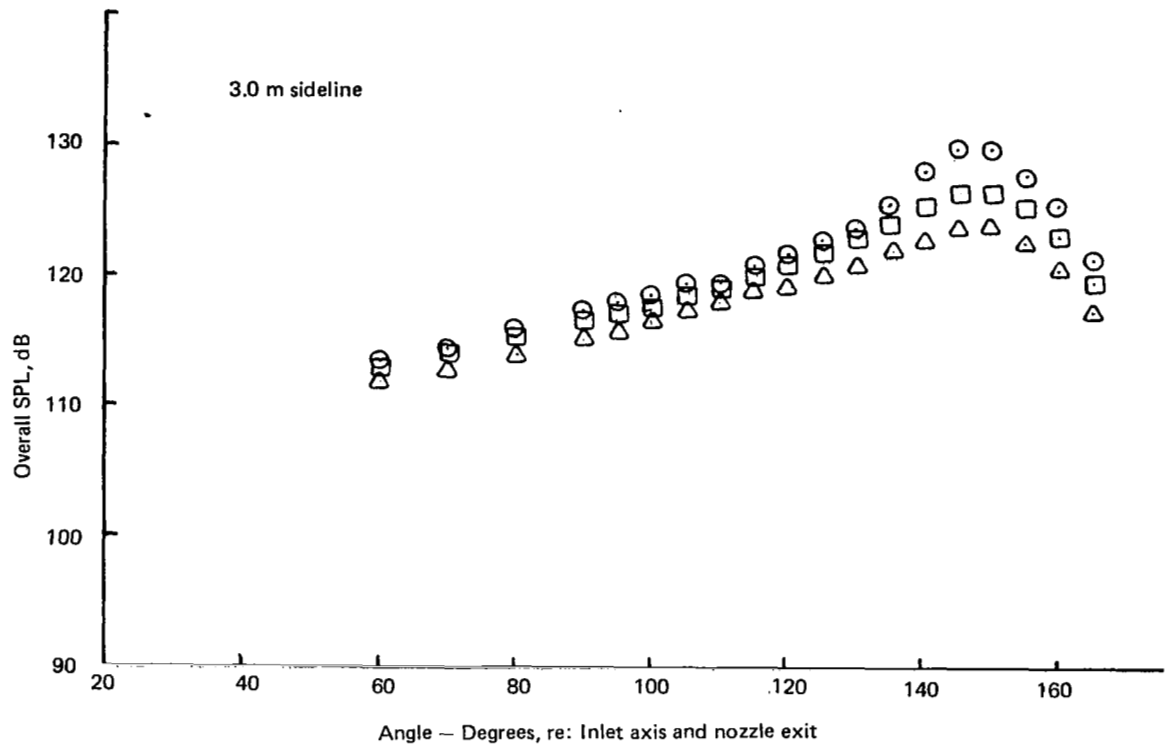
Figure 21.—(Continued)
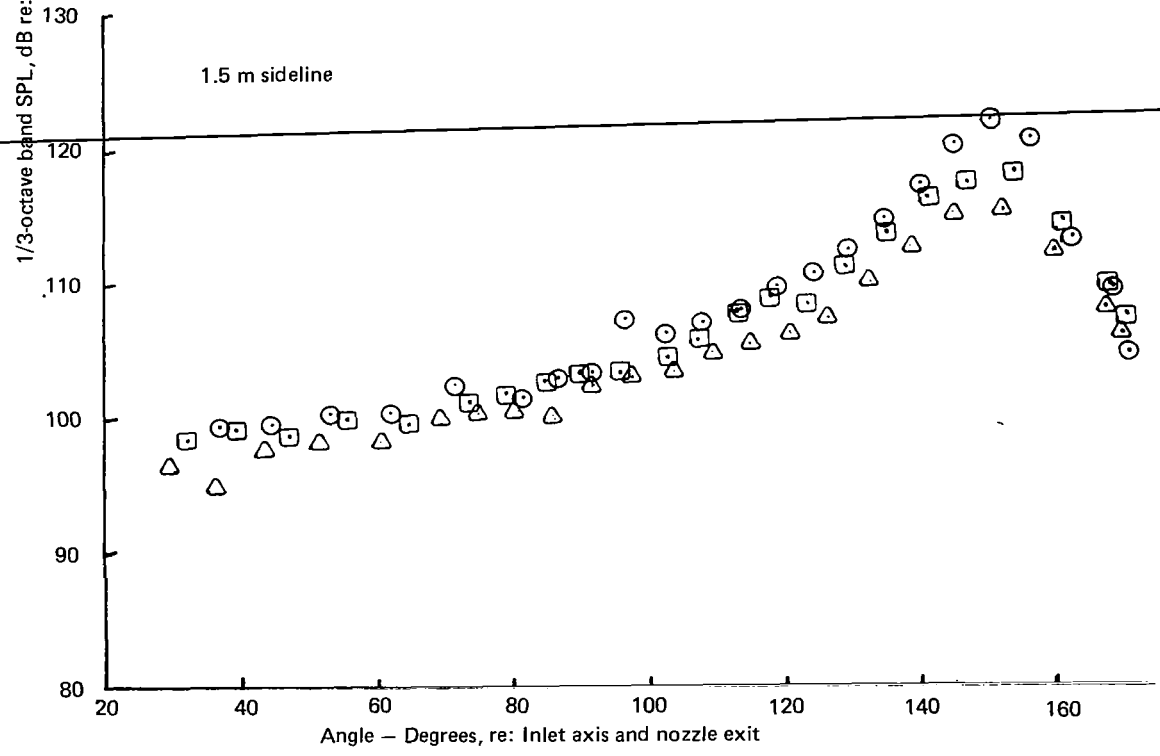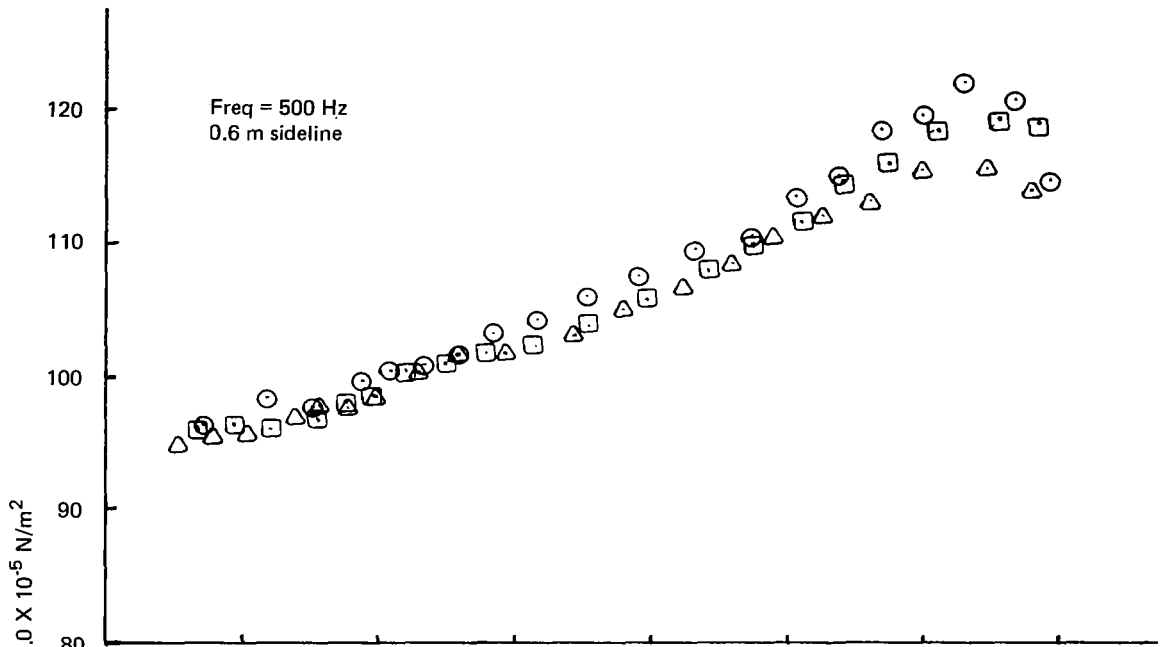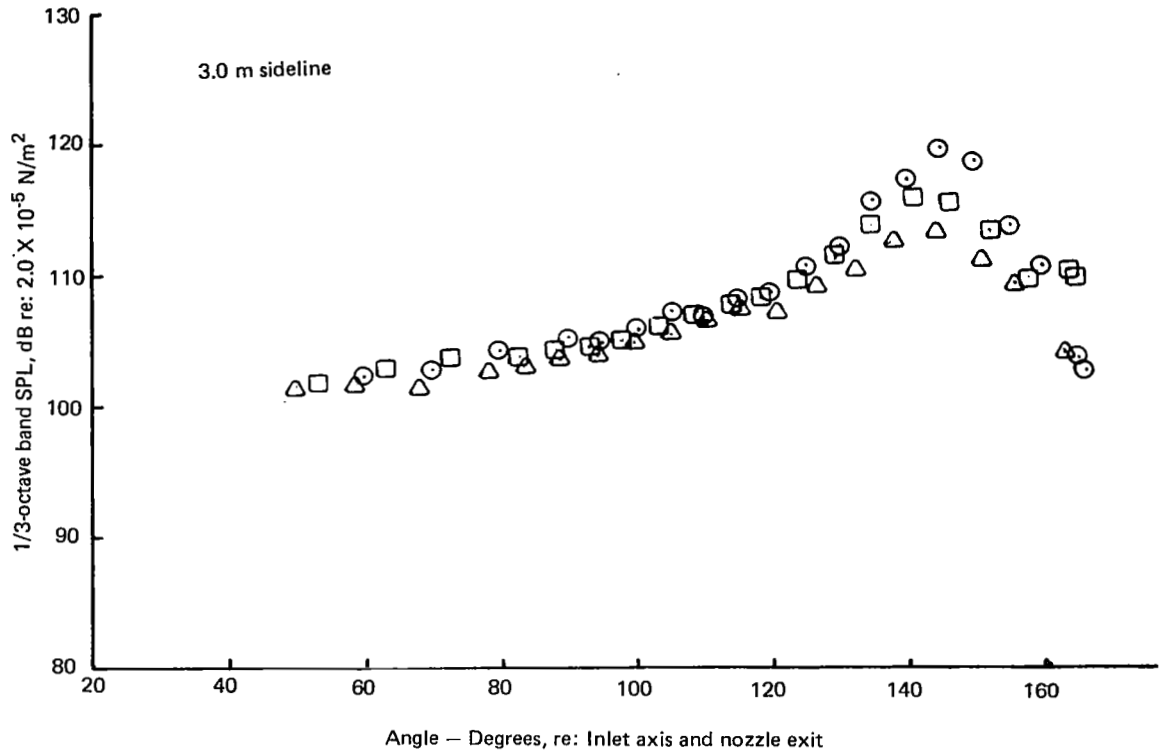
Figure 21.—(Continued)

Figure 21.—(Continued)

Figure 21.—(Continued)

Figure 21.—(Continued)

Figure 21.—(Continued)

3.0 m sideline
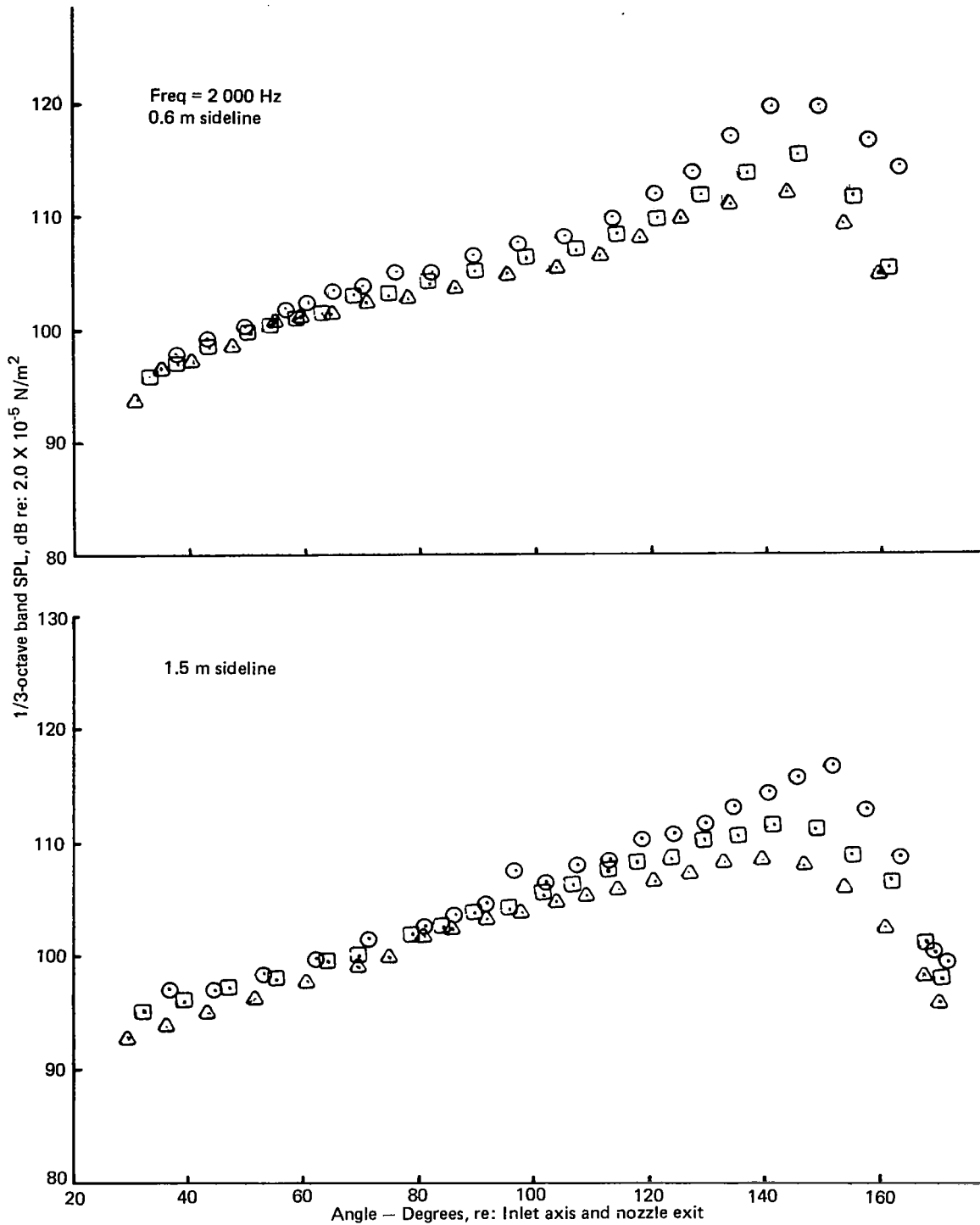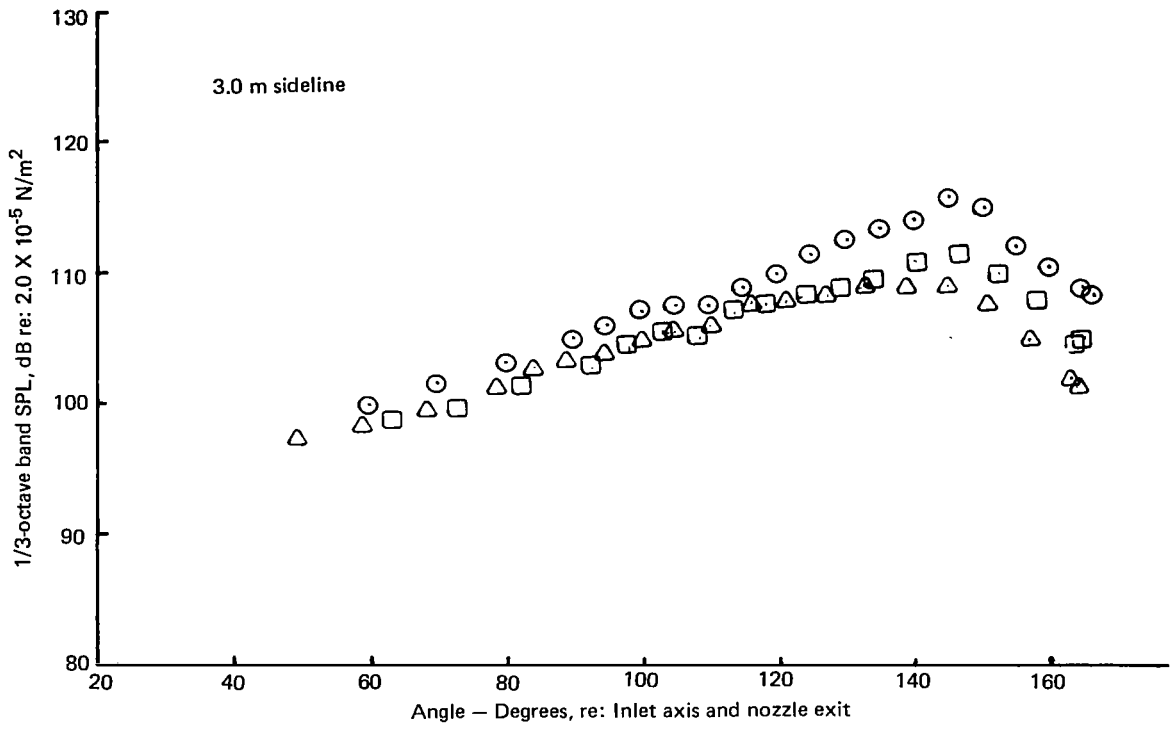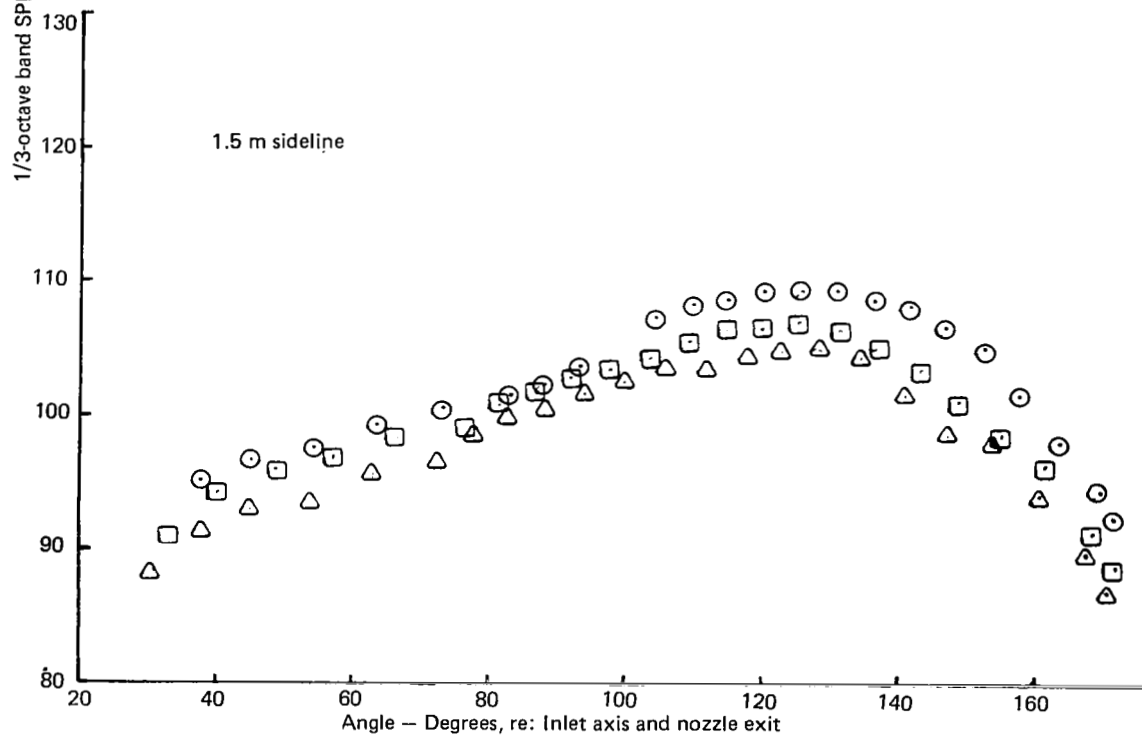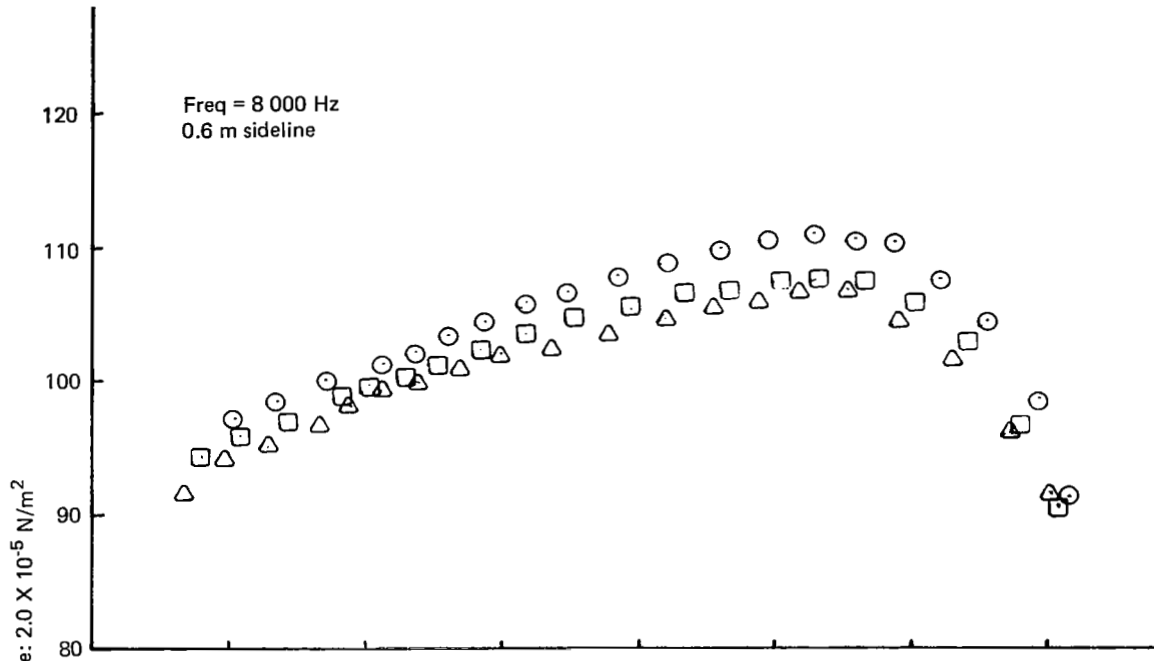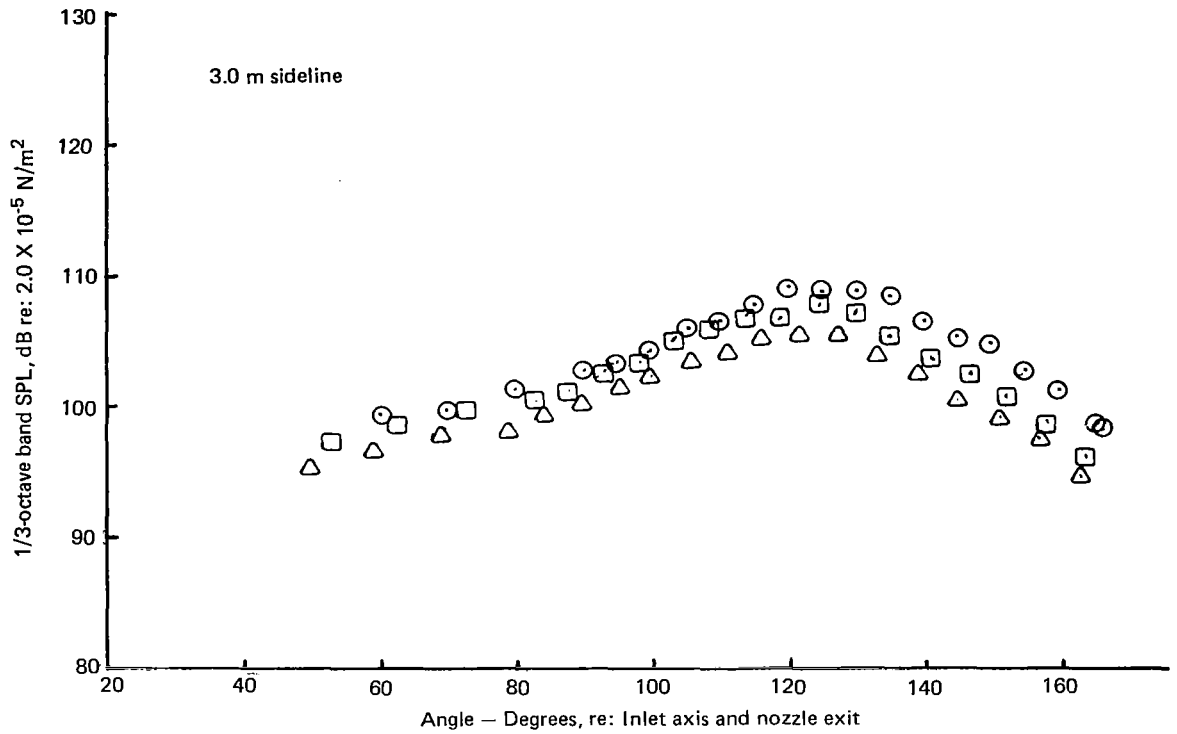
Figure 21.—(Concluded)
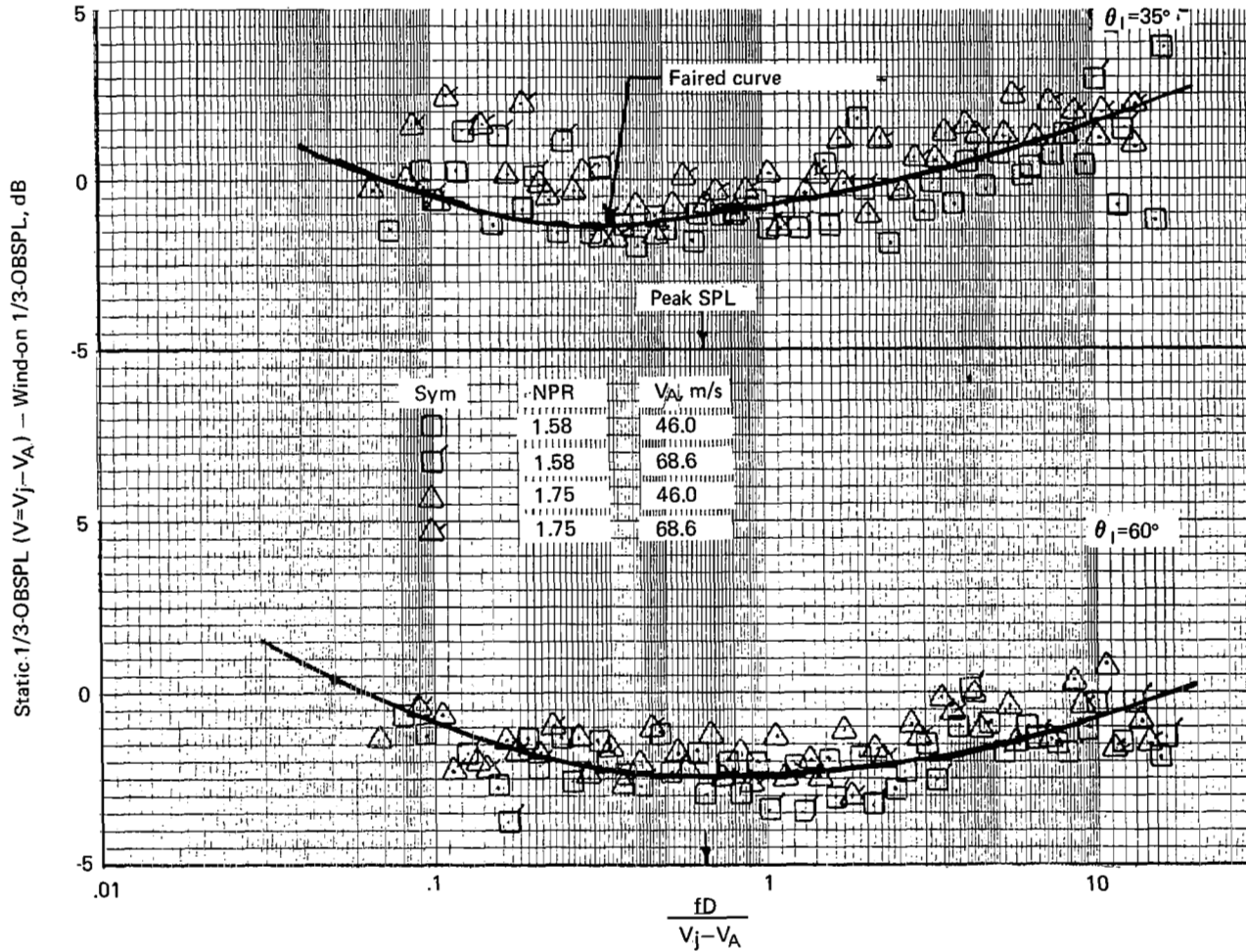
Figure 22.—Effect of Ambient Velocity on Subsonic Jet Noise Spectra or an RC Nozzle Referenced to the Static Case Where $V=V_j-V_A$, $T_T = 844K$
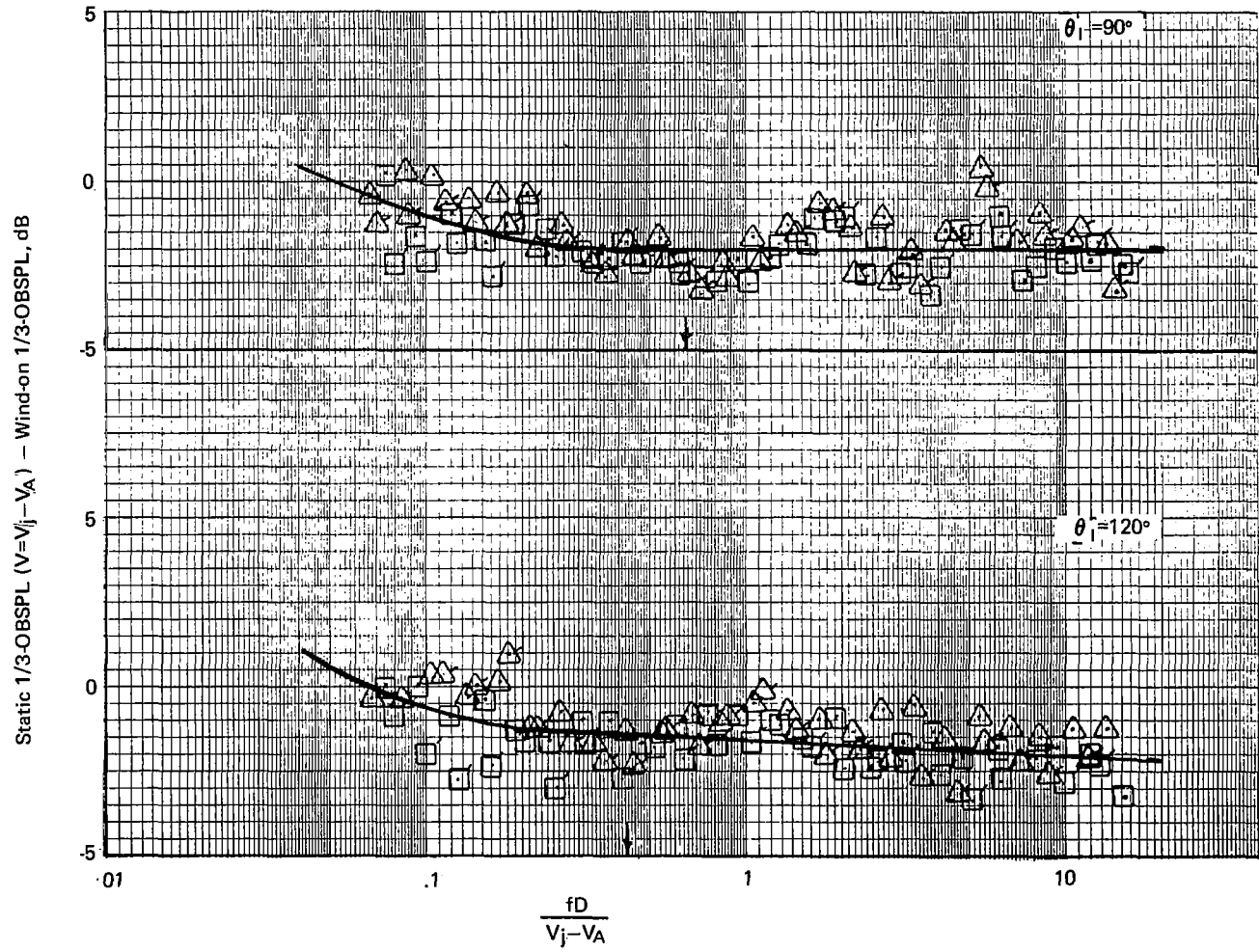
Figure 22.—(Continued)
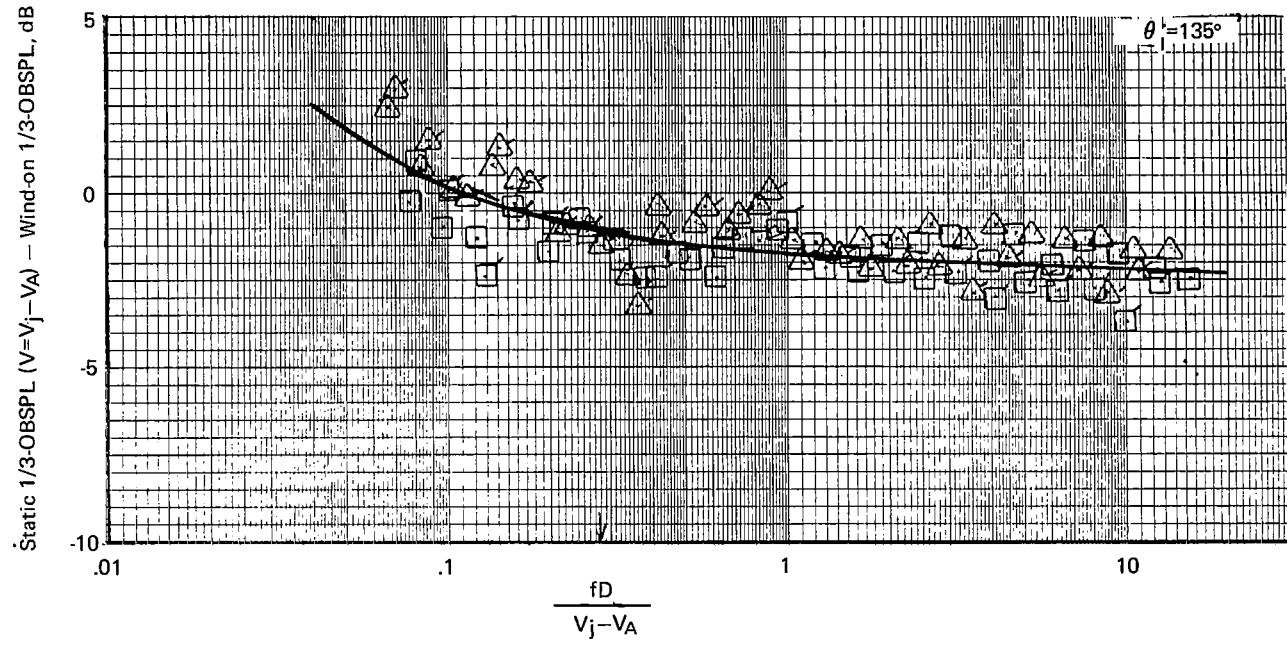
Figure 22.—(Continued)
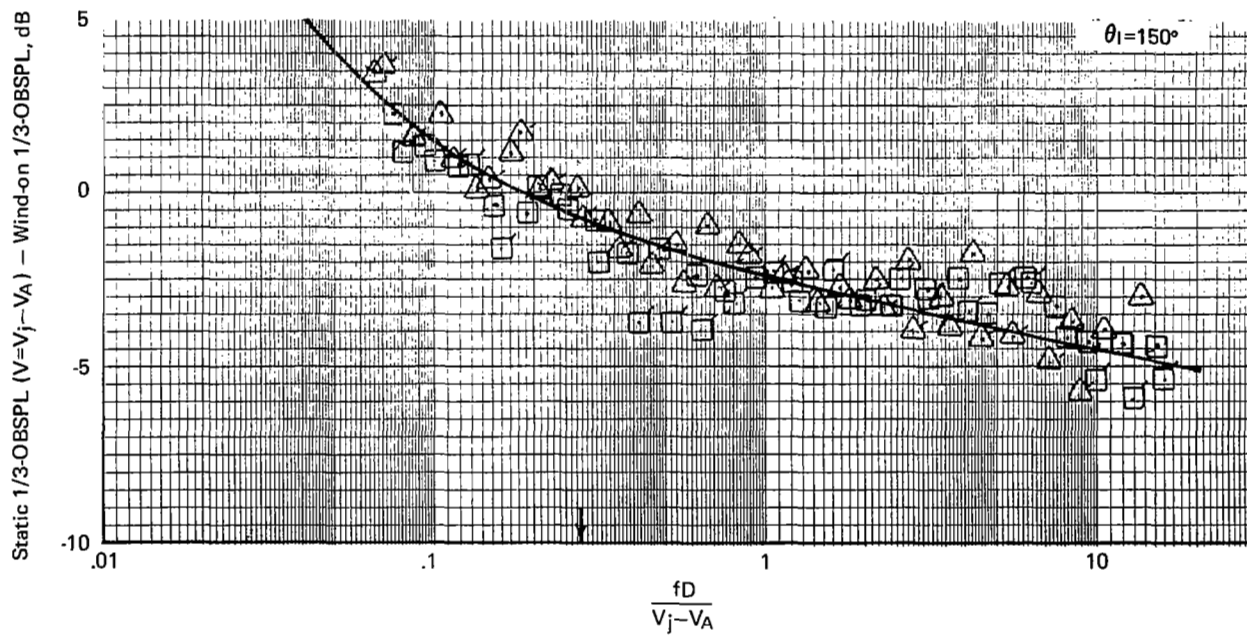
Figure 22.—(Continued)

Figure 22.—(Concluded)

$$0 \leq \text{Log}_{10} \frac{V_j}{a_A} \leq 0.2$$

Symbols and line derived from ref. 15

$$m = \frac{\left[\text{OASPL} - 10\,\text{Log}_{10}\left(\frac{\rho_j}{\rho_A}\right)^{\omega}\right]_{V_j} - \left[\text{OASPL} - 10\,\text{Log}_{10}\left(\frac{\rho_j}{\rho_A}\right)^{\omega}\right]_{(V_j - V_A)}}{10\,\text{Log}_{10}\left(\frac{V_j}{V_j - V_A}\right)}$$

from ref. 15
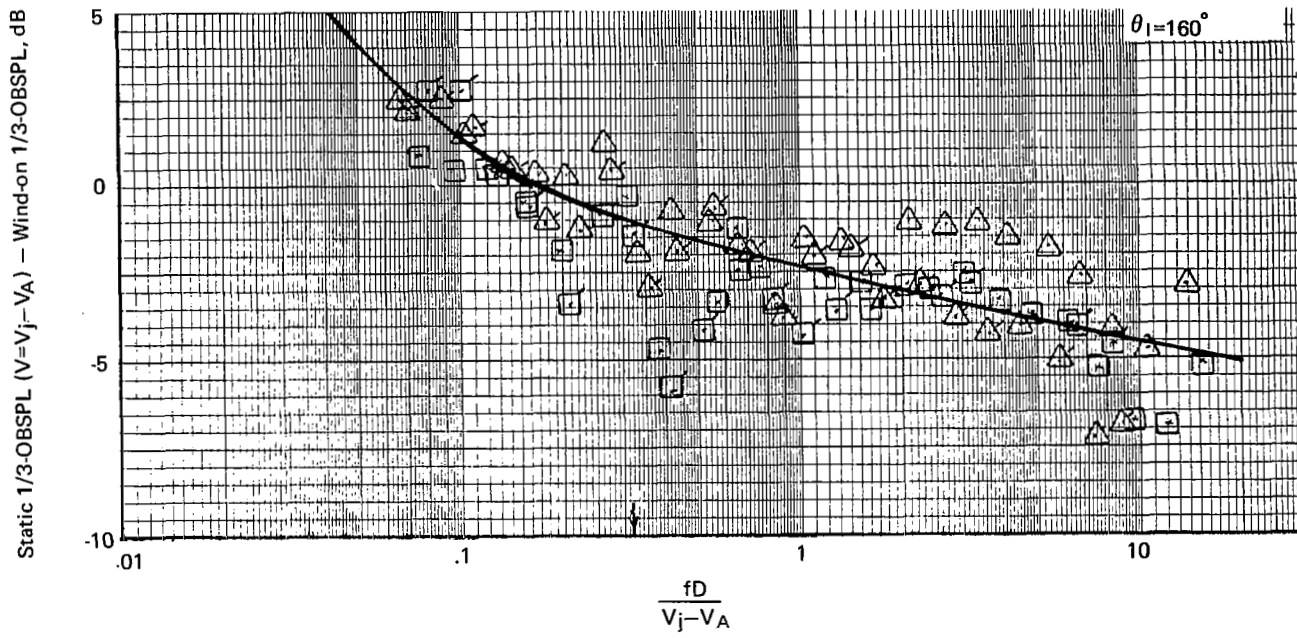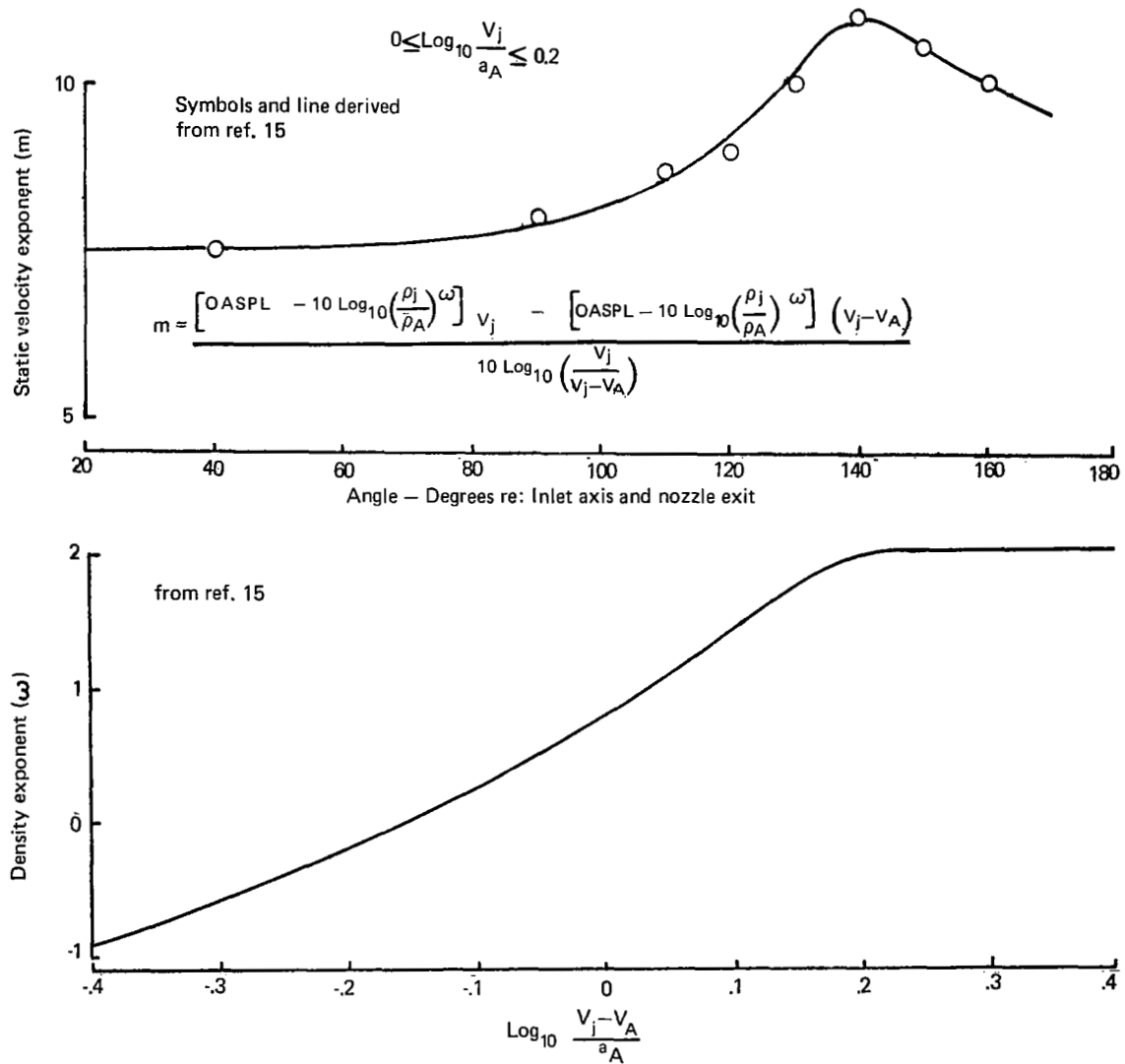
Figure 23.—Static Velocity Exponent for an RC Nozzle
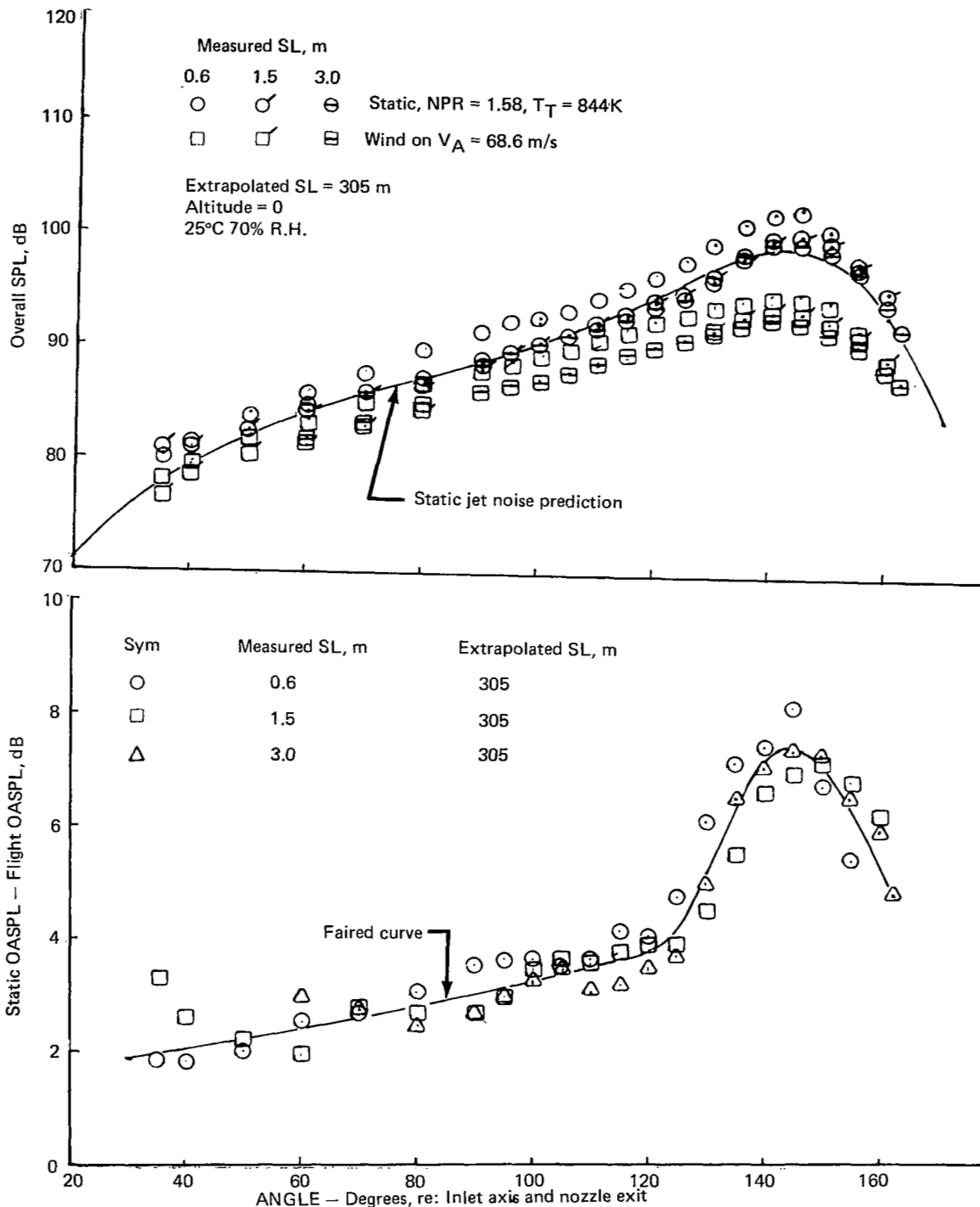
Figure 24.—0.76 m RC Nozzle Flight Effects Based on 40 by 80 Tunnel Measurements
V_j = 457 m/s V_A= 68.6 m/s
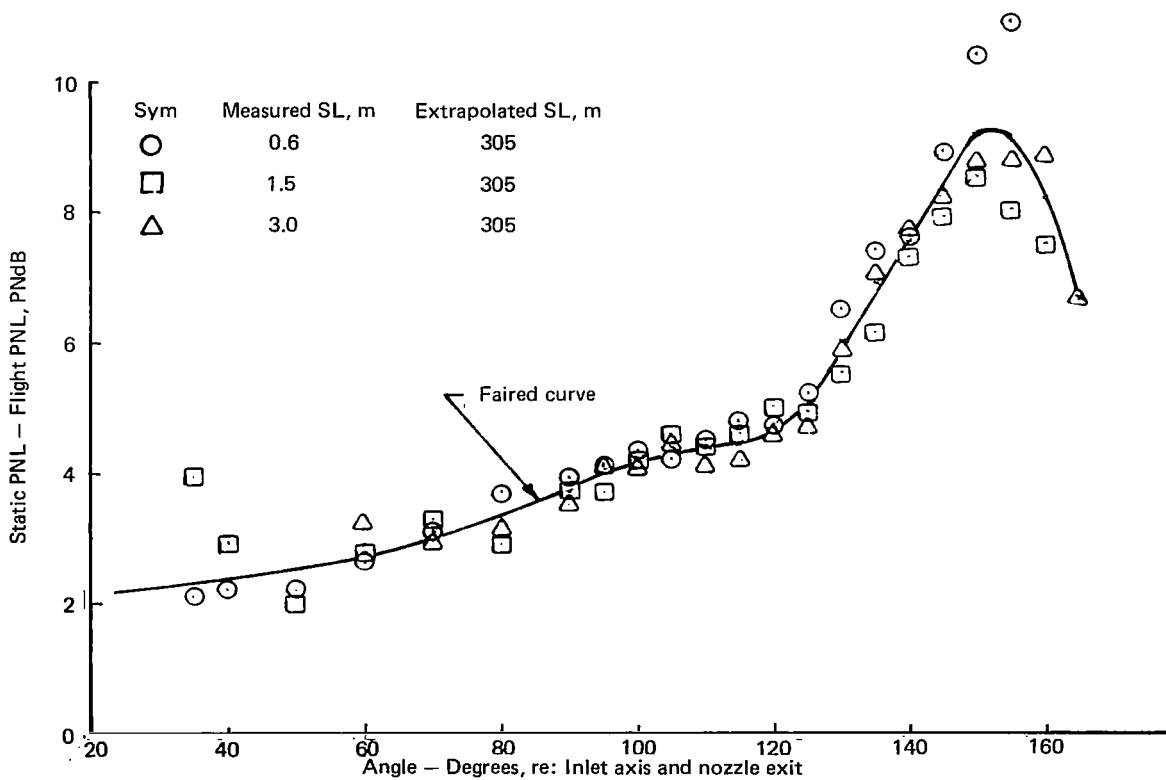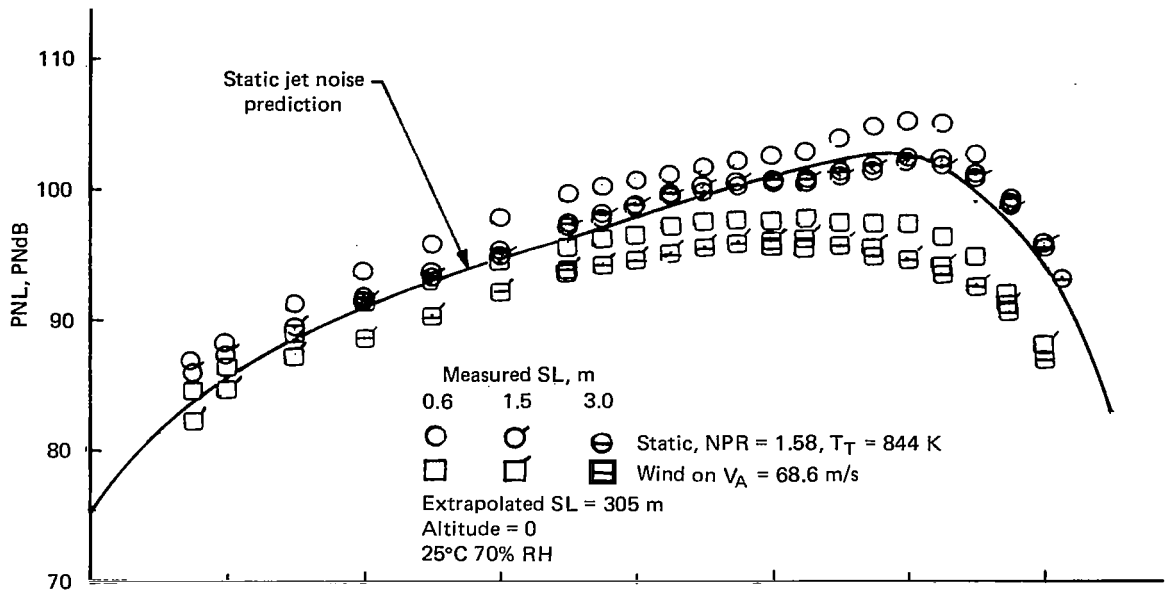
Figure 24.—(Concluded)
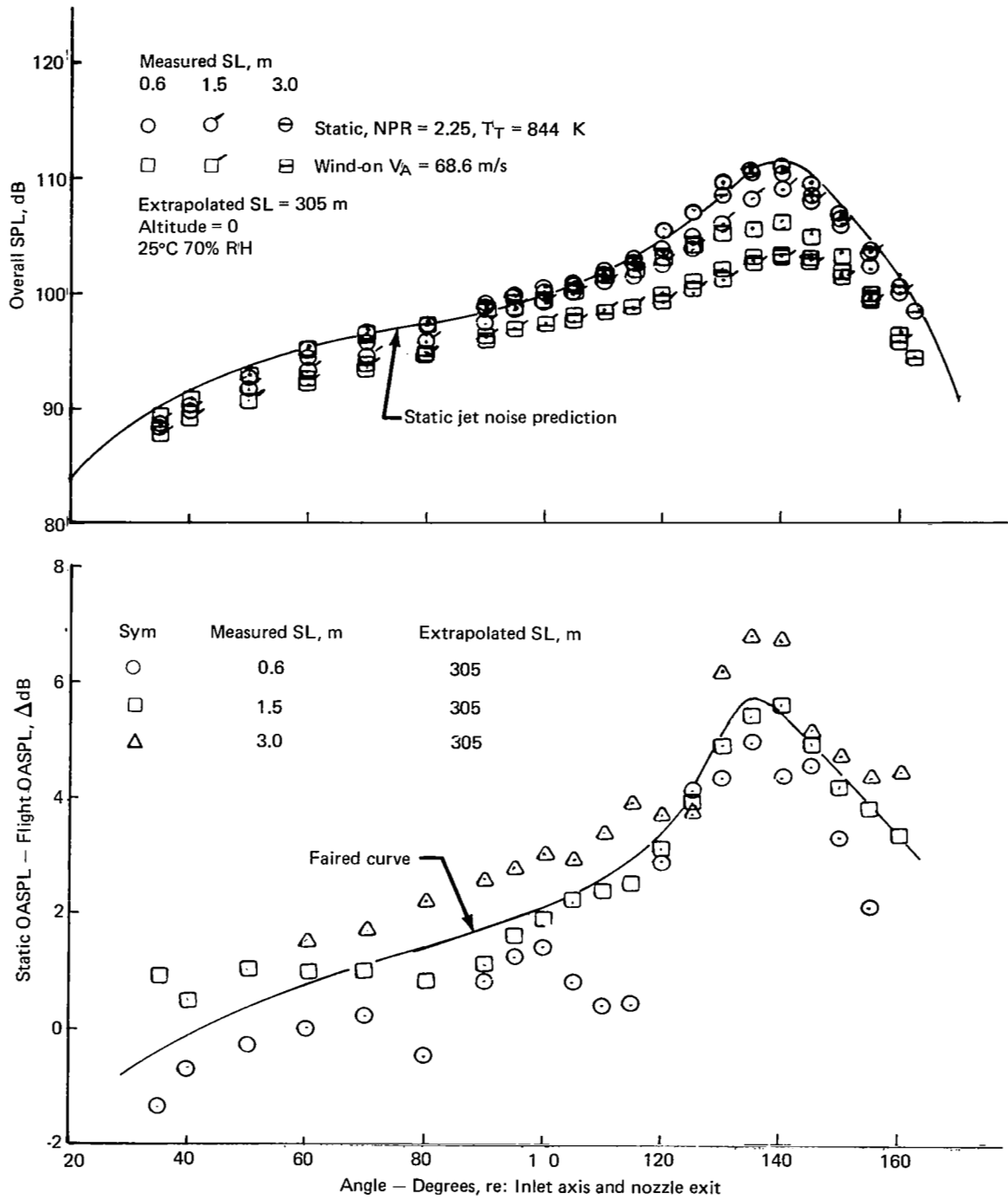
Figure 25.—0.76 m RC Nozzle Flight Effects Based on 40 by 80 Tunnel Measurements
V_j = 594 m/s V_A = 68.6 m/s
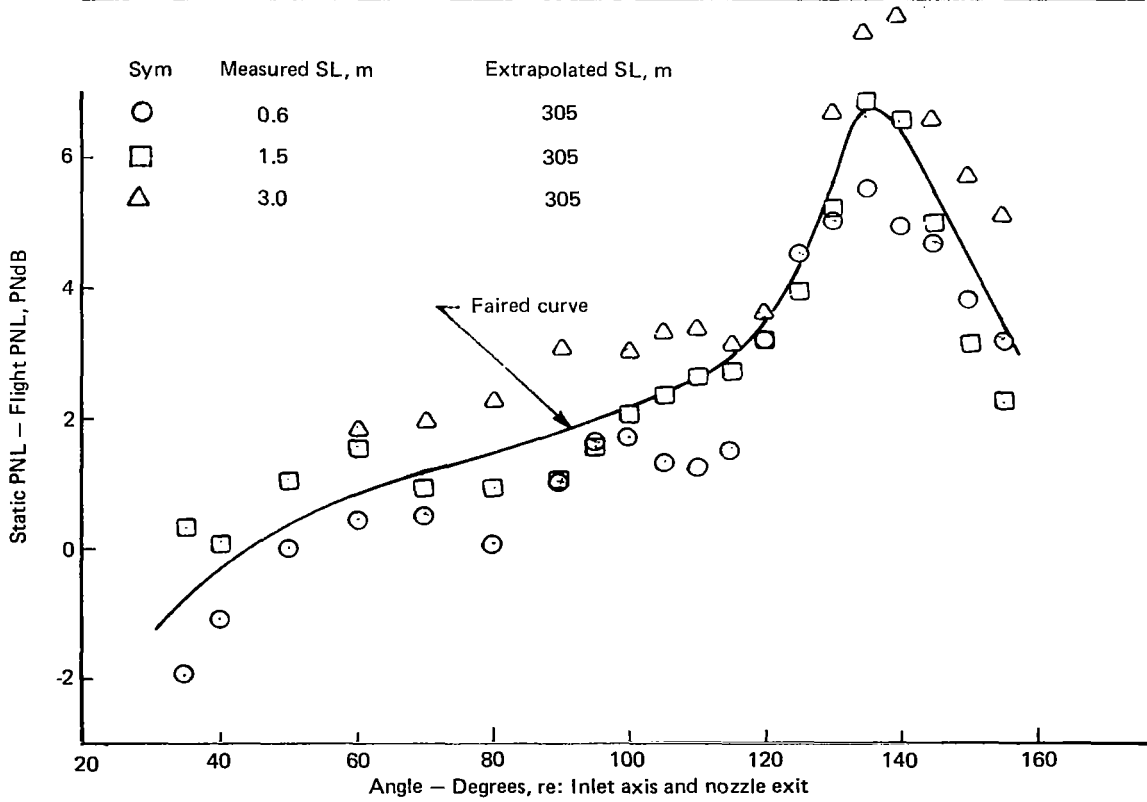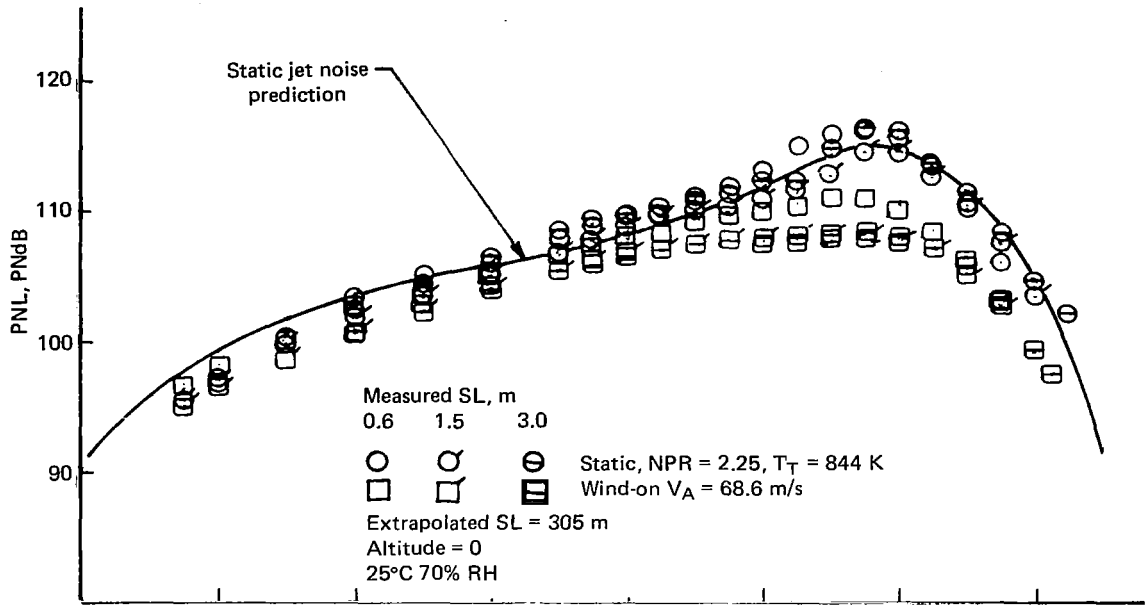
Figure 25.— (Concluded)
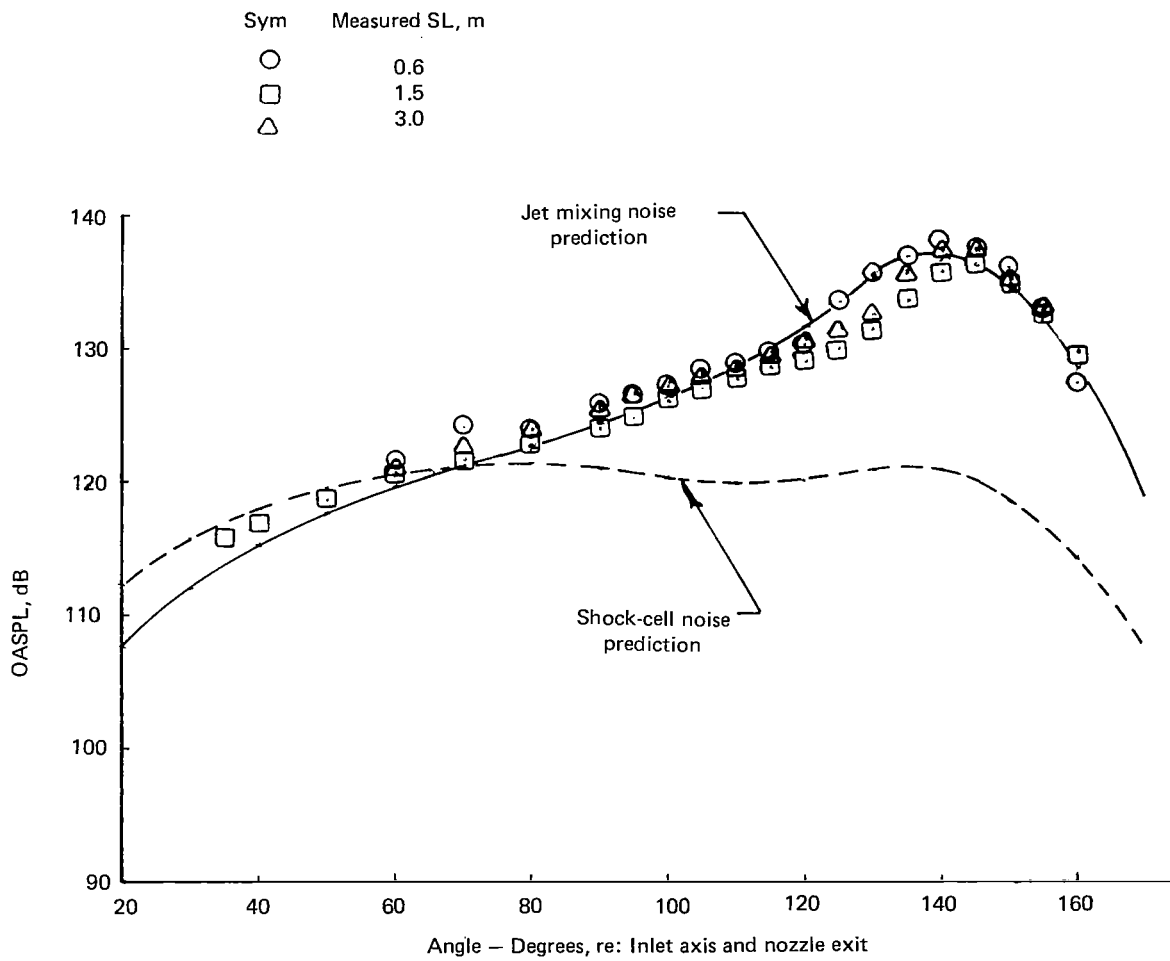
Figure 26.—OASPL Directivity and Jet Noise Spectra for a 15.24 cm RC Nozzle
Extrapolated to a 3.05 m Sideline, NPR = 2.25, V_A = 0 m/s

Figure 26.—(Continued)

Figure 26.—(Continued)

Figure 26.—(Continued)

73
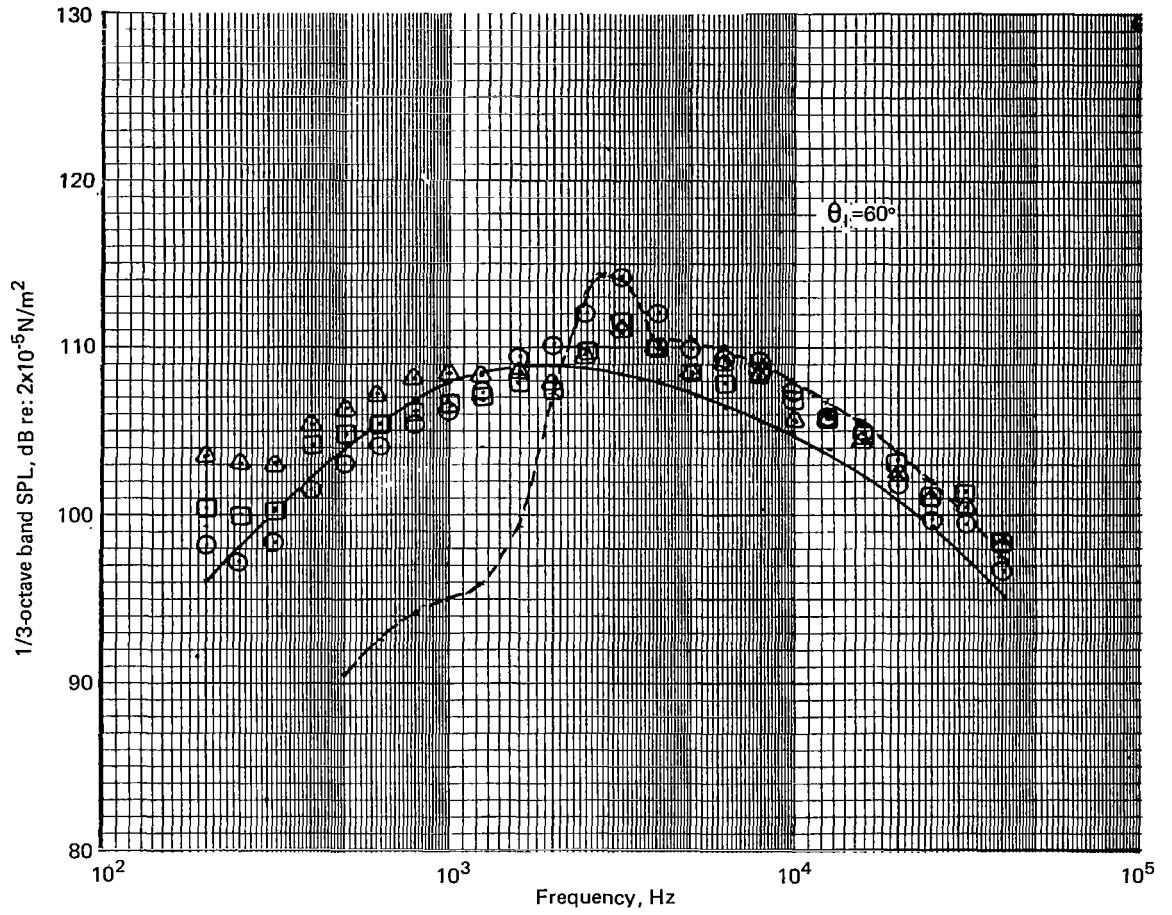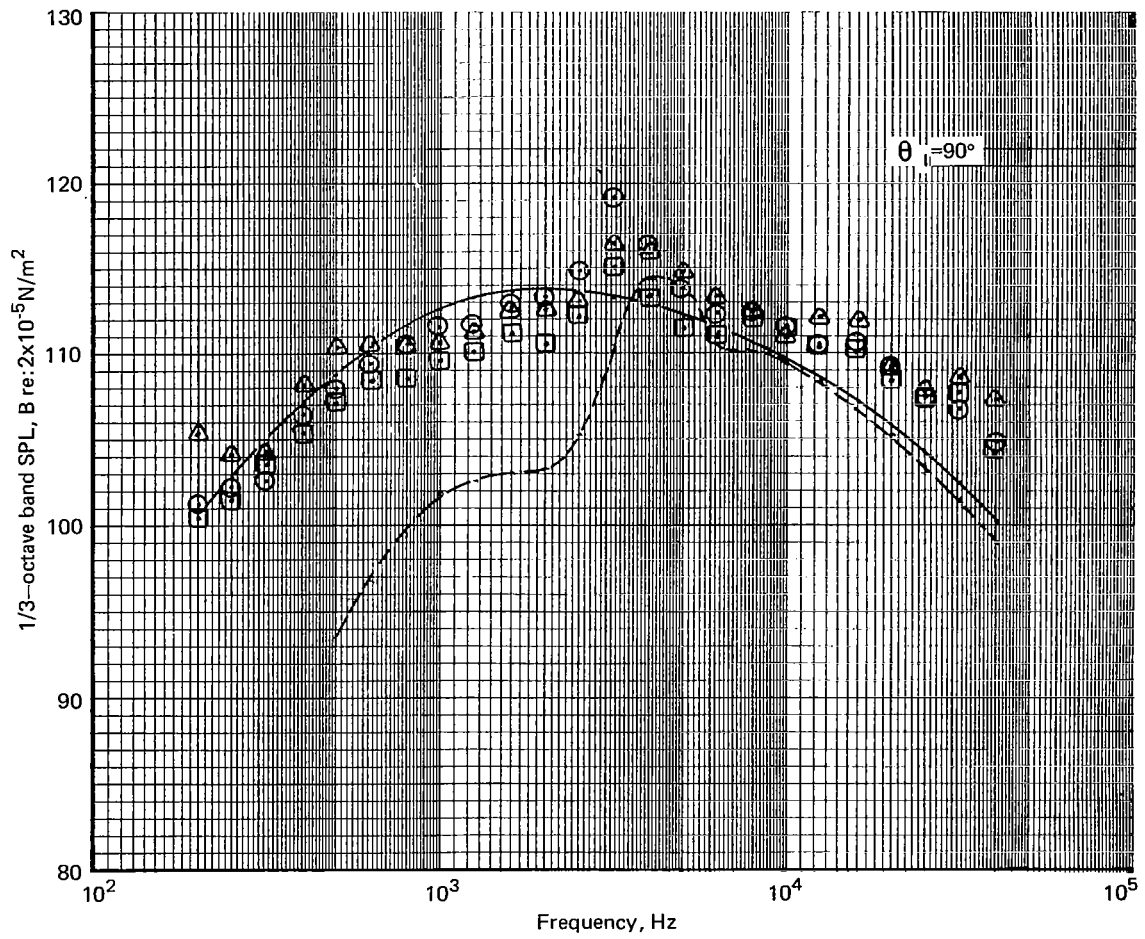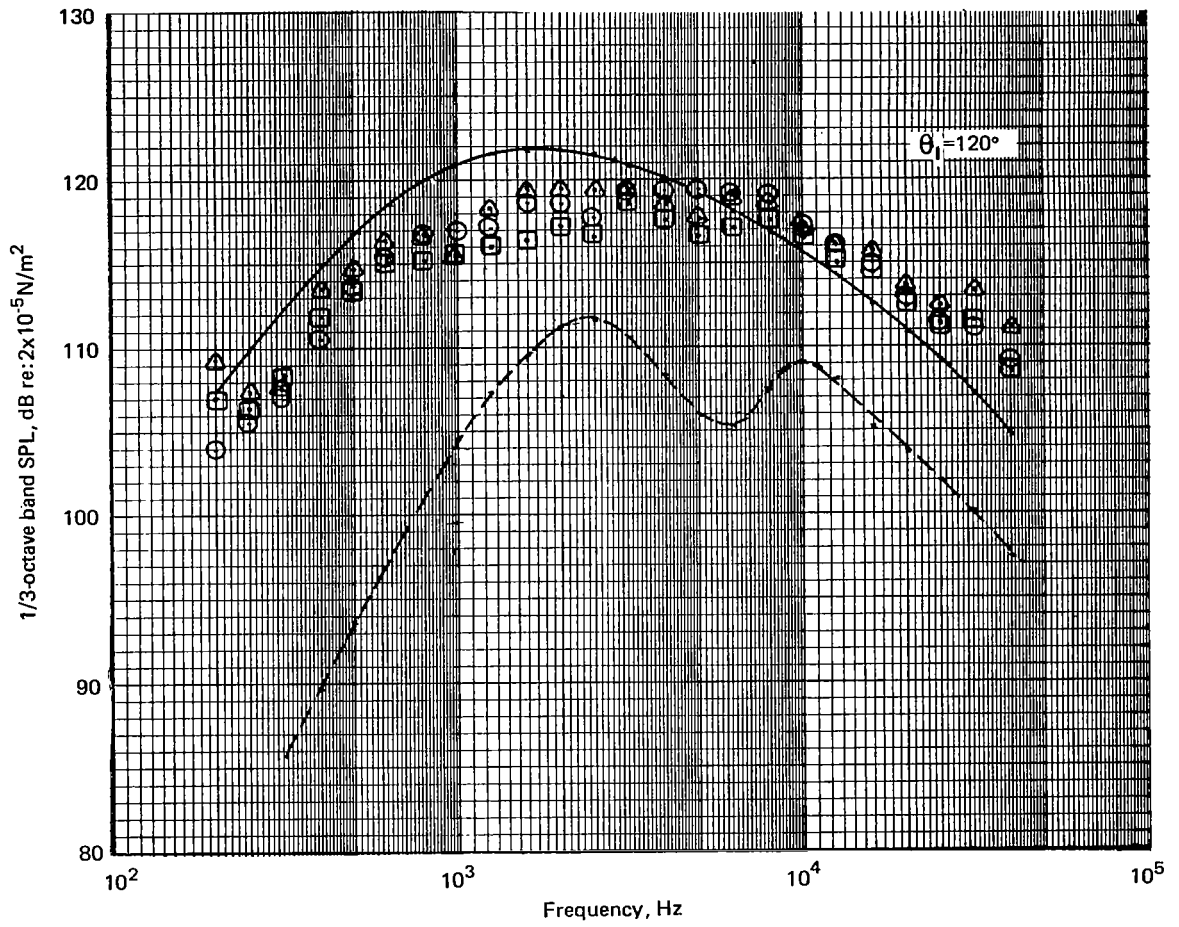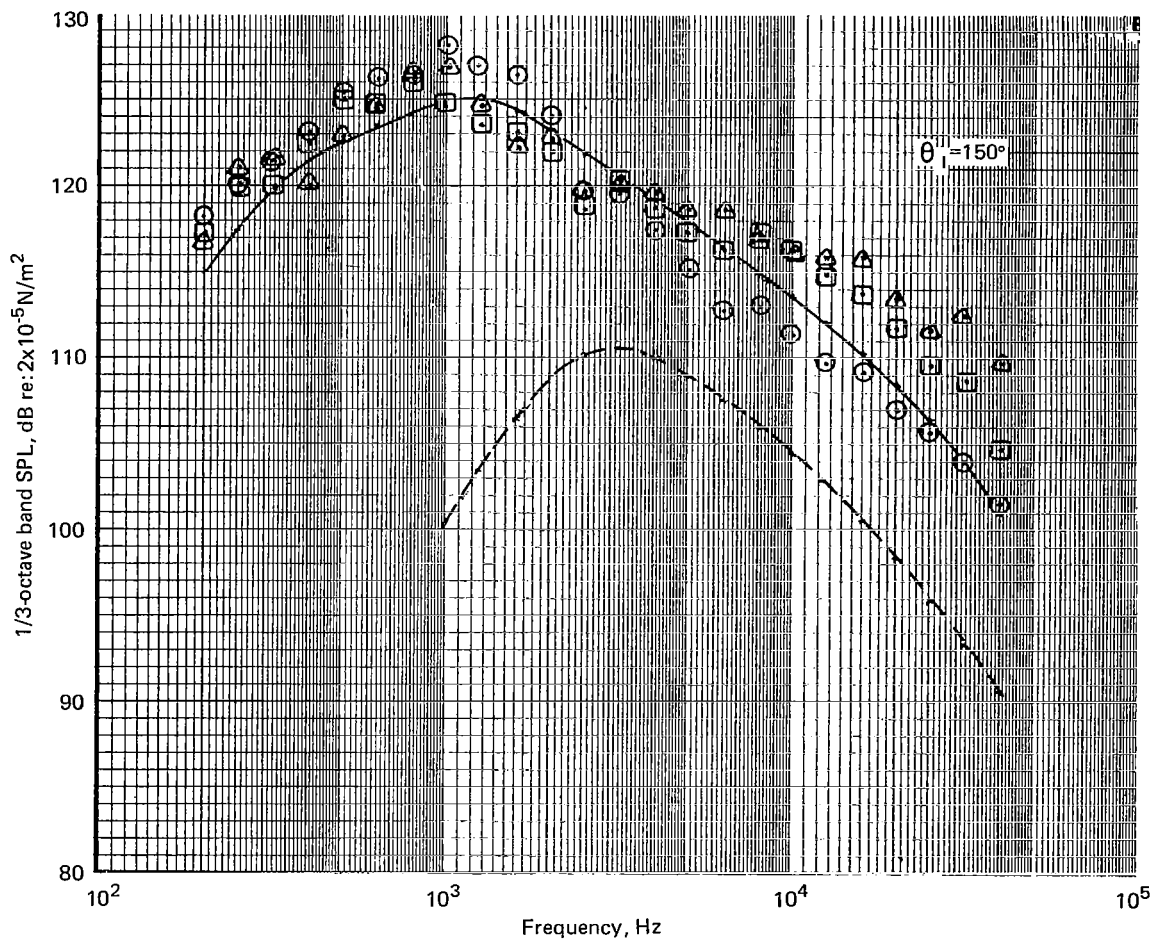
Figure 26.—(Concluded)
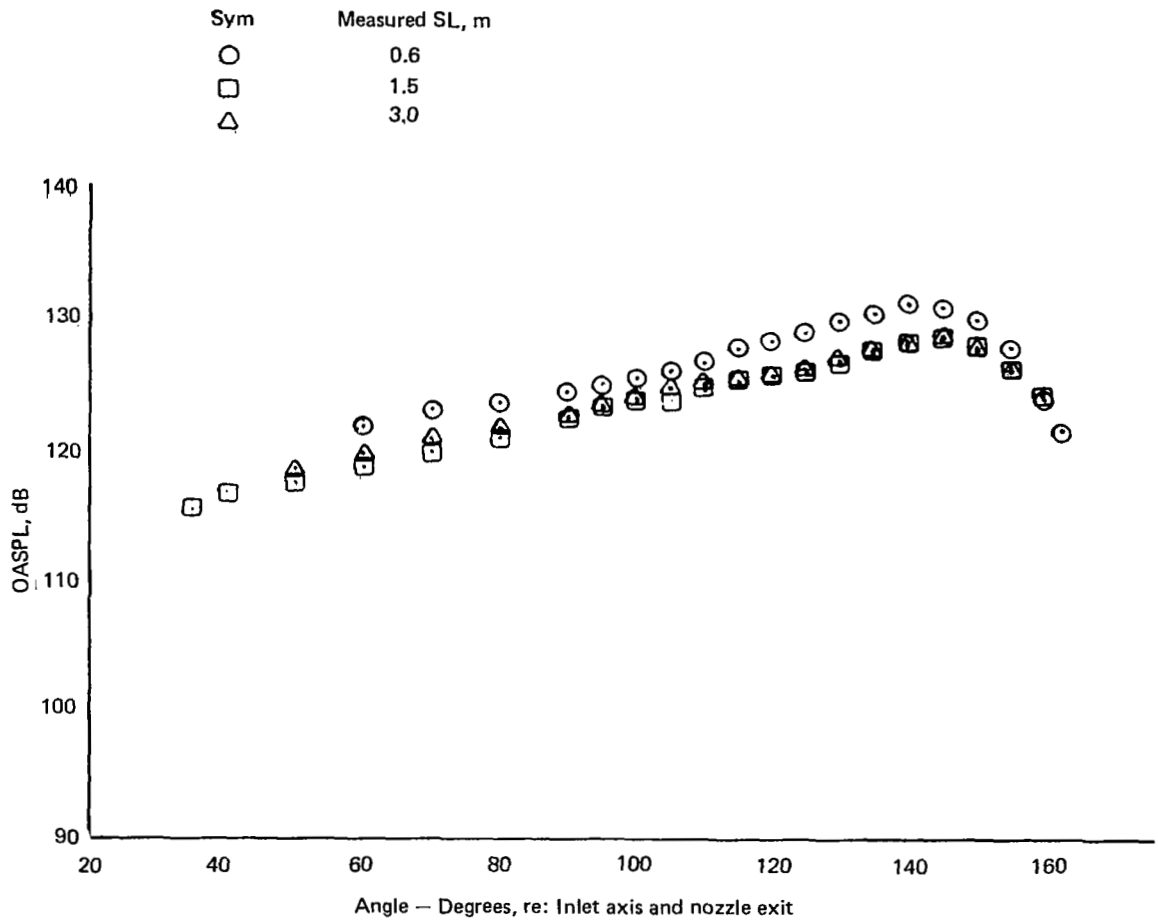
Figure 27.—OASPL Directivity and Jet Noise Spectra for a 15.24 cm RC Nozzle
Extrapolated to a 3.05 m Sideline, NPR = 2.25, V_A = 91.5 m/s
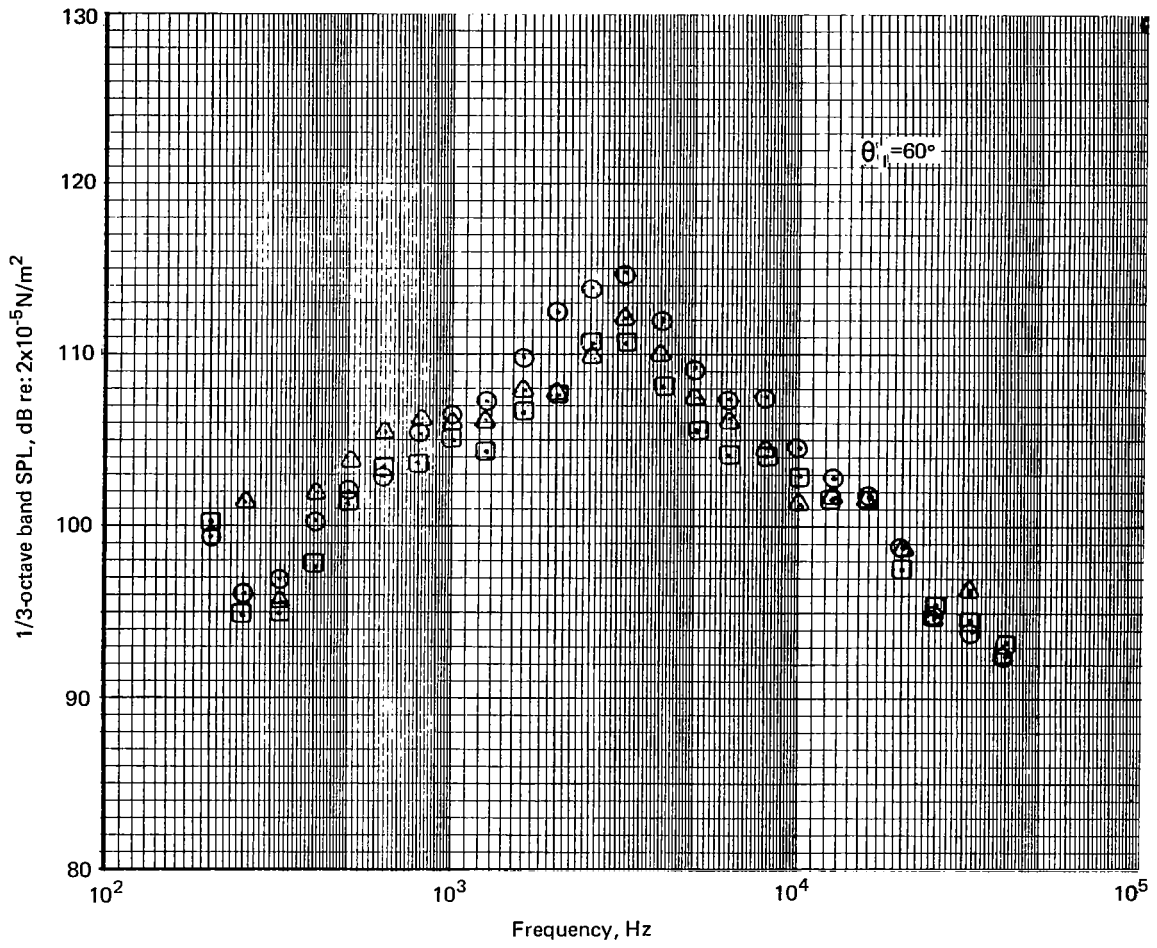
Figure 27.—(Continued)
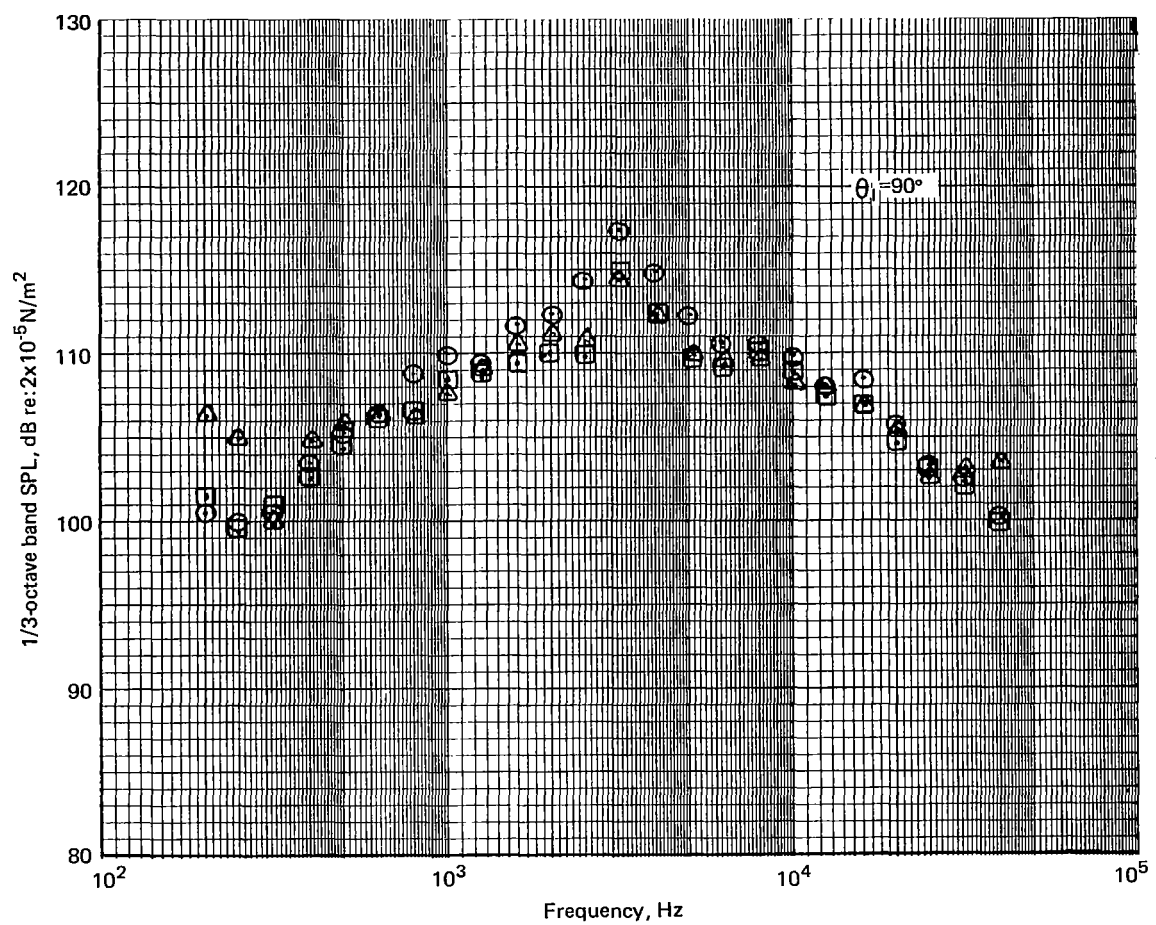
Figure 27.—(Continued)
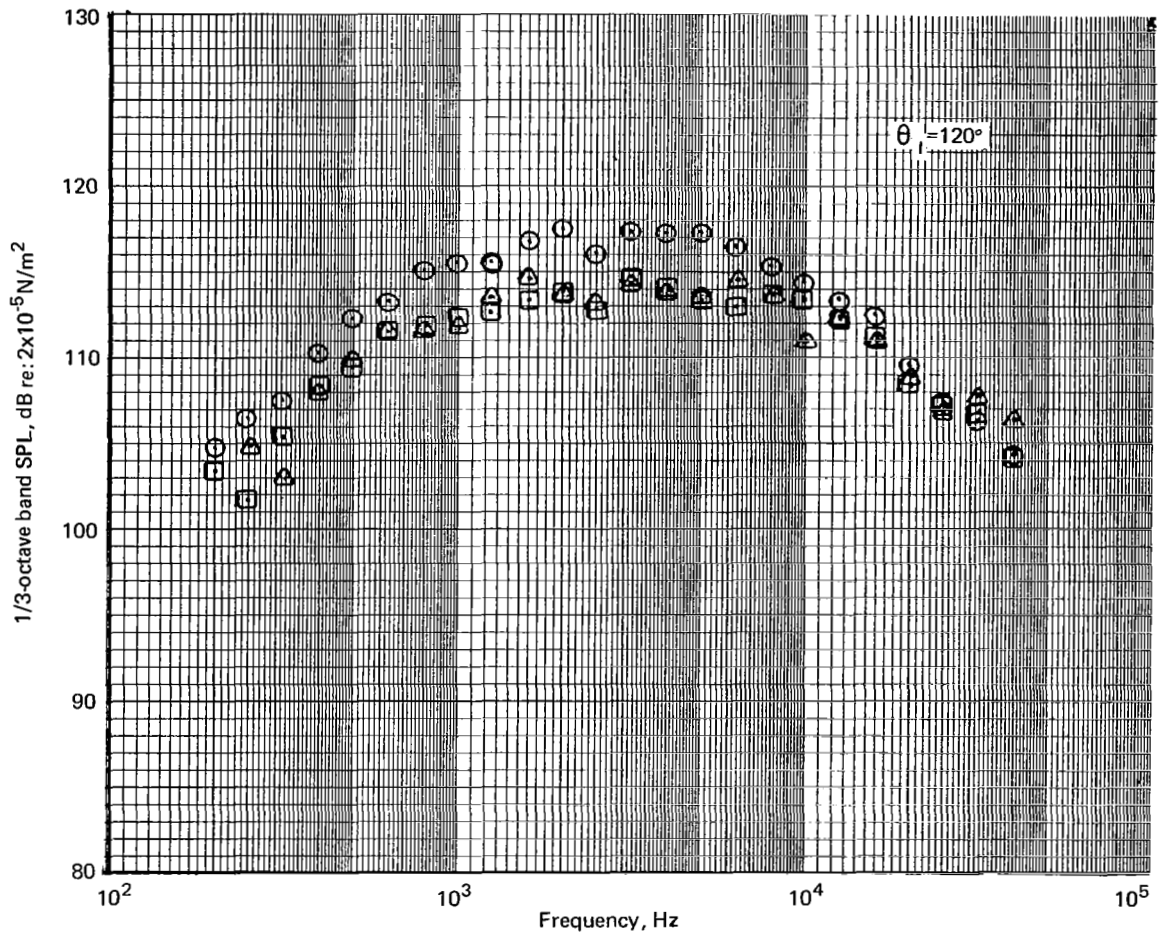
Figure 27.—(Continued)
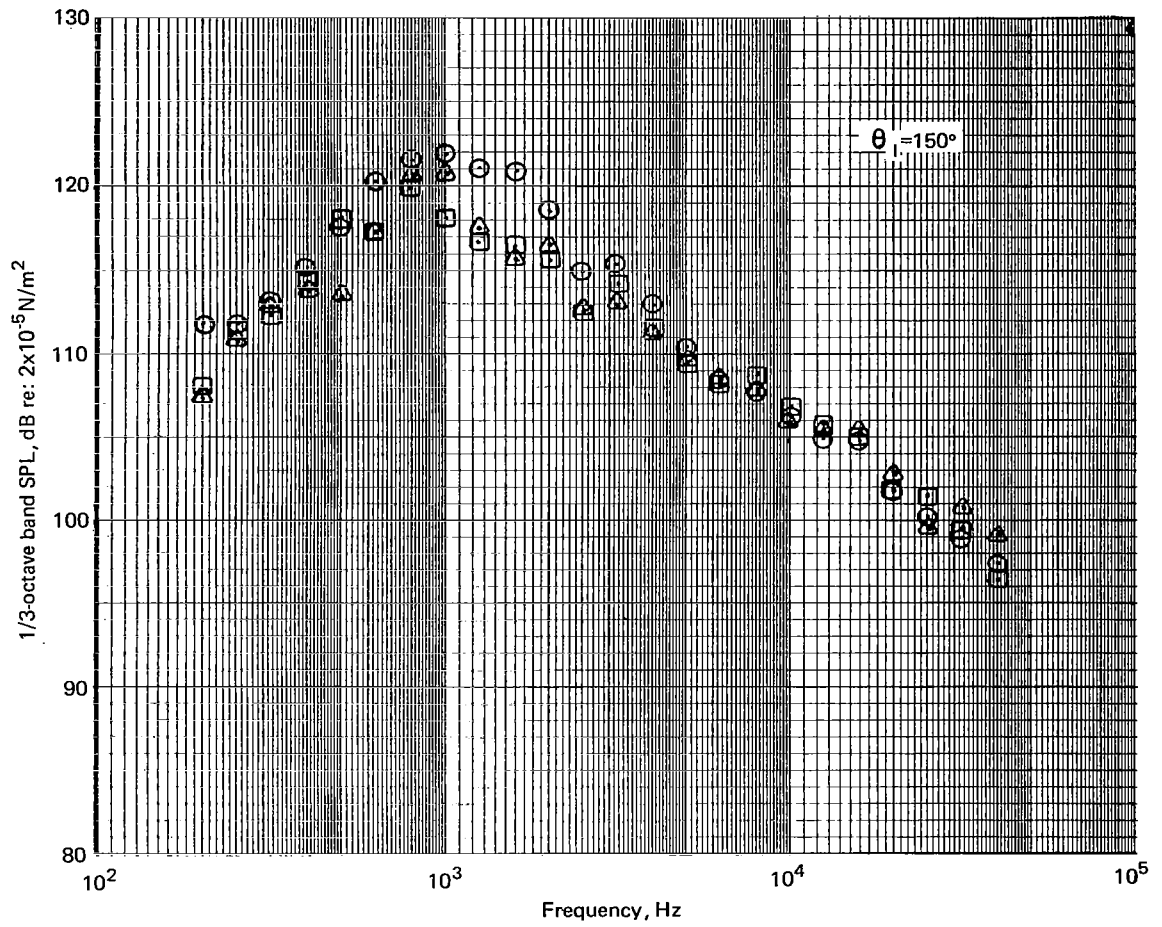
Figure 27.—(Concluded)
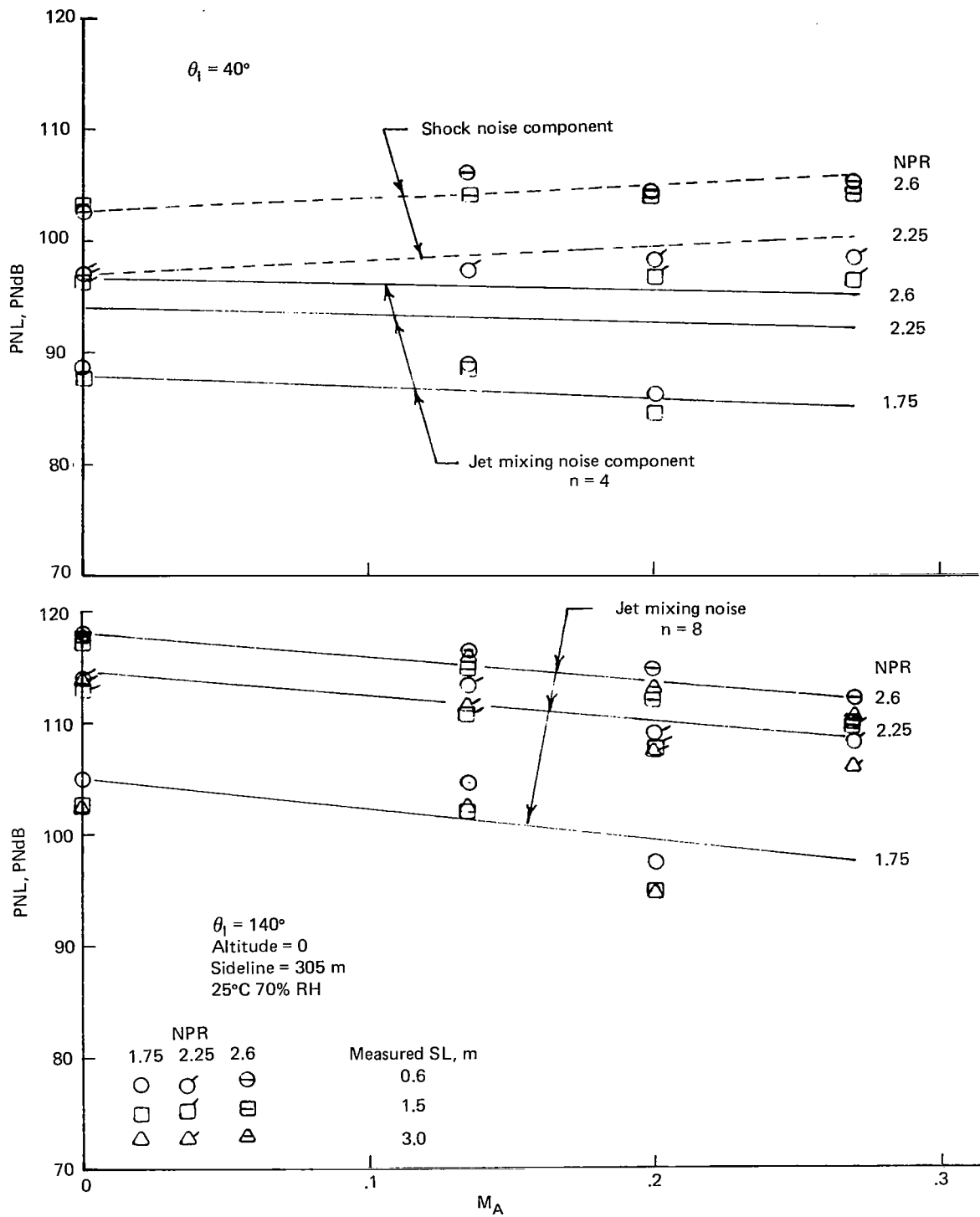
Figure 28.—Effect of Ambient Velocity on Shock-Cell Noise from an RC Nozzle
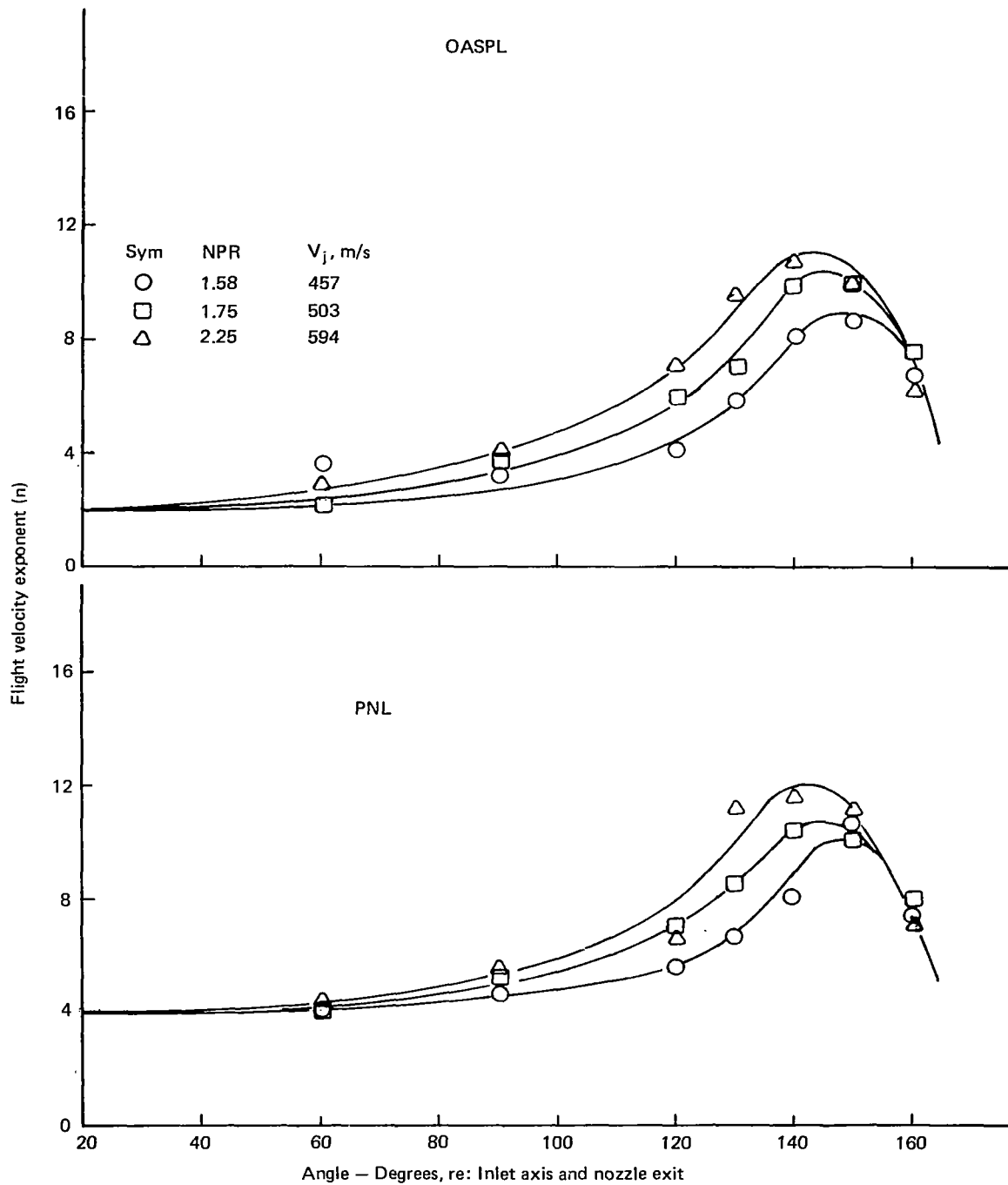
Figure 29.—RC Nozzle Flight Velocity Exponent Based on 40 by 80 Tunnel Data
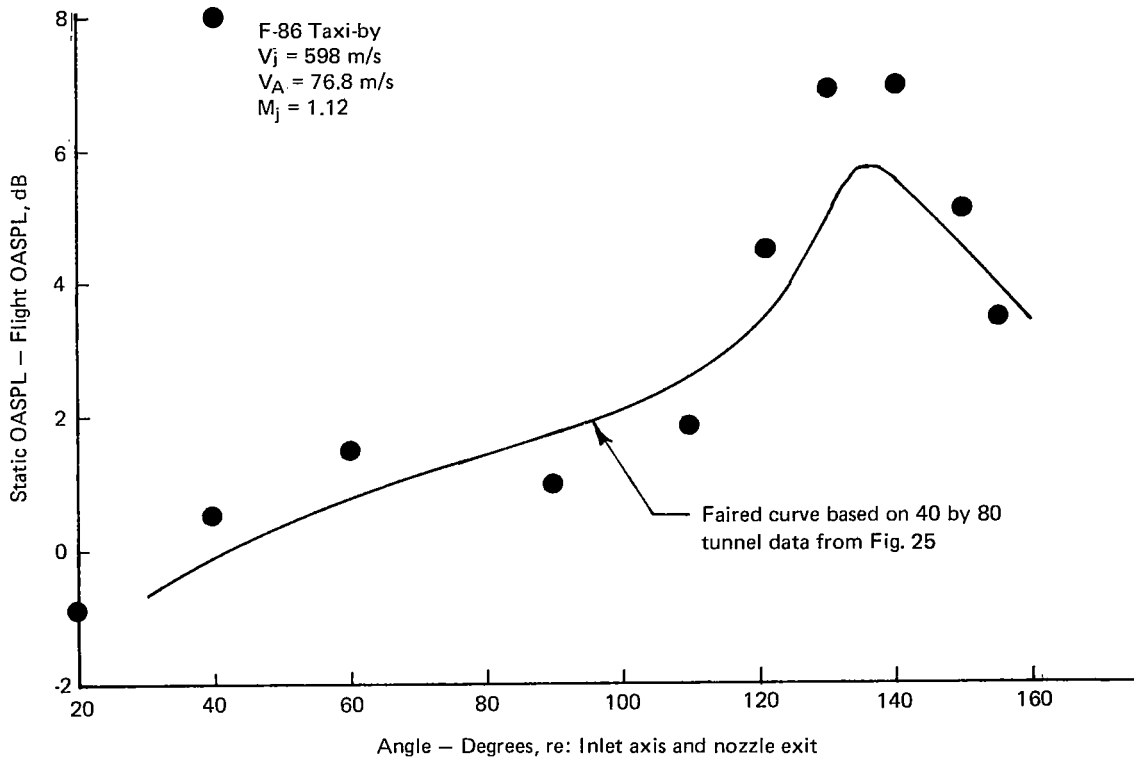
Figure 30.—Comparison of Flight Effects on OASPL Measured in the 40 by 80 Tunnel with F-86 Taxi-By Results
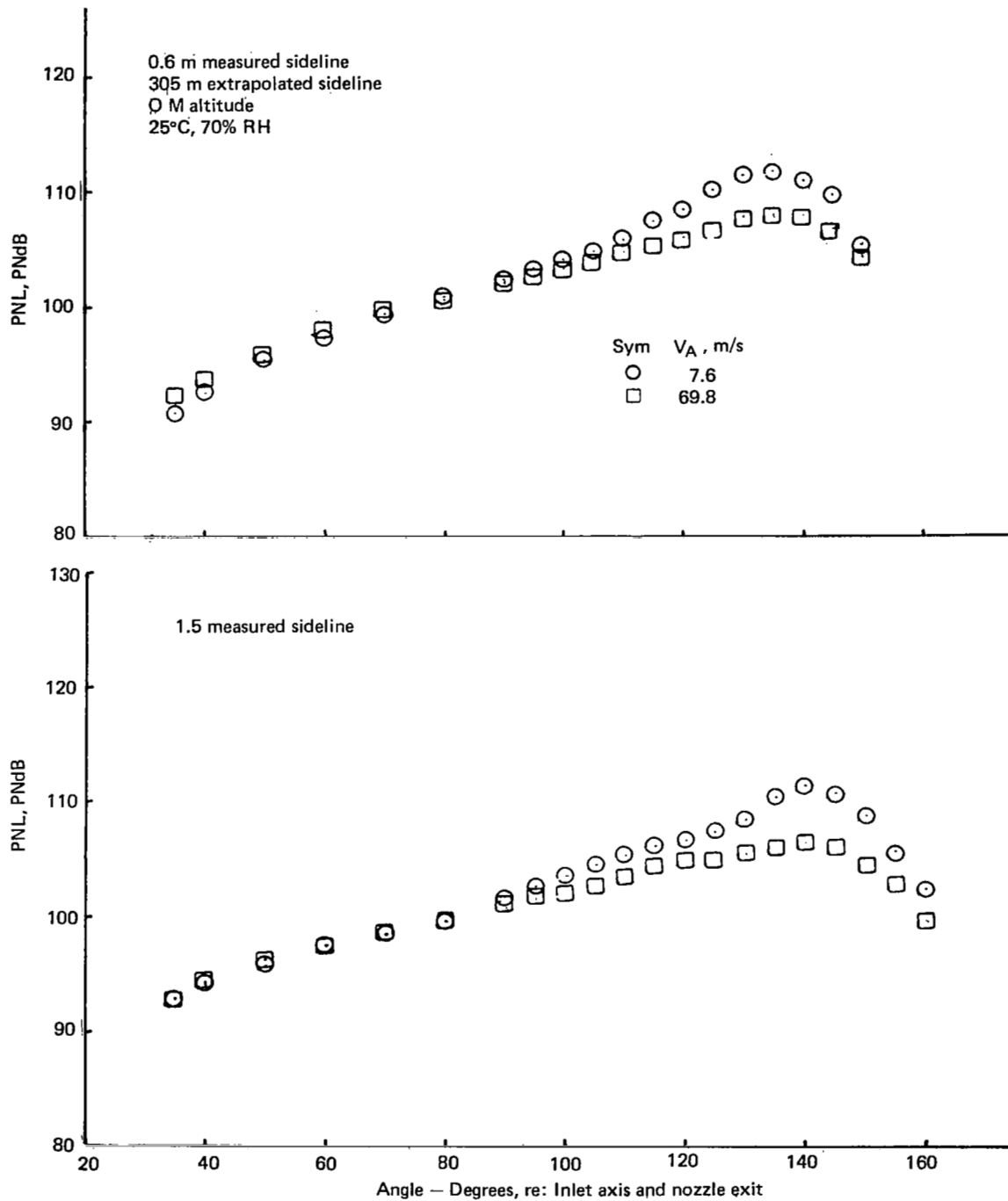
Figure 31.—Flight Effects on PNL of an Annular Nozzle NPR = 2.25, V_j = 594 m/s
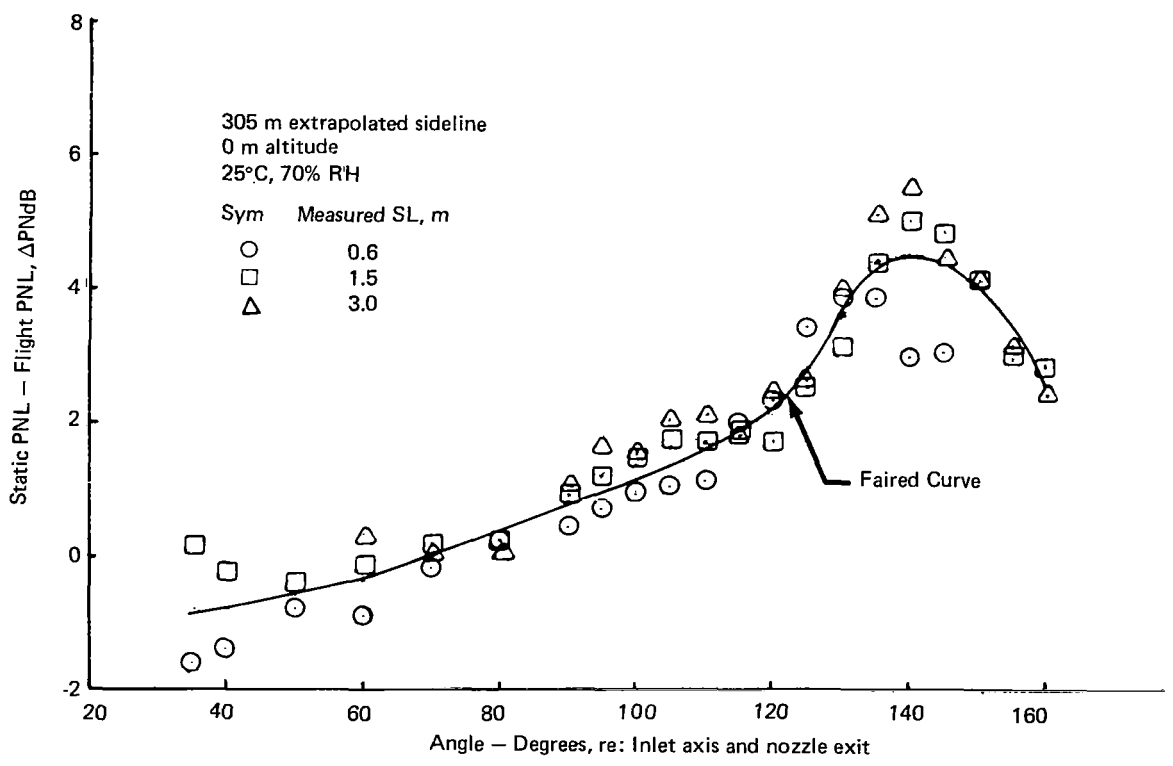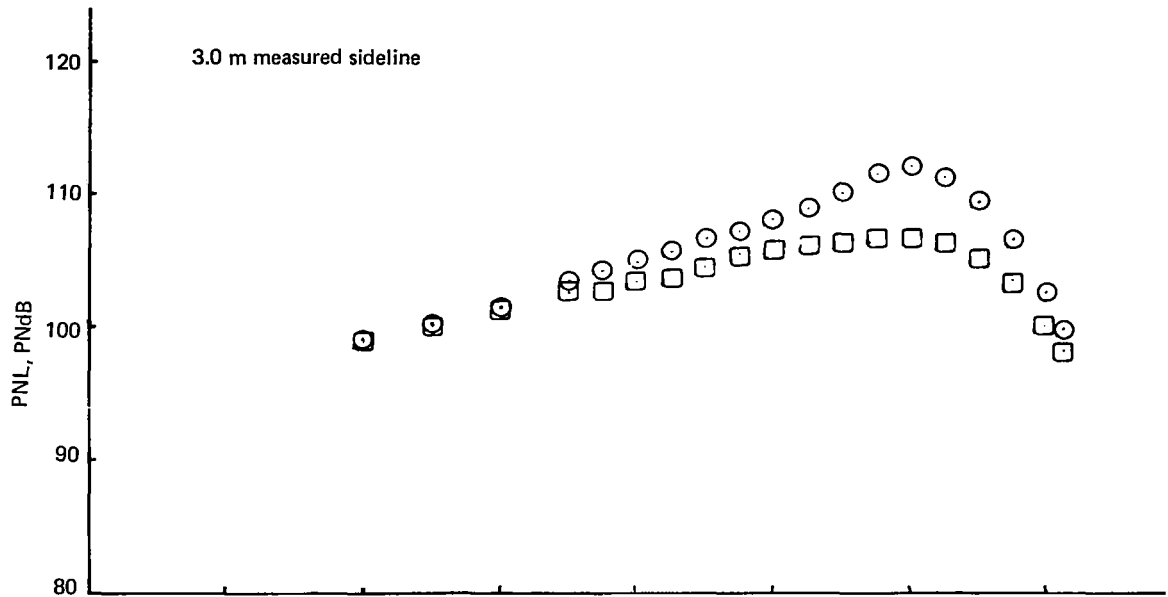
Figure 31.— (Concluded)
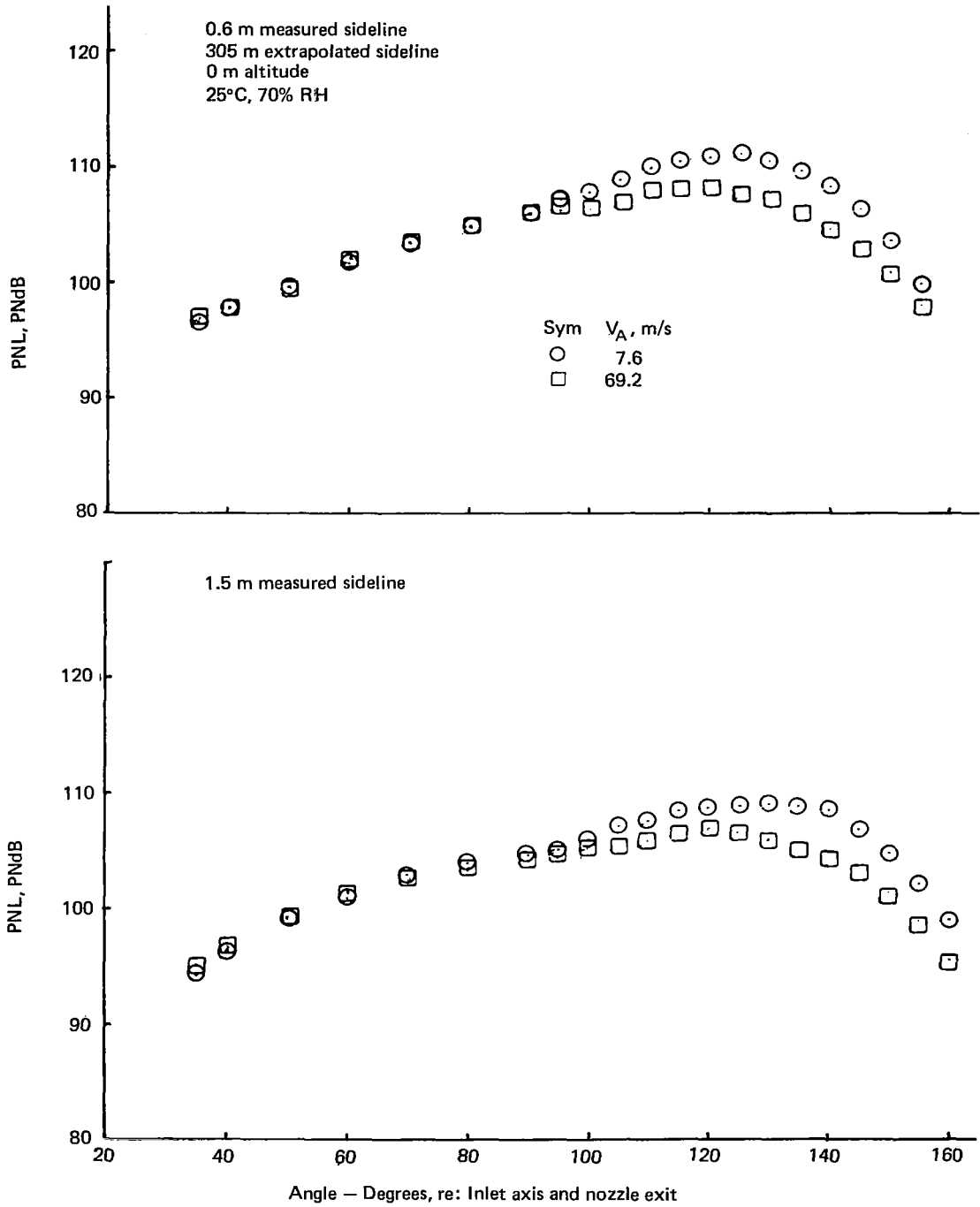
Figure 32.—Flight Effects on PNL of a 20-Lobe Nozzle NPR = 2.25, V_j = 594 m/s

Inside the top chart:

0.6 m measured sideline
305 m extrapolated sideline
0 m altitude
25°C, 70% RH

Sym	V_A, m/s
○	7.6
□	69.2

Inside the bottom chart:

1.5 m measured sideline

Axis labels: PNL, PNdB (vertical, both charts); Angle — Degrees, re: Inlet axis and nozzle exit (horizontal)
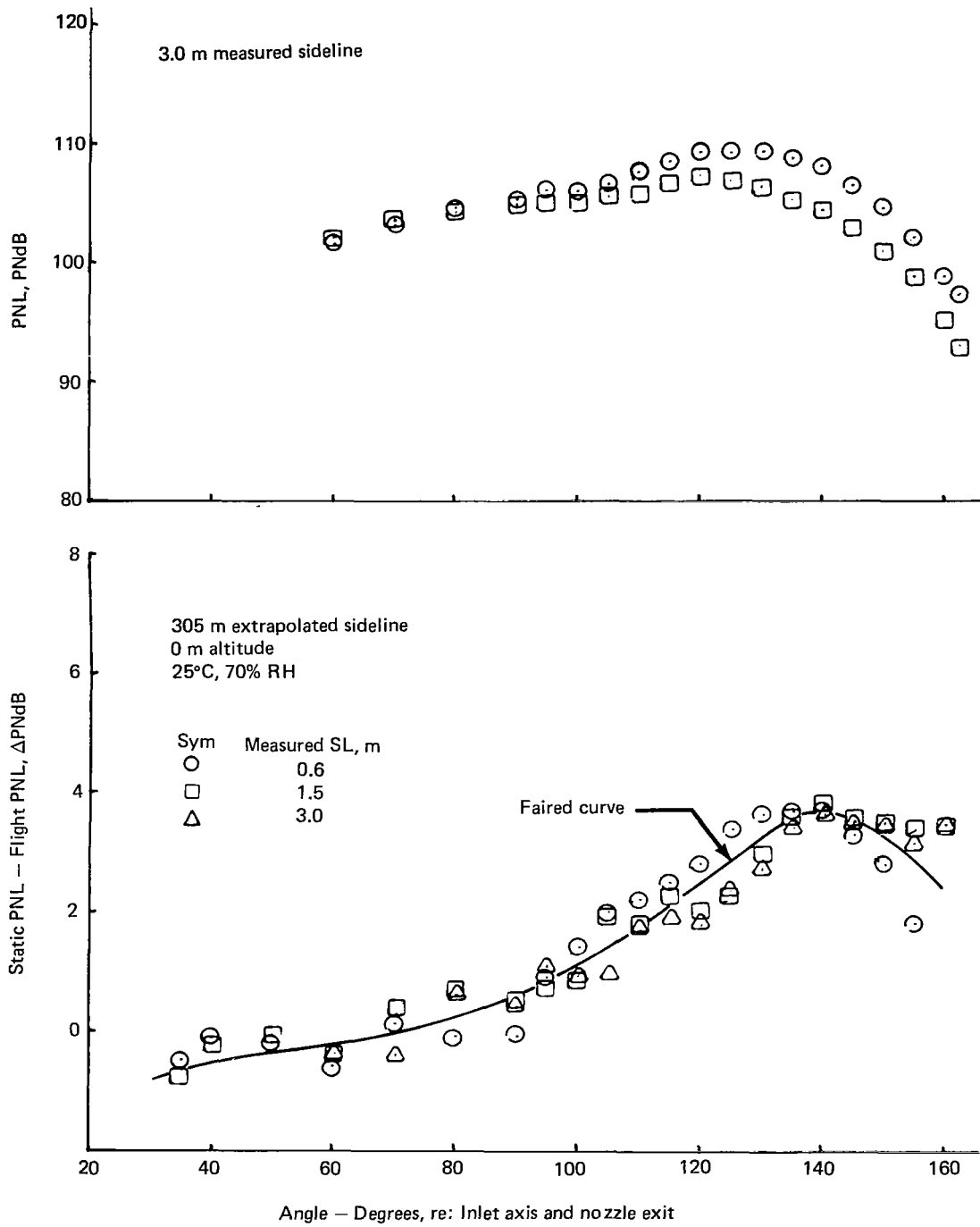
Figure 32.—(Concluded)
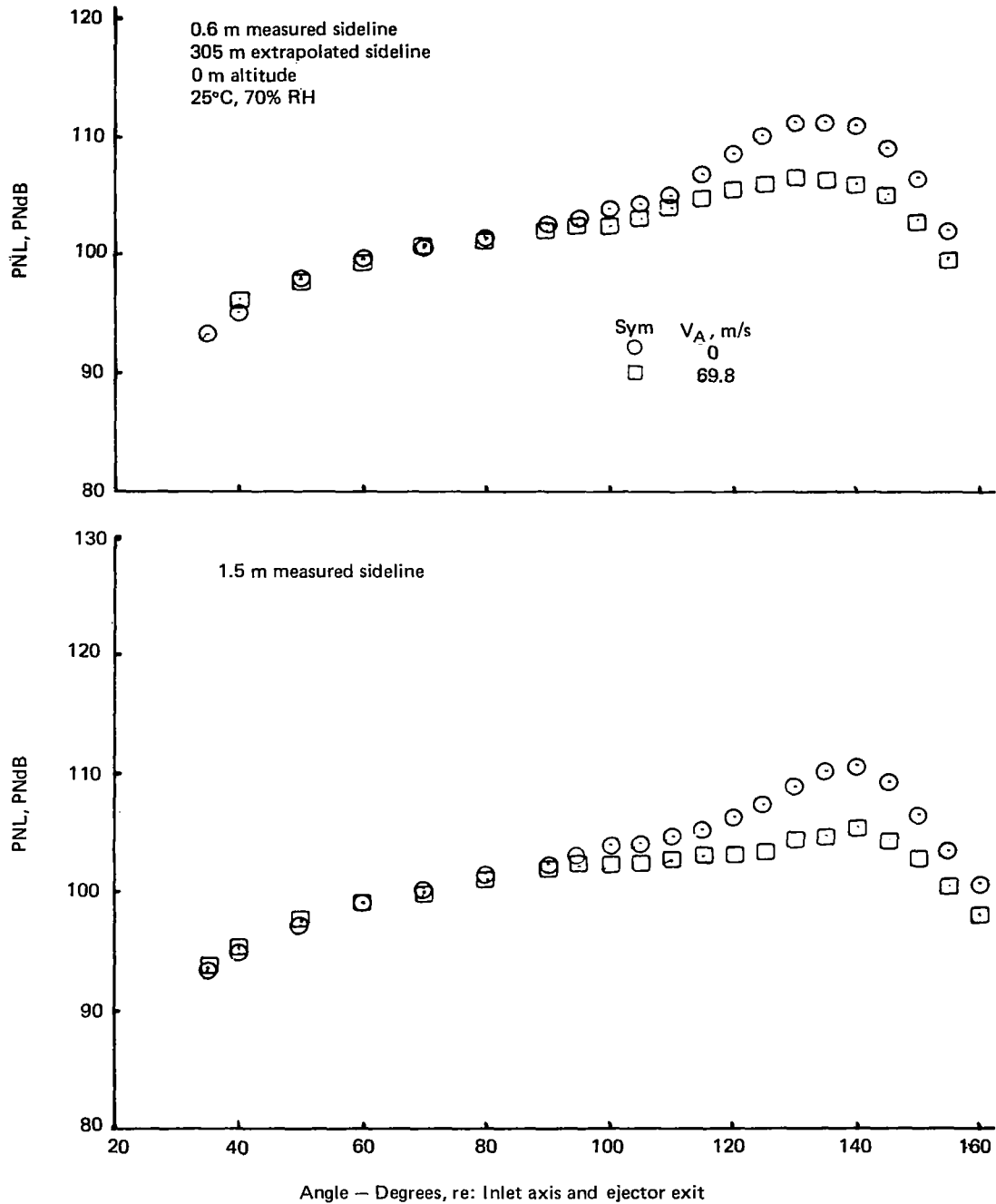
Figure 33.—Flight Effects on PNL of an Annular Nozzle with Lined Ejector
NPR = 2.25, V_j = 594 m/s
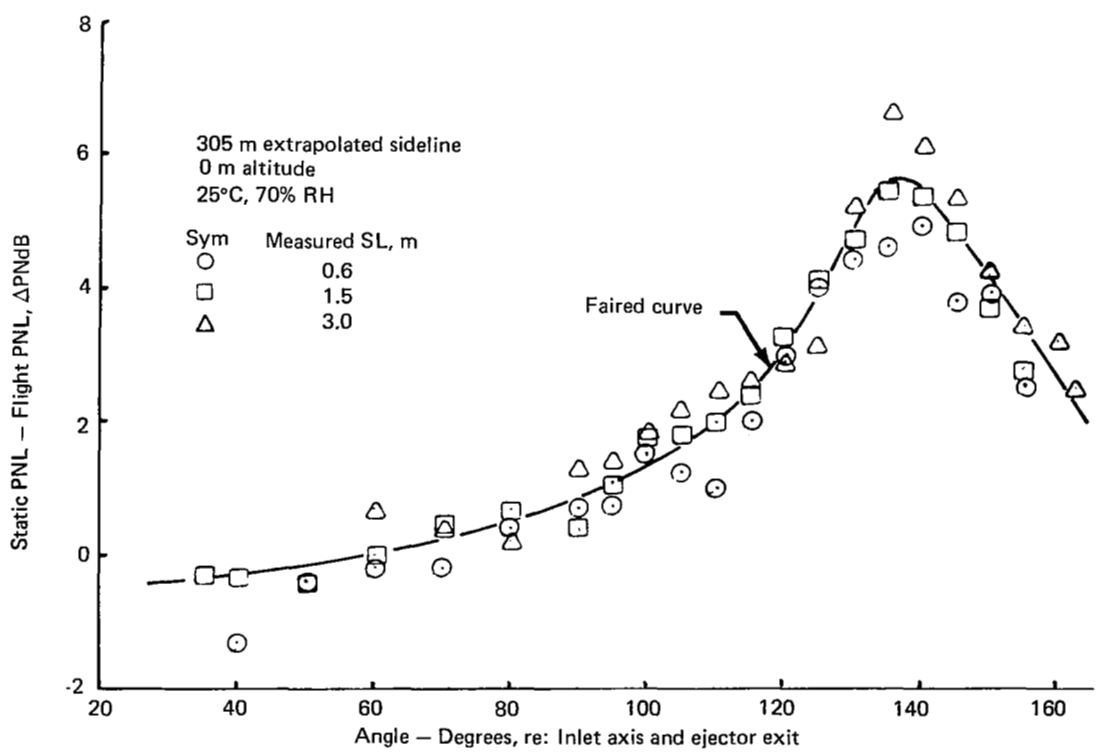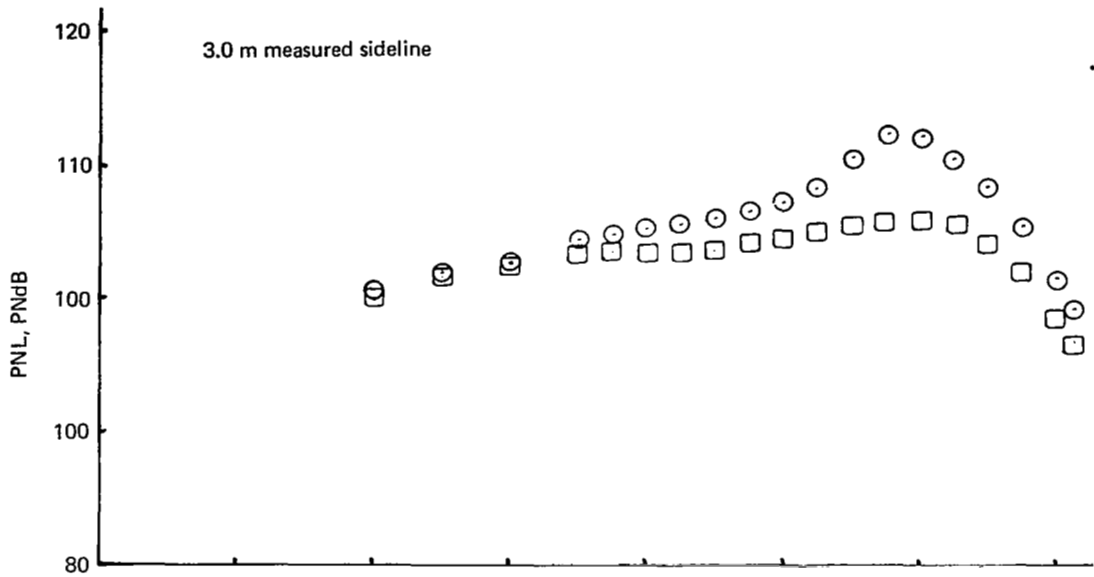
Figure 33.—(Concluded)
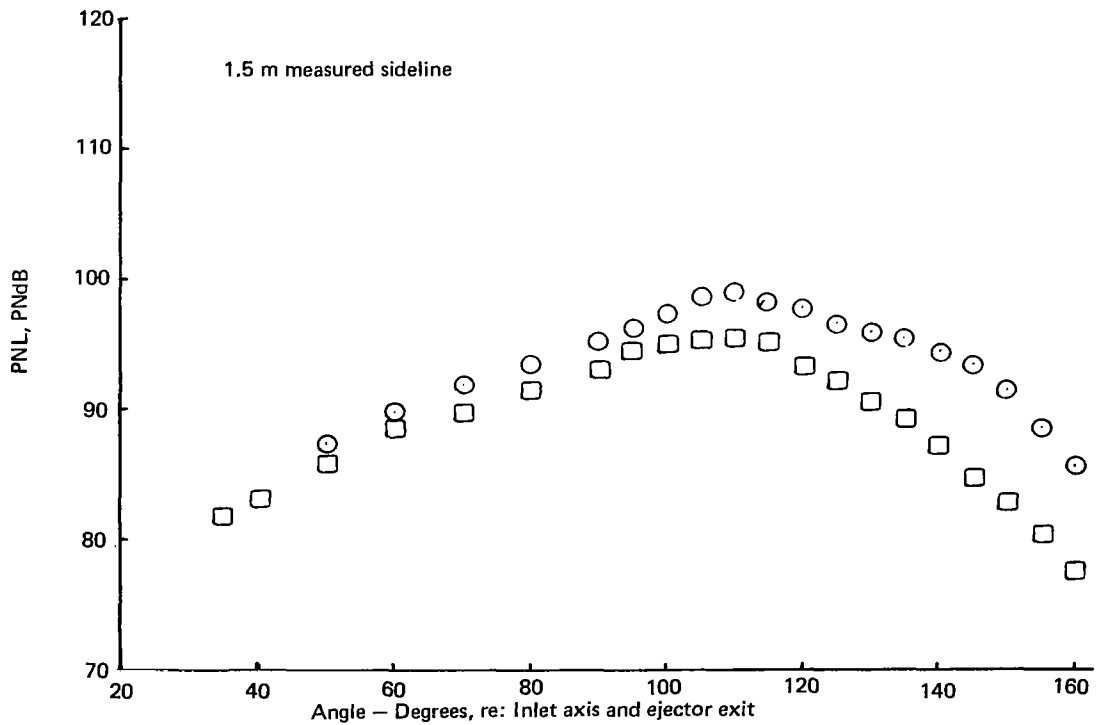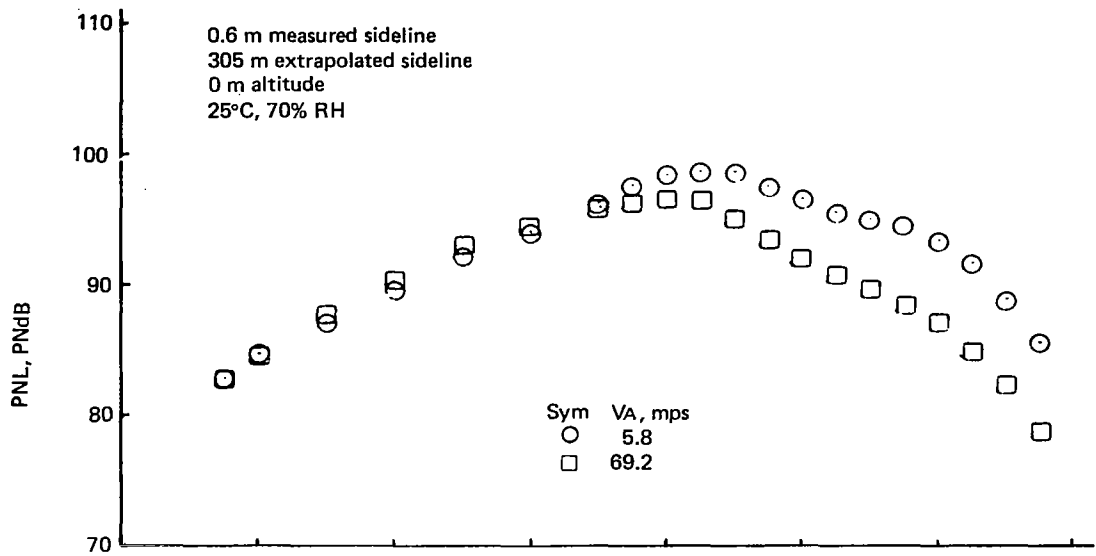
Figure 34.—Flight Effects on PNL of a 20-Lobe Nozzle with Ejector
$$NPR = 2.25 \ V_j = 594 \ m/s$$
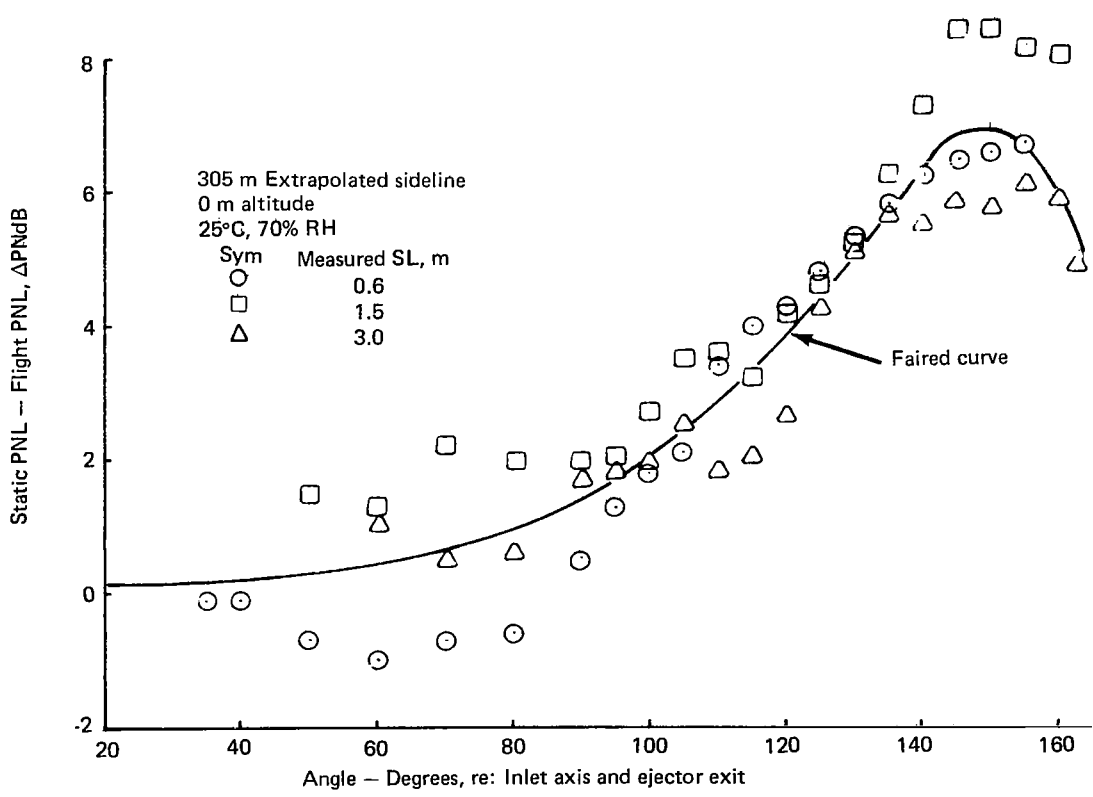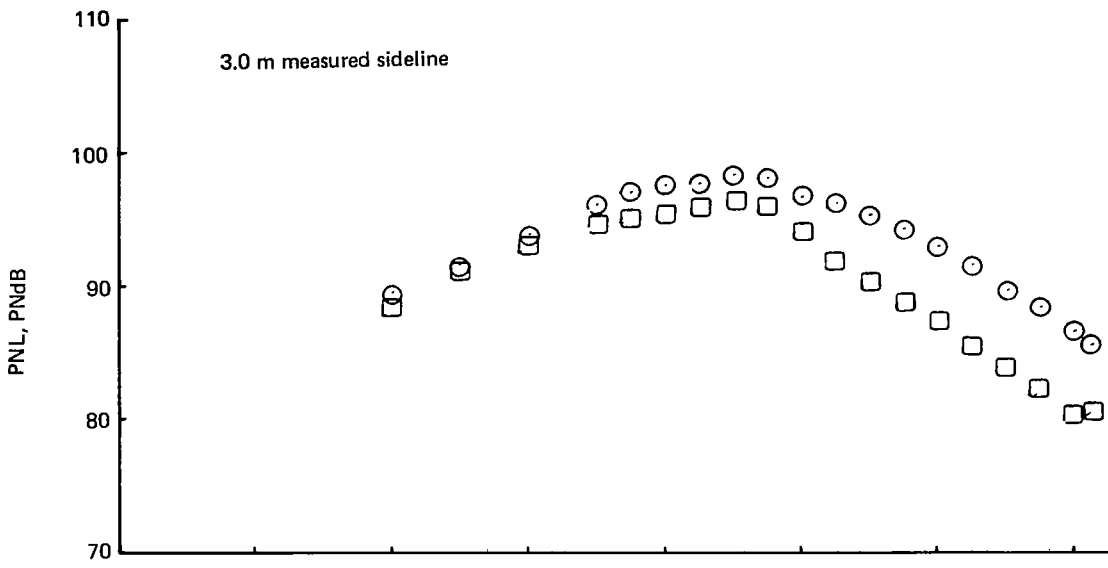
Figure 34.—(Concluded)
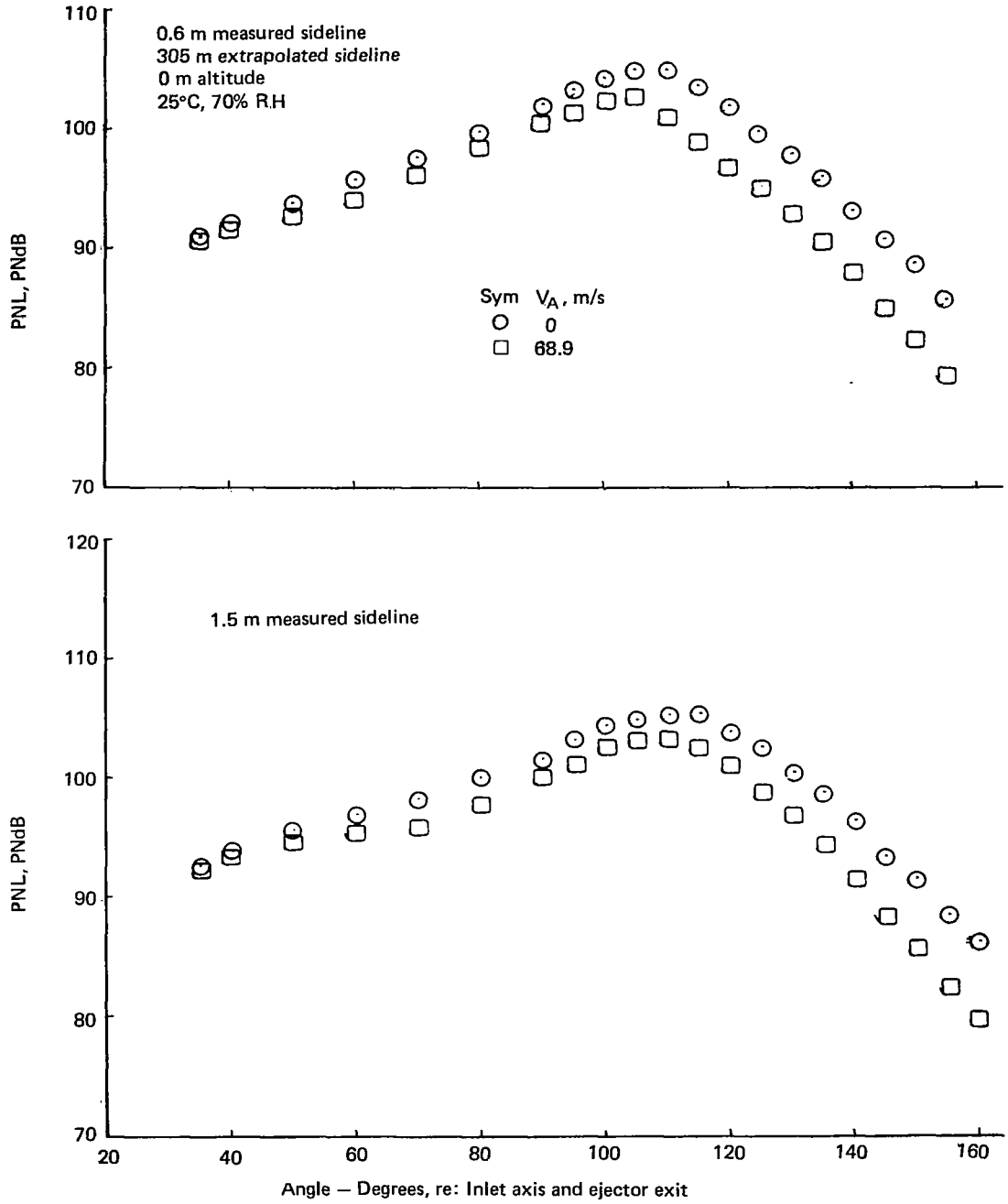
Figure 35.—Flight Effects on PNL of a 57-Tube Nozzle with Ejector
NPR = 2.25 V_j = 594 m/s
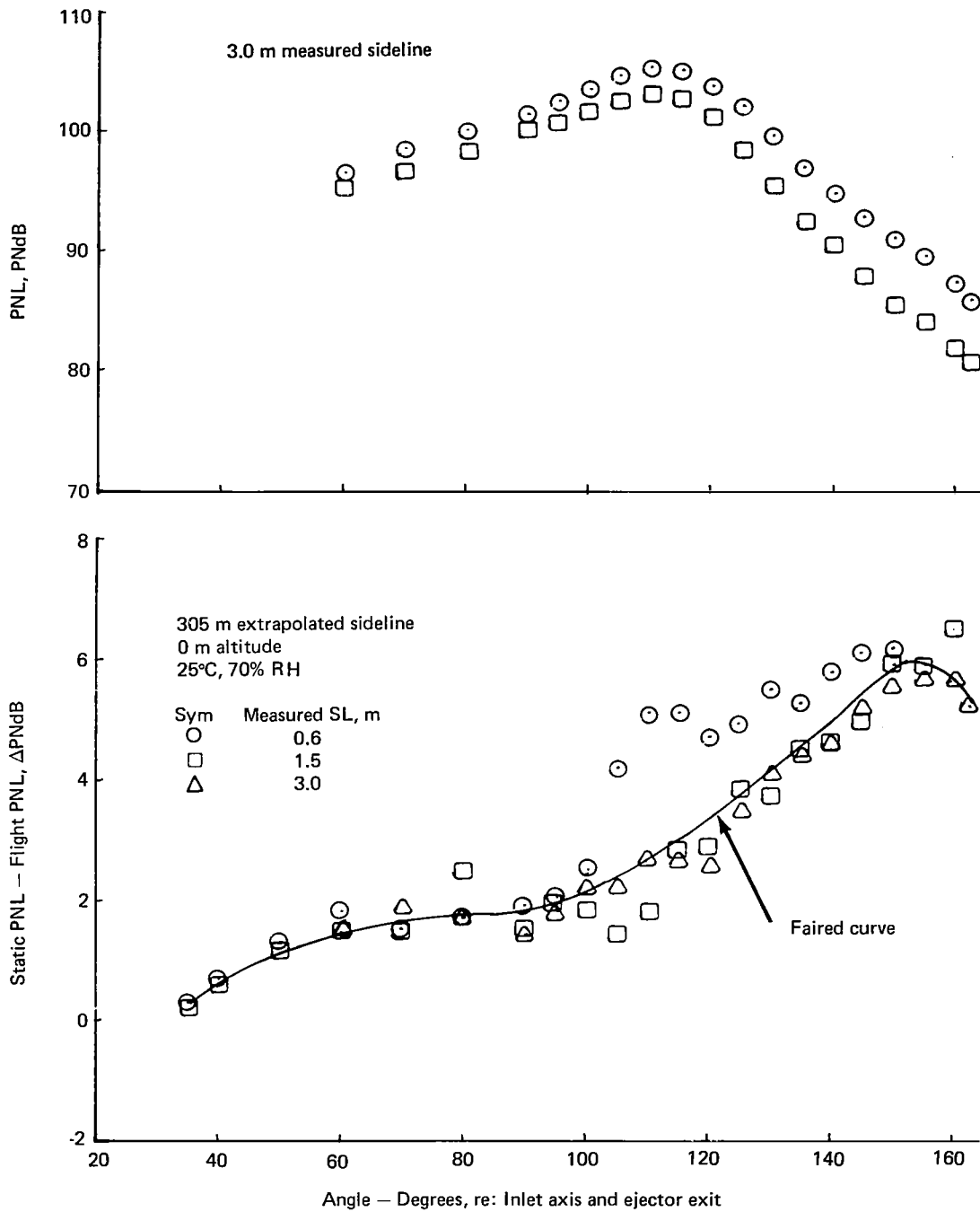
Figure 35.—(Concluded)
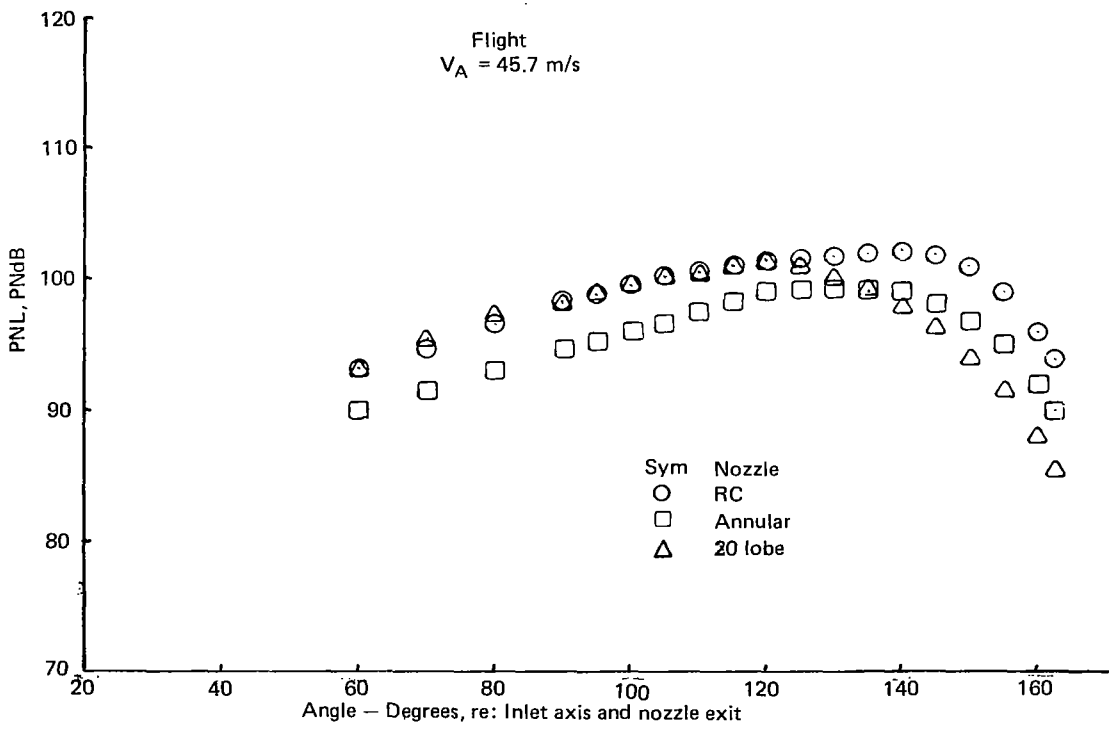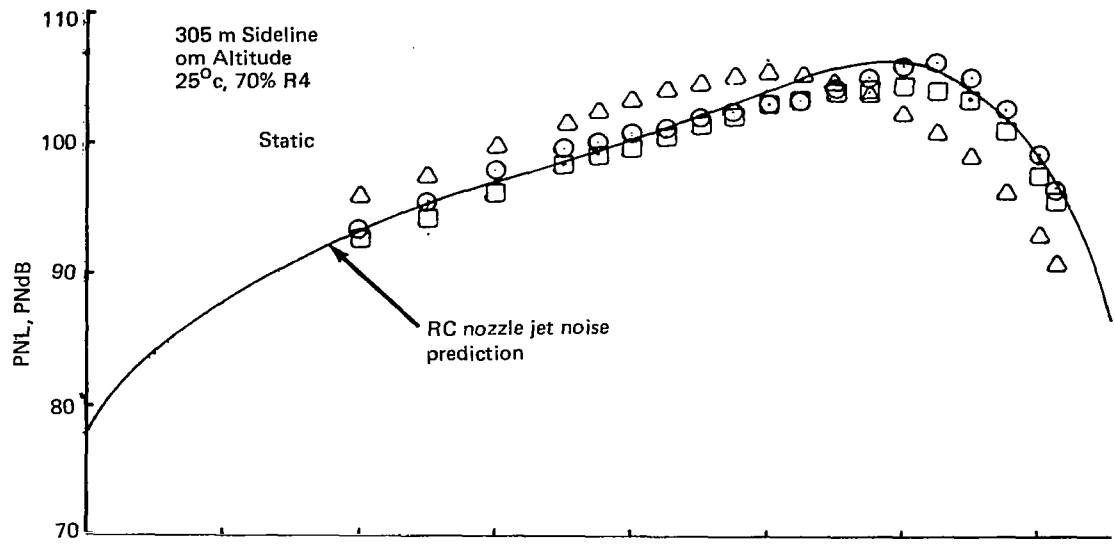
Figure 36.—Comparison of Baseline and Suppressor Nozzles on Basis of PNL Directivity
NPR = 1.75 V_j = 503 m/s
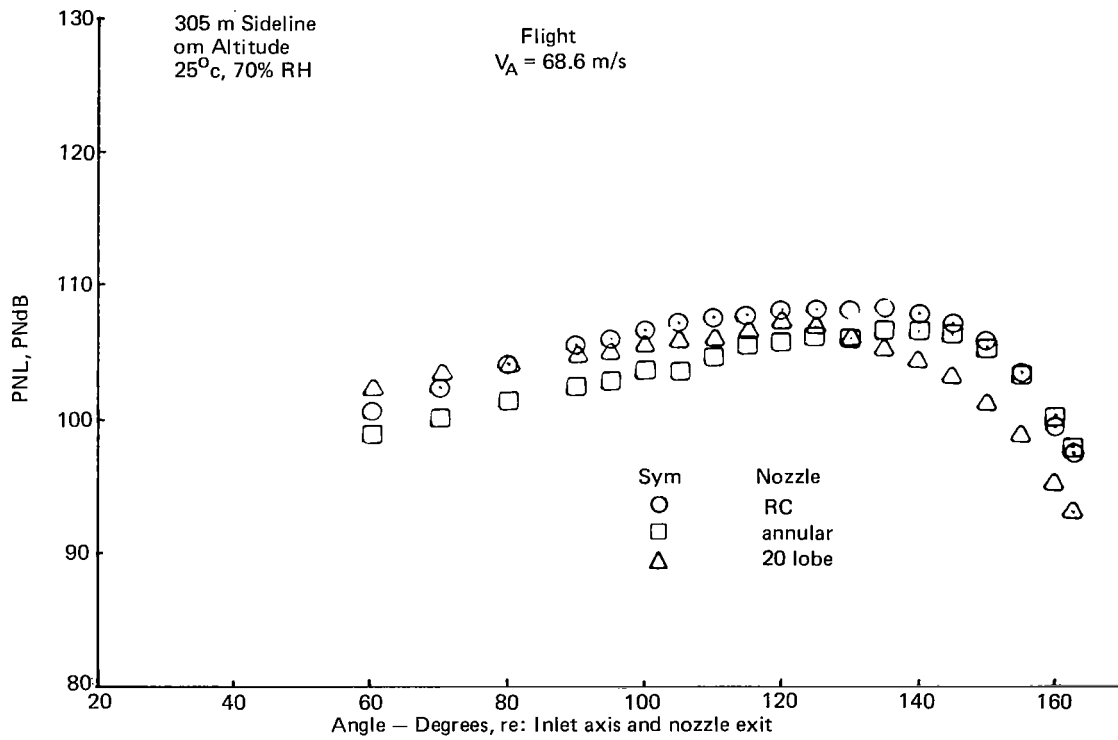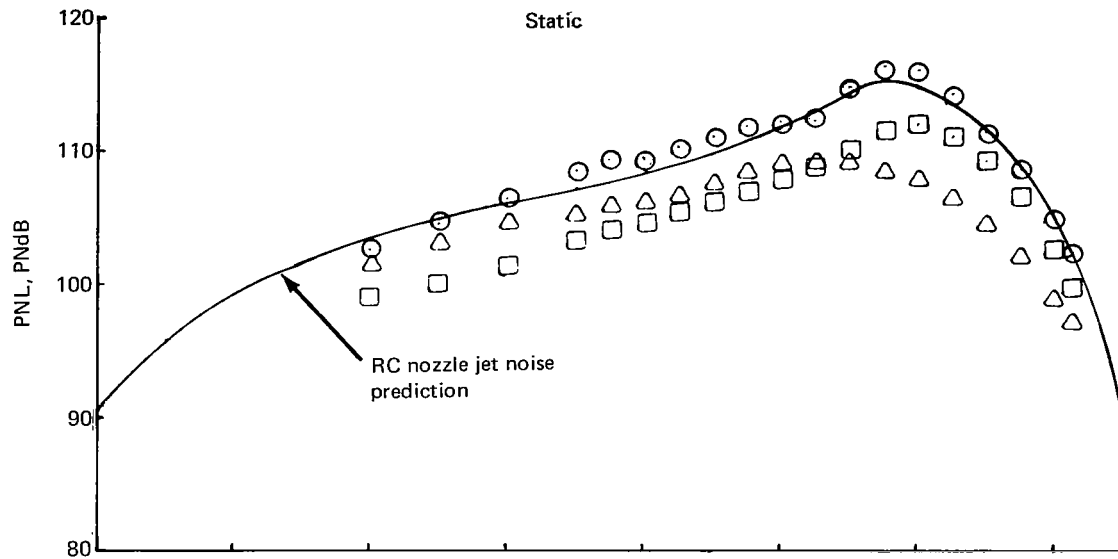
Figure 37.—Comparison of Baseline and Suppressor Nozzle on Basis of PNL Directivity
NPR = 2.25 V_j = 594 m/s
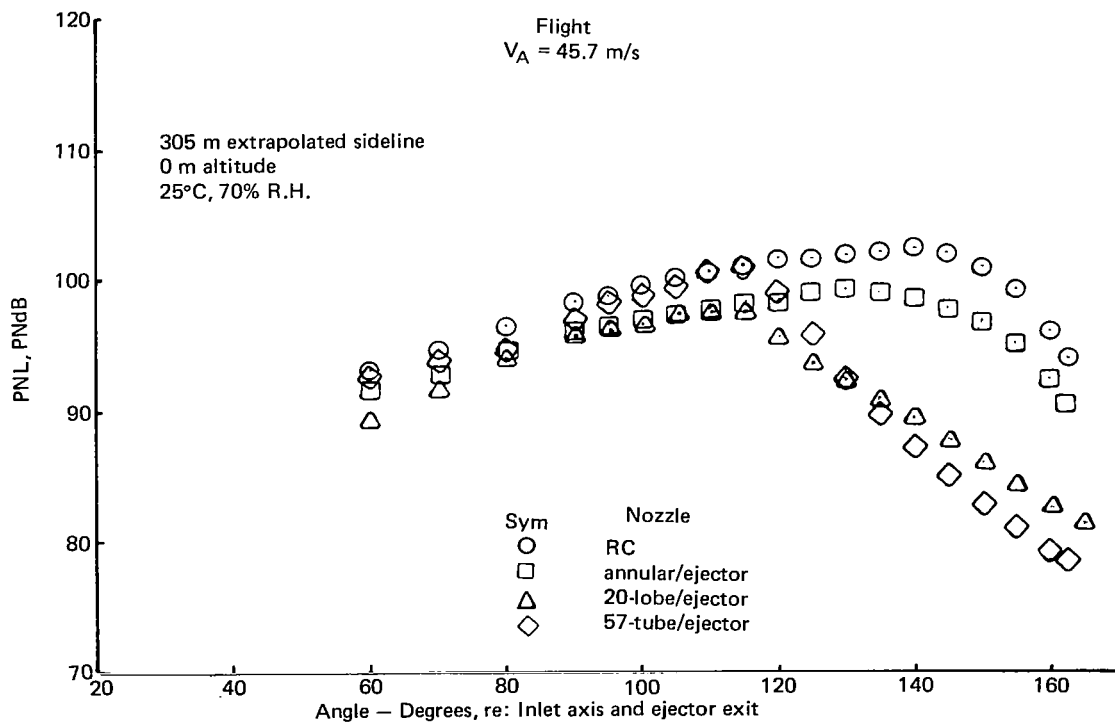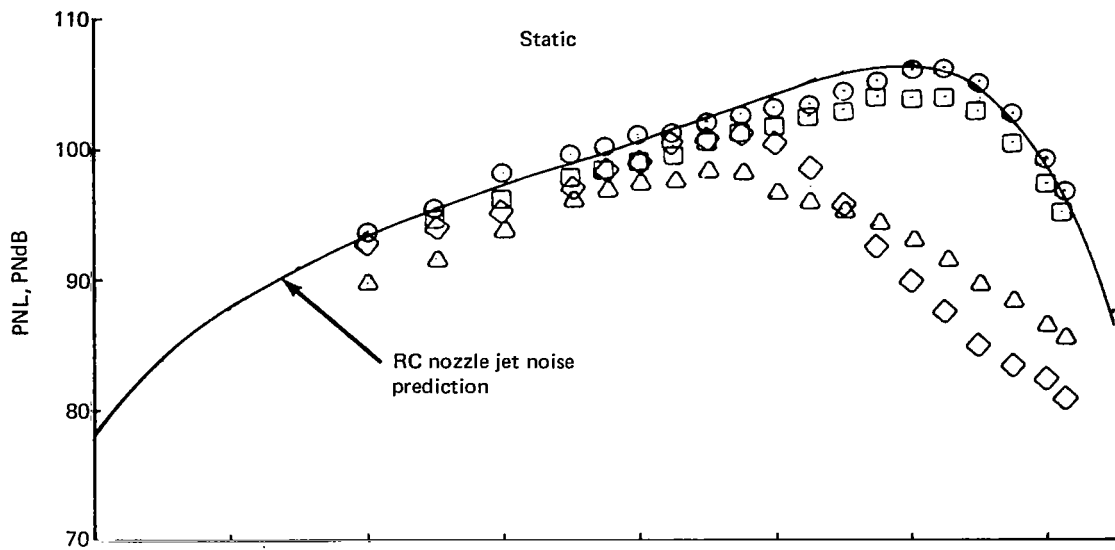
Figure 38.—Comparison of Baseline Nozzle and Suppressor Ejector Configurations on Basis of PNL Directivity NPR = 1.75 V_j = 503 m/s
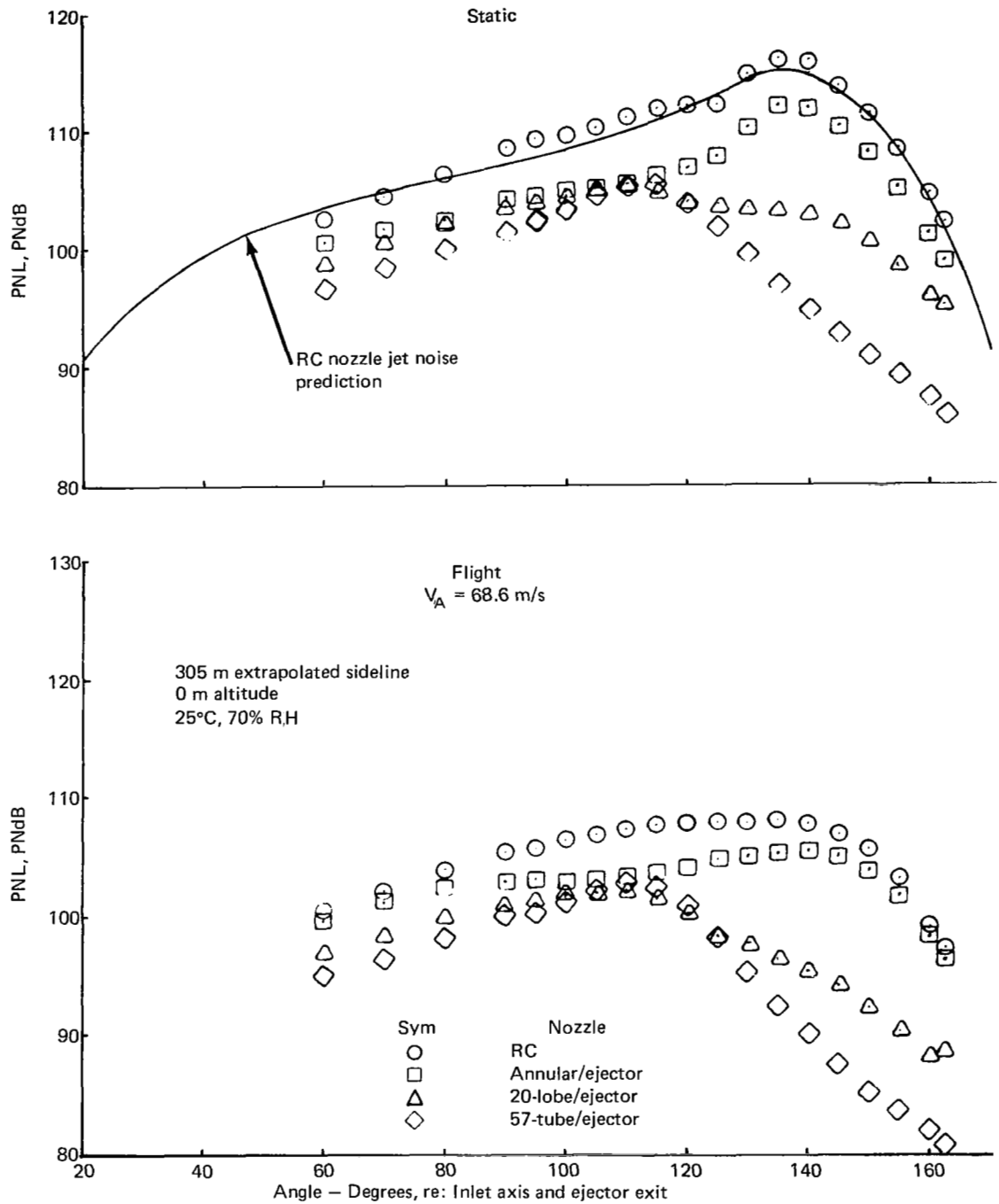
Figure 39.—Comparison of Baseline Nozzle and Suppressor Ejector Configurations on Basis of PNL Directivity NPR = 2.25 V_j = 594 m/s

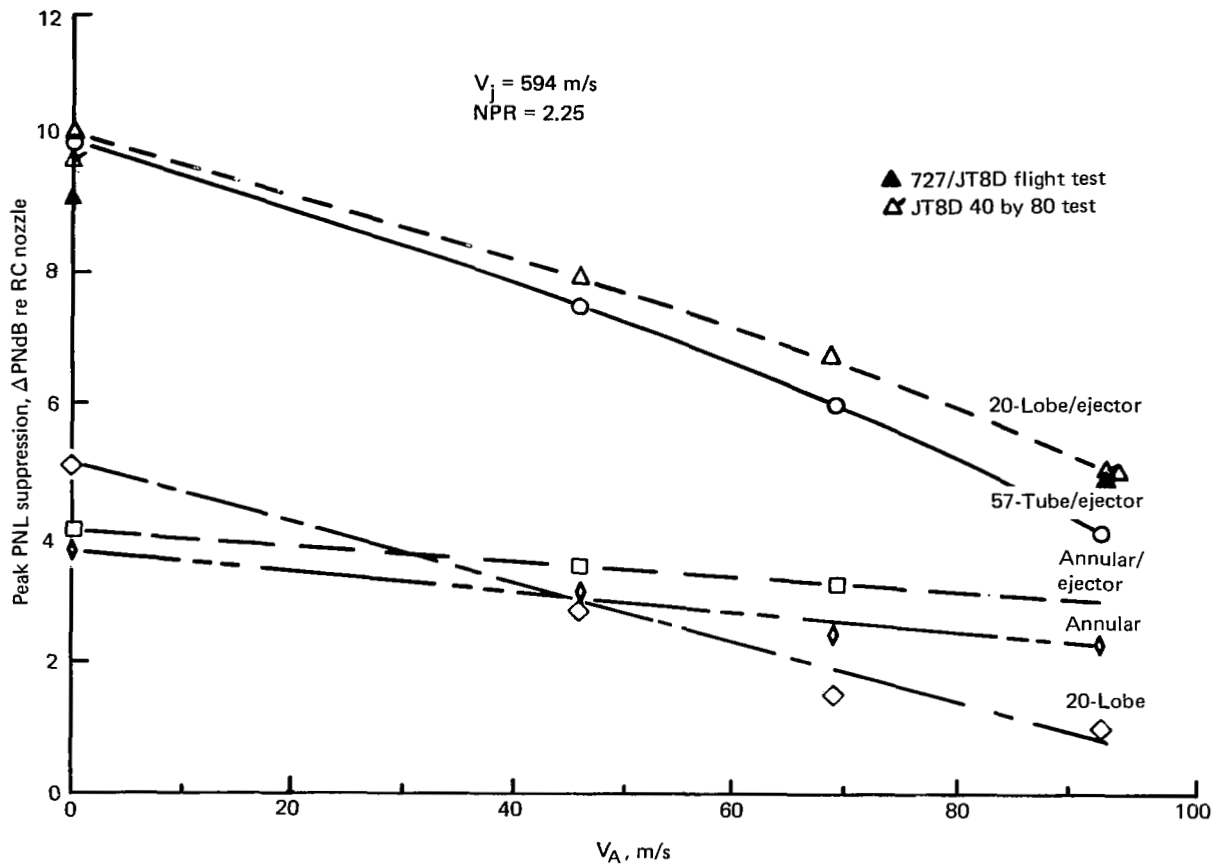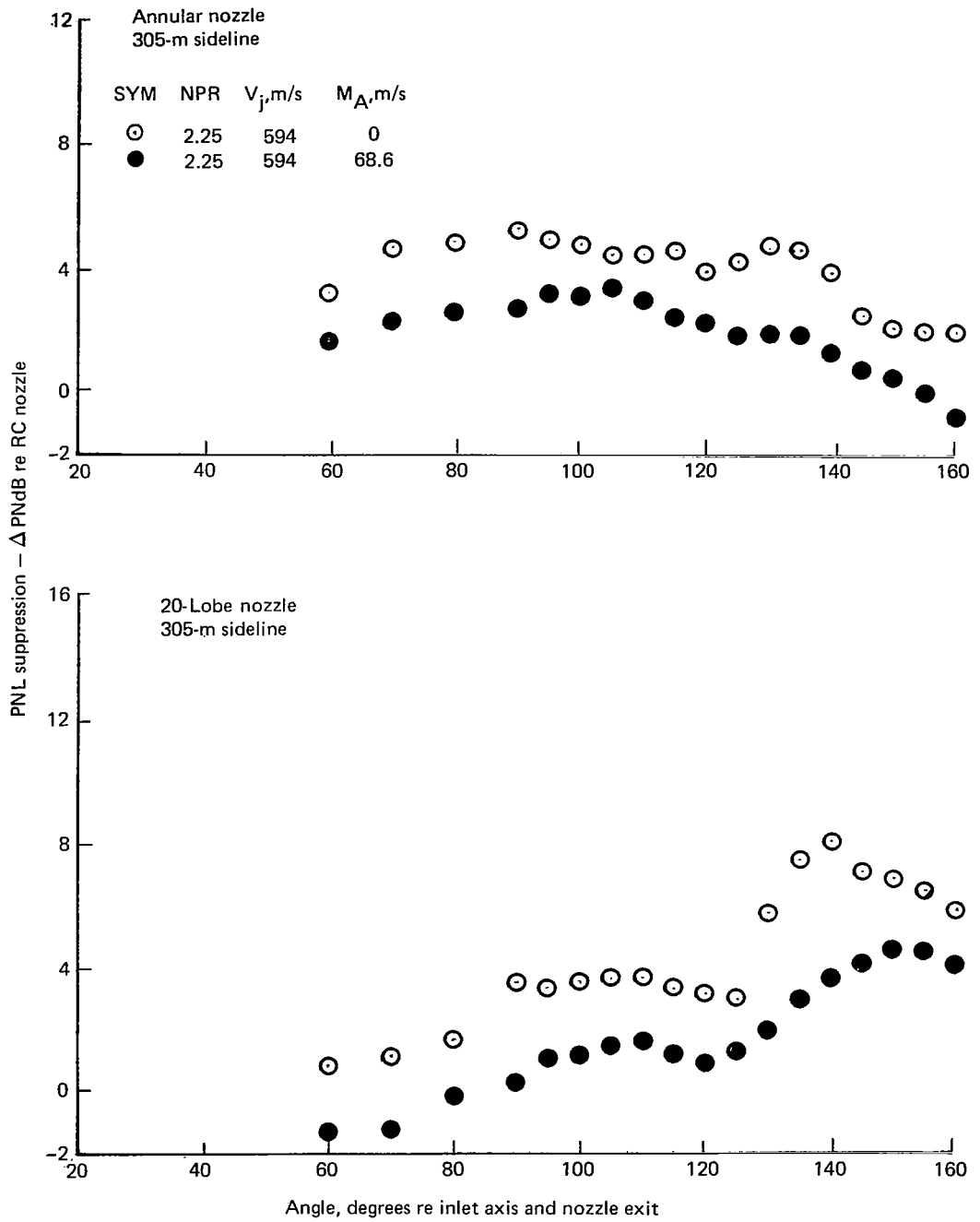Figure 40.--Peak PNL Suppression Characteristics

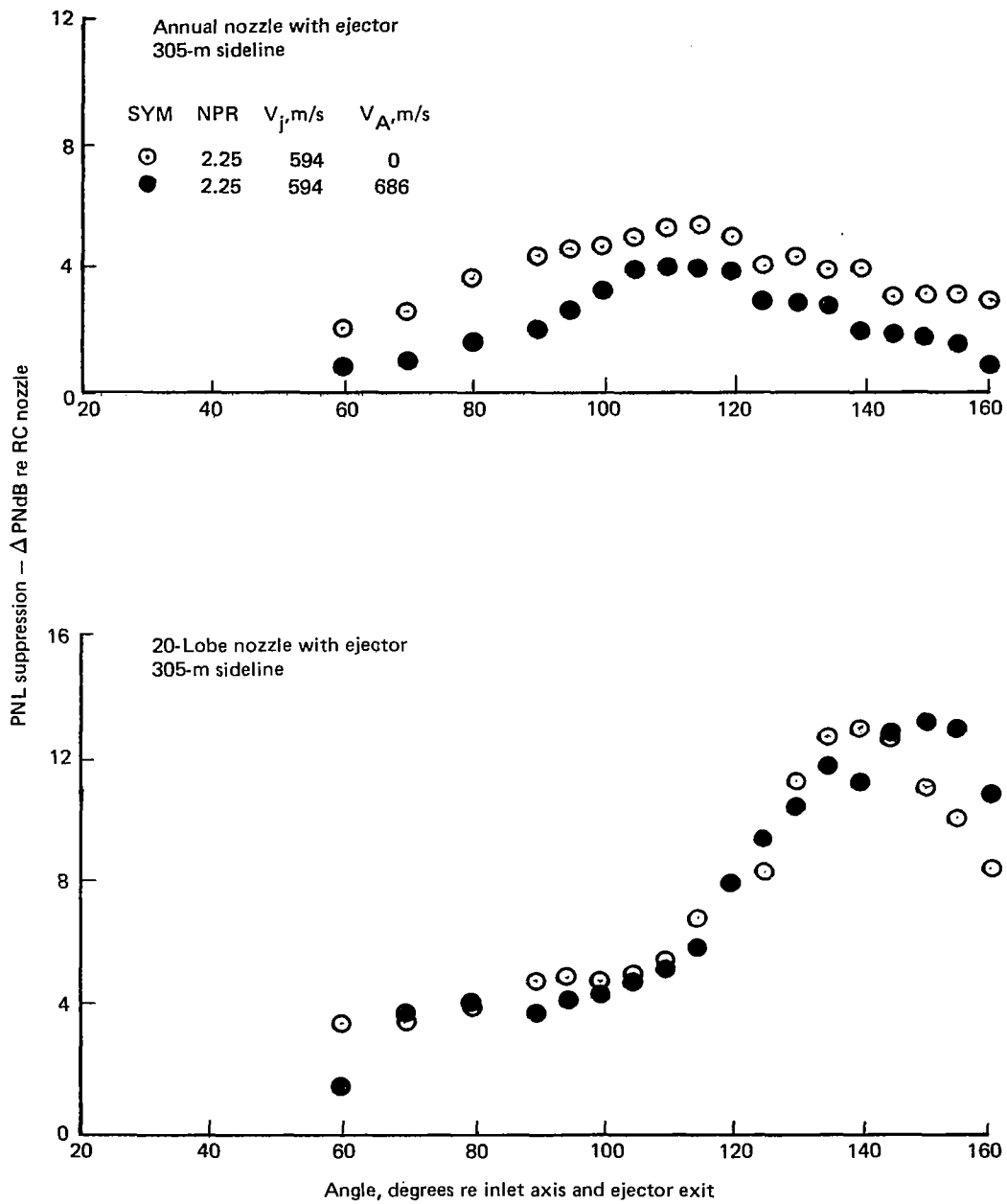Figure 41.—PNL Suppression for the Suppressor Nozzles

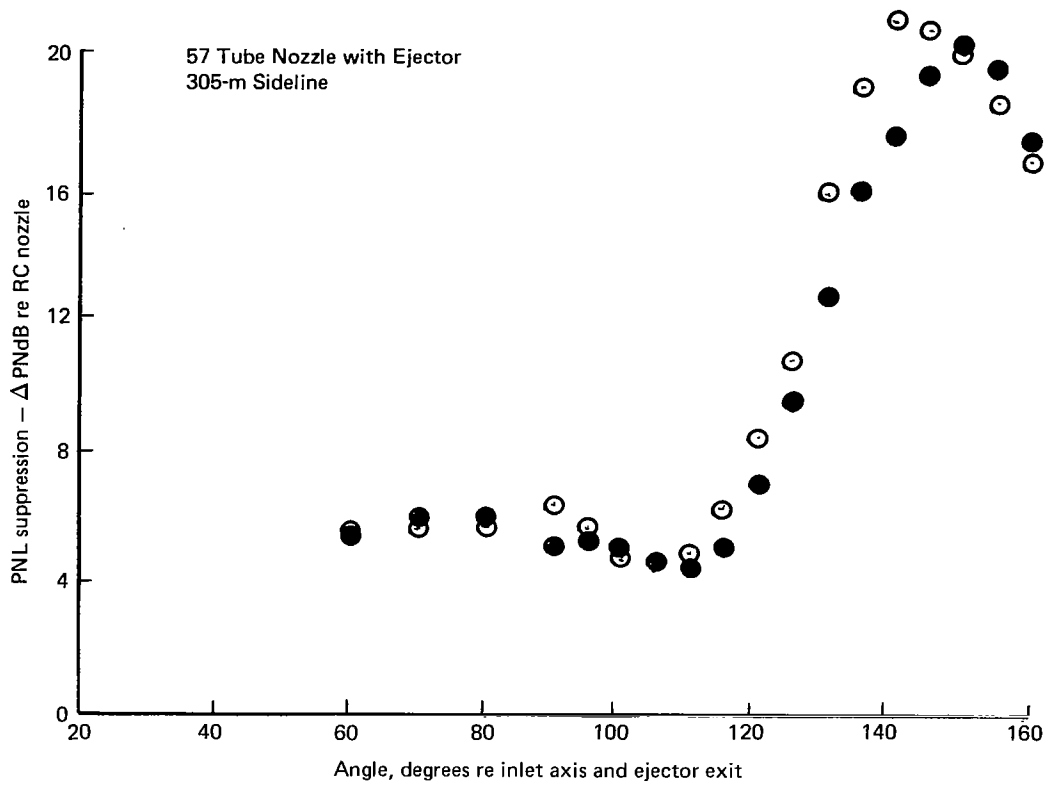*Figure 42.—PNL Suppression for the Ejector/Suppressor Configurations*

Figure 42.—(Concluded)